Waste-to-energy conversion of dried sewage sludge using sorption-enhanced thermochemical technology

By

Xiaoxia Yang

A THESIS SUBMITTED TO MACQUARIE UNIVERSITY

FOR THE DEGREE OF

DOCTOR OF PHILOSOPHY

SCHOOL OF ENGINEERING

June 2020

I certify that the work in this thesis has not previously been submitted for a degree nor has it been submitted as part of requirements for a degree to any other university or institution other than Macquarie University.

Xiaoxia Yang 8-June-2020

Acknowledgements

I would like to express my gratitude to all those who helped me during the past three years of my PhD candidature. My deepest gratitude goes first and foremost to my supervisor, Associate Professor Yijiao Jiang, she has offered me valuable ideas, suggestions, and criticisms with her profound knowledge and rich research experience. Besides, she always puts a high priority on our PhD project and is willing to discuss it with me anytime available. Her patience, kindness, constant encouragement and guidance are greatly appreciated.

Second, I greatly acknowledge the Australian Research Council Industrial Transformation Research Hub (IH140100035) for financial support. Besides, I greatly appreciate the HDR funding support from the School of Engineering at Macquarie University (MQ) throughout my PhD program. I also acknowledge the Postgraduate Research Fund from MQ to support my oral presentation at an international conference and three laboratory visits in the USA. I also would like to express my gratitude to the International Research Training Program (iRTP) Scholarship.

Completion of my PhD program would not have been possible without technical support from Dr Susan Law, Wendy Tao, Dr Aleksei Marianov, and Dr Aaron Colusso from the School of Engineering at MQ. I would also acknowledge Professor Vladimir Strezov and Dr Tao Kan from the Department of Earth and Environmental Sciences at MQ to access the TGA, FTIR, and GC-MS analysis. I would also like to thank Walther Adendorff and Sam Borg in Macquarie Engineering & Technical Services.

All my group members and lab colleagues at MQ are greatly acknowledged, especially Dr Zichun Wang, Dr Yuxiang Zhu, Dr Aleksei Marianov, Dr Dedong He, Shengsheng Gu, Haimei Xu, Wenwen Zhang, Yutong Zhao, Amanj Kheradmand, and Alena Kochubei, all of whom

have helped me in many ways. Special thanks should go to Dr Zishan Liu, Dr Honghui Xu, and Lingmeng Li, who accompanied me through that period of loneliness when I first arrived in Australia.

I am indebted to my parents, my boyfriend Xiaolong Guo, my sister Lixia Yang, my brother-in-law Bernard, my nephew Arden for their continuous support, thoughtfulness, and encouragement all the time.

Last but not least, I express my sincere gratitude to the examiners for reviewing my thesis and for their valuable comments.

List of publications

Journal publications included in the thesis

[1] **Xiaoxia Yang**, Sicong Tian, Tao Kan, Yuxiang Zhu, Honghui Xu, Vladimir Strezov, Peter Nelson, Yijiao Jiang, 2019. Sorption-enhanced thermochemical conversion of sewage sludge to syngas with intensified carbon utilization. Applied Energy, 254: 113663. (Chapter 3)

[2] **Xiaoxia Yang**, Tao Kan, Amanj Kheradmand, Haimei Xu, Vladimir Strezov, Aibing Yu, Yijiao Jiang, 2020. Tunable syngas production from two-stage sorption-enhanced steam gasification of sewage sludge. Chemical Engineering Journal, 404: 126069. (Chapter 4)

[3] **Xiaoxia Yang**, Shengshen Gu, Amanj Kheradmand, Tao Kan, Jing He, Vladimir Strezov, Ruiping Zou, Aibing Yu, Yijiao Jiang. Syngas production from co-gasification of sewage sludge with biochar using two-stage sorption-enhanced catalytic thermochemical conversion process. (Chapter 5)

Other publications

[1] **Xiaoxia Yang**, Xiaoteng Zhou, Tao Kan, Vladimir Strezov, Peter Nelson, Tim Evans, Yijiao Jiang, 2019. Characterization of size resolved atmospheric particles in the vicinity of iron and steelmaking industries in China. Science of The Total Environment, 694:133534.

[2] Yuxiang Zhu, Xianlin Zheng, Yiqing Lu, **Xiaoxia Yang**, Amanj Kheradmand, Yijiao Jiang, 2019. Efficient upconverting carbon nitride nanotubes for near-infrared-driven photocatalytic hydrogen production. Nanoscale, 42: 20274-20283.

[3] Xiaoteng Zhou, Vladimir Strezov, Yijiao Jiang, **Xiaoxia Yang**, Tao Kan, Tim Evans, 2020. Contamination identification, source apportionment and health risk assessment of trace elements at different fractions of atmospheric particles at iron and steelmaking areas in China. PLOS One, 15: e0230983.

[4] Xiaoteng Zhou, Vladimir Strezov, Yijiao Jiang, **Xiaoxia Yang**, Jing He, Tim Evans, 2020. Life cycle impact assessment of airborne metal pollution near selected iron and steelmaking industrial areas in China. Aerosol and Air Quality Research, https://doi.org/10.4209/aaqr.2019.10.0552.

[5] Xiaoteng Zhou, Vladimir Strezov, **Xiaoxia Yang**, Tim Evans, Yijiao Jiang, 2019. Characterising trace element profiles in atmospheric particles at iron and steelmaking industrial areas in China. Chemeca 2019: Chemical Engineering Megatrends and Elements, 30.

Conference presentations

[1] **Xiaoxia Yang**, Yijiao Jiang. Waste-to-energy conversion of biomass using a new two-stage sorption-enhanced thermochemical technology (Abstracts of Papers the American Chemical Society). ACS Fall 2019 National Meeting & Expo, San Diego, CA, USA, Sep 25-29, 2019, Oral Presentation.

[2] **Xiaoxia Yang**, Yijiao Jiang. Two-stage thermochemical conversion of sewage sludge to syngas with intensified carbon utilization. School HDR conference, Macquarie University, Australia, June 20, 2019, Poster Presentation.

[3] **Xiaoxia Yang**, Yijiao Jiang. Waste-to-energy conversion of sewage sludge using sorption-enhanced thermochemical technology. The 2nd International Symposium on Computational Particle Technology and The 13th International Conference on Computational Fluid Dynamics, Melbourne, Australia, Dec 4-8, 2018, Oral Presentation.

[4] **Xiaoxia Yang**, Yijiao Jiang. Waste-to-energy conversion of sewage sludge using sorption-enhanced thermochemical technology. Inaugural School of Engineering HDR conference, Macquarie University, Australia, June 7, 2018, Best Oral Presentation Award.

Abstract

Thermochemical conversion of sewage sludge (SS) into bioenergy is a promising and sustainable approach to combat the energy crisis and mitigate the climate change. Among all the products from the thermochemical conversion, syngas, a mixture of hydrogen (H_2) and carbon monoxide (CO), has attracted increasing attention since it is a versatile and flexible platform feedstock for the production of value-added chemicals and fuels via Fischer-Tropsch synthesis (FTS) process. However, conventional thermochemical conversion of biomass mainly focuses on H_2 production, and effective approaches for CO production are still lacking. In this thesis we proposed a novel two-stage sorption-enhanced (TSSE) thermochemical conversion process, which relies on the integration of a CaO-based CO_2 carrying cycle, to intensify the utilization of sludge carbon. In the process, the CO_2 generated from SS at the first stage (a lower temperature around 500-600 °C) is captured and stored in the form of $CaCO_3$ to enhance H_2 production and is then released at the second stage (a higher temperature around 700-800 °C) to gasify the sludge char for CO production. Thus, the syngas production from the TSSE thermochemical conversion of SS is significantly improved in the following two aspects: (1) producing syngas with separated H_2- and CO-rich streams at the first stage and the second stage, respectively, and (2) improving the utilization efficiency of carbon for CO production. The TSSE pyrolysis of SS sample with a CaO/SS mass ratio of 1:1 (Ca/SS-1:1) could produce 284.7 $NmL/g_{dry\ ss}$ of syngas with the gross H_2/CO molar ratio of 0.4, obtaining 62.4 vol% of H_2-rich gas stream at 550 °C and 72.5 vol% of CO-rich gas stream at 750 °C, respectively. The carbon utilization in the SS could reach as high as 20.4% using the proposed TSSE pyrolysis process, and the yield of CO is remarkably higher than that using other conventional sorption-enhanced thermochemical conversion processes.

The maximum conversion of syngas into downstream synthetic products via the FTS process requires a controllable H_2/CO ratio in the syngas to match the usage ratio of the FTS reactors, while the lack of tunable H_2/CO ratio in the syngas limits direct industrial application of SS-derived syngas. By the introduction of steam into the first stage of the TSSE steam gasification of SS, the H_2 production at the first stage is significantly enhanced, and the H_2/CO ratio of produced syngas is tunable from 0.9 to 4.7 by controlling the CaO and steam contents. The SS sample with a CaO/SS mass ratio of 3:7 (Ca/SS-3:7) produces the maximum syngas production reaching 323.8 NmL/$g_{dry\ SS}$ with an H_2-rich gas stream (72.2 vol% purity) at the first stage and a CO-rich gas stream (60.5 vol% purity) at the subsequent second stage. The performance characterization of the TSSE steam gasification process shows a high yield of tar, indicating that the proposed TSSE steam gasification process still has a great potential to promote the decomposition of tar for enhanced syngas production.

The tar in syngas would block and corrode the downstream equipment, restricting the industrial and practical application of syngas. To address the issue of tar removal in the syngas and further enhance the syngas production, the Ni-CaO/Al_2O_3 catalyst and biochar were introduced into the TSSE steam gasification of SS. A synergistic effect of CaO and Ni in the Ni-CaO/Al_2O_3 catalyst was observed to enhance the H_2 production at the first stage, while CaO is a factor of vital importance for CO production at the second stage. The presence of steam and Ni_5Ca_{40}/Al catalyst shows unprecedented performance in enhancing the H_2 production at the first stage due to the promotion of tar cracking/reforming and water-gas shift reaction. Biochar supplements carbon source for CO production, remarkably promoting the CO production at the second stage. Upon introducing steam, Ni_5Ca_{40}/Al catalyst and biochar, a 9.3 times higher yield (396.9 NmL/$g_{dry\ SS}$) of H_2 at the first stage was obtained compared to the TSSE pyrolysis of Ca/SS-3:7, and the yield of CO (208.4 NmL/$g_{dry\ SS}$) at the second stage triples that without biochar (66.6 NmL/$g_{dry\ SS}$). Therefore, there is a complementary effect of steam, Ni-CaO/Al_2O_3

catalyst, and biochar on the enhancement in H_2 production at the first stage and CO production at the second stage. With the introduction of steam, Ni-CaO/Al_2O_3 catalyst, and biochar, the yield of syngas further increases to 645.5 NmL/$g_{dry\ SS}$ with an 88.2 vol% of H_2 at the first stage and a 55.6 vol% of CO at the second stage, and a H_2/CO ratio of 2 is achieved, which is desirable for the downstream synthesis of value-added chemicals and fuels via FTS process. And the percentage of tar is eliminated by 22.0% and the total gas increases by 42.7% compared to those from the TSSE steam gasification process.

This work develops a new TSSE thermochemical conversion process that has been demonstrated to effectively utilize the carbon in SS for high-purity CO production in addition to the sorption-enhanced production of high-purity H_2, and to achieve the production of syngas with tunable H_2-to-CO molar ratios through the inherent separation of H_2 and CO generation. This technology makes it possible to achieve the waste-to-energy conversion by direct integration of the TSSE thermochemical conversion with the syngas application via FTS process where H_2 and CO could be mixed in desirable ratios for the downstream synthesis of value-added chemicals and fuels.

Table of Contents

Chapter 1 Introduction

1.1. Background

With the population growth and rapid economic development, the global energy demand continues to escalate. The depletion of fossil fuels and environmental pollution caused by the consumption of fossil fuels are gradually aggravated [1, 2]. There is an urgent need to transit the energy source from fossil fuels to renewable sources [3]. Among all the renewable sources, biomass has attracted intensive attention since it is abundantly available, less dependent on geographical and climatic conditions, and easily storable and transportable [4].

As one kind of biomass source, sewage sludge (SS) is generated in large quantities during wastewater treatment. The risk of pathogens, persistent organic pollutants and heavy metals make SS a hazardous waste, which is mainly disposed of by landfill and land applications so far [5, 6]. However, rapid urbanization worldwide results in an increasing amount of wastewater required for treatment, and therefore, a quick growth in SS generation [7]. This poses a significant challenge to conventional approaches for SS treatment considering the land shortage and environmental concerns [8, 9]. Therefore, efficient approaches to treat SS in an environmentally benign and sustainable manner are in urgent demand.

To date, one promising approach would be the thermochemical treatment of SS, which could not only lead to an effective minimization of SS but also make use of the bioenergy it contains [10-12]. Incineration power generation is a commonly considered thermochemical treatment technique for SS at present, other emerging technologies mainly include pyrolysis and gasification [6]. Unlike incineration that directly recovers heat from SS [5], pyrolysis and gasification can produce value-added chemicals or fuels, such as biochar [13-15], liquid fuels [16-18], and syngas[19, 20].

Among these products, syngas, which consists mainly of hydrogen (H_2) and carbon monoxide (CO), has gained increasing interests due to its high calorific value and wide application as a platform feedstock for a wide range of high value-added fuels and chemicals via well-established industrial processes, such as Fischer-Tropsch synthesis (FTS) process [21]. Considering that H_2 is carbon-free energy and versatile in the chemical industry, a lot of research effort is spent on pursuing high yield and purity of H_2 from biomass [22, 23]. A process was proposed named sorption-enhanced thermochemical conversion of biomass with calcium oxide (CaO), aiming to enhance H_2 production by the introduction of the CaO carbonation reaction to capture the carbon dioxide (CO_2) released during biomass reforming [24]. The purity of H_2 in the gas stream obtained after the sorption-enhanced steam gasification of biomass can reach as high as 70-80 vol% [25]. However, less attention was paid to another important component of the syngas, CO production from the biomass, and effective approaches for biomass-derived CO production are lacking.

There are still some challenges to restrict the industrial and practical application of the syngas via well-established industrial processes. Firstly, different synthetic products and FTS operation modes demand different H_2/CO ratios in the syngas [26, 27]. The maximum conversion efficiency of syngas into downstream synthetic products requires that the composition of the syngas matches the overall usage ratio of the FTS reactors [28]. However, an uncontrollable H_2/CO ratio in the biomass-derived syngas incurs additional process and cost of refining. Secondly, a tar limit of 0.05 g/m^3 or less is generally required for the industrial application of the biomass-derived syngas [29]. Nevertheless, the tar contents in the biomass-derived syngas are always beyond the limit value, which would block and corrode the downstream equipment [30]. Therefore, it is of great significance to precisely control the H_2/CO ratio and eliminate the tar in the biomass-derived syngas.

1.2. Objectives and scope

This thesis presents a novel two-stage sorption-enhanced (TSSE) thermochemical conversion process integrating of a CaO-based CO_2 carrying cycle to produce syngas from SS. More specifically, the CO_2 generated from SS is captured to enhance H_2 production at the first stage, and is then released to gasify the sludge char for CO production at the second stage. Besides, the yield and purity of H_2 and CO are further enhanced and optimised by adding steam and catalysts. Moreover, the performance characterisation of the TSSE thermochemical conversion process on product distributions, tar compositions, and elemental utilization are also investigated.

The specific objectives of this thesis are:

(1) To intensify the carbon utilization of SS for CO production.

(2) To produce syngas from SS with separated H_2-rich gas stream at the first stage and CO-rich gas stream at the second stage.

(3) To obtain a tunable H_2/CO ratio in the SS-derived syngas.

(4) To clearly understand the mechanism of the proposed TSSE thermochemical conversion process.

(5) To eliminate tar for the enhancement in the syngas production over bio-functional Ni-CaO catalyst and biochar.

The background, objectives and scope of this thesis are described in **Chapter 1**. In **Chapter 2,** the current status and challenges of global energy supply and SS treatment, recent developments of the sorption-enhanced thermochemical conversion process of biomass for syngas production and tar elimination methods are reviewed. **Chapter 3** presents a novel TSSE thermochemical conversion process of SS for syngas production and the improvement in the utilization efficiency of carbon in the SS. **Chapter 4** presents the SS-derived syngas production with a tunable H_2/CO

ratio via the introduction of steam into the TSSE steam gasification process. Besides, studies on the performance characterisation of the novel TSSE thermochemical conversion process are also exhibited in this chapter. **Chapter 5** shows the catalytic activity of the bi-function Ni-CaO/Al_2O_3 catalyst and biochar on the tar elimination for syngas production. Thereinto, the role of Ni and CaO contents in the Ni-CaO/Al_2O_3 catalyst on syngas production and the stability of the Ni-CaO/Al_2O_3 catalyst are also studied. Besides, the synergistic effect of steam, Ni-CaO/Al_2O_3 catalyst and biochar on the syngas production is also studied in this chapter. **Chapter 6** summarises the main findings of this work and suggests the prospects for the future work on SS-derived syngas via the TSSE thermochemical conversion process.

References

1. Panwar, N.L., S.C. Kaushik, and S. Kothari, *Role of renewable energy sources in environmental protection: A review.* Renewable and Sustainable Energy Reviews, 2011. **15**(3): p. 1513-1524.
2. Ellabban, O., H. Abu-Rub, and F. Blaabjerg, *Renewable energy resources: Current status, future prospects and their enabling technology.* Renewable and Sustainable Energy Reviews, 2014. **39**: p. 748-764.
3. Lund, H., *Renewable energy strategies for sustainable development.* Energy, 2007. **32**(6): p. 912-919.
4. Sikarwar, V., et al., *An overview of advances in biomass gasification.* Energy & Environmental Science, 2016. **9**(10).
5. Syed-Hassan, S.S.A., et al., *Thermochemical processing of sewage sludge to energy and fuel: Fundamentals, challenges and considerations.* Renewable and Sustainable Energy Reviews, 2017. **80**: p. 888-913.

6. He, C., et al., *Hydrothermal gasification of sewage sludge and model compounds for renewable hydrogen production: A review.* Renewable and Sustainable Energy Reviews, 2014. **39**: p. 1127-1142.

7. Yang, G., G. Zhang, and H. Wang, *Current state of sludge production, management, treatment and disposal in China.* Water Research, 2015. **78**: p. 60-73.

8. Magdziarz, A. and S. Werle, *Analysis of the combustion and pyrolysis of dried sewage sludge by TGA and MS.* Waste Management, 2014. **34**(1): p. 174-179.

9. Peng, L., et al., *Co-gasification of wet sewage sludge and forestry waste in situ steam agent.* Bioresource Technology, 2012. **114**: p. 698-702.

10. Hernández, A.B., F. Okonta, and N. Freeman, *Thermal decomposition of sewage sludge under N_2, CO_2 and air: Gas characterization and kinetic analysis.* Journal of Environmental Management, 2017. **196**(C): p. 560-568.

11. Fytili, D. and A. Zabaniotou, *Utilization of sewage sludge in EU application of old and new methods—A review.* Renewable and Sustainable Energy Reviews, 2008. **12**(1): p. 116-140.

12. Peccia, J. and P. Westerhoff, *We should expect more out of our sewage sludge.* Environmental Science & Technology, 2015. **49**(14): p. 8271-8276.

13. Tripathi, M., J.N. Sahu, and P. Ganesan, *Effect of process parameters on production of biochar from biomass waste through pyrolysis: A review.* Renewable and Sustainable Energy Reviews, 2016. **55**: p. 467-481.

14. Li, J., et al., *Biochar from microwave pyrolysis of biomass: A review.* Biomass and Bioenergy, 2016. **94**: p. 228-244.

15. Leng, L., et al., *Study on demetalization of sewage sludge by sequential extraction before liquefaction for the production of cleaner bio-oil and bio-char.* Bioresource Technology, 2016. **200**: p. 320-327.

16. Xie, Q., et al., *Fast microwave-assisted catalytic pyrolysis of sewage sludge for bio-oil production.* Bioresource Technology, 2014. **172**: p. 162-168.

17. Sánchez, M.E., et al., *Effect of pyrolysis temperature on the composition of the oils obtained from sewage sludge.* Biomass and Bioenergy, 2009. **33**(6): p. 933-940.

18. Fonts, I., et al., *Sewage sludge pyrolysis for liquid production: A review.* Renewable and Sustainable Energy Reviews, 2012. **16**(5): p. 2781-2805.

19. Nipattummakul, N., et al., *High temperature steam gasification of wastewater sludge.* Applied Energy, 2010. **87**(12): p. 3729-3734.

20. Watson, J., et al., *Gasification of biowaste: A critical review and outlooks.* Renewable and Sustainable Energy Reviews, 2018. **83**: p. 1-17.

21. Jiao, F., et al., *Selective conversion of syngas to light olefins.* Science (New York, N.Y.), 2016. **351**(6277): p. 1065-1068.

22. Ren, N.-Q., et al., *A review on bioconversion of lignocellulosic biomass to H_2: Key challenges and new insights.* Bioresource Technology, 2016. **215**: p. 92-99.

23. Patra, T.K. and P.N. Sheth, *Biomass gasification coupled with producer gas cleaning, bottling and HTS catalyst treatment for H_2-rich gas production.* International Journal of Hydrogen Energy, 2019. **44**(23): p. 11602-11616.

24. Harrison, D.P., *Sorption-enhanced hydrogen production: A review.* Industrial & Engineering Chemistry Research, 2008. **47**(17): p. 6486-6501.

25. Florin, N.H. and A.T. Harris, *Enhanced hydrogen production from biomass with in situ carbon dioxide capture using calcium oxide sorbents.* Chemical Engineering Science, 2008. **63**(2): p. 287-316.

26. Dry, M.E., *The Fischer–Tropsch process: 1950–2000.* Catalysis Today, 2002. **71**(3-4): p. 227-241.

27. Schulz, H., *Short history and present trends of Fischer-Tropsch synthesis.* Applied Catalysis A: General, 1999. **186**(1-2): p. 3-12.

28. Dry, M.E., *The Fischer-Tropsch process: 1950-2000.* Catalysis Today, 2002. **71**(3-4): p. 227-241.

29. Han, J. and H. Kim, *The reduction and control technology of tar during biomass gasification/pyrolysis: An overview.* Renewable and Sustainable Energy Reviews, 2008. **12**(2): p. 397-416.

30. Shen, Y. and K. Yoshikawa, *Recent progresses in catalytic tar elimination during biomass gasification or pyrolysis-A review.* Renewable and Sustainable Energy Reviews, 2013. **21**: p. 371-392.

Chapter 2 Literature review

2.1. Renewable Energy

The growing global population and rapid economic development contribute to an increase in energy demand. The global energy consumption continues to rapidly grow at a growth rate of 2.9% in 2018, which is the fastest growth since 2010 and almost double the average rate of 1.5% over the last ten years, leading to the fastest increase rate of 1.7% of energy-related CO_2 emissions for the past seven years [1]. Fossil fuels still accounted for 81.1% share of global primary energy consumption in 2017, including oil (31.9%), coal (27.1%), and natural gas (22.1%) (Fig. 2.1) [2]. Due to continuously increasing energy demand and overwhelmingly relying on fossil fuels, human beings are facing unprecedented risks, such as fossil fuel depletion and environmental pollution [3, 4]. Given that, much research emphasis has been put on the exploitation and utilisation of renewable energy that is of great importance to the sustainable development of global energy [5-7].

Renewable energy supply also continues to grow at an average annual rate of 2.0% since 1990, providing an estimated 13.7% of the global total primary energy consumption in 2017 [2]. Thereinto, bioenergy originated from biomass is the largest contributor to the global renewable energy supply, accounting for nearly 68% of the entire contribution of renewable energy, followed by hydro (18.5%), wind (5.1%), and geothermal (4.5%), etc. (Fig. 2.1). However, the traditional use of biomass to supply energy for residential cooking and heating is the main utilisation method of biomass nowadays, accounting for 83.4% of solid biomass consumption in 2017, mainly in developing countries, like Asia and Africa [2]. The traditional use of biomass for residential cooking and heating has been used for thousands of years, usually in simple and inefficient devices,

posing negative effects on air pollution and human health [8, 9]. Quaschning [10] reported that $1.55 \cdot 10^{11}$ tonnes of biomass are produced annually, while roughly 1% of that amount is used worldwide as a source of heat. There is still enormous potential for biomass to be exploited and utilised. Compared to other renewable energy sources, biomass has the advantages of abundant availability, low dependence on geographical and climatic conditions [11]. Besides, biomass can be converted into easily storable and transportable bioenergy, like syngas, liquid fuels via the modern biomass-to-energy technologies, i.e. pyrolysis and gasification, to compensate for the shortcomings of other renewable energy sources such as solar and wind, which greatly fluctuate in supply [10]. Therefore, biomass plays a crucial role in providing a reliable renewable energy supply.

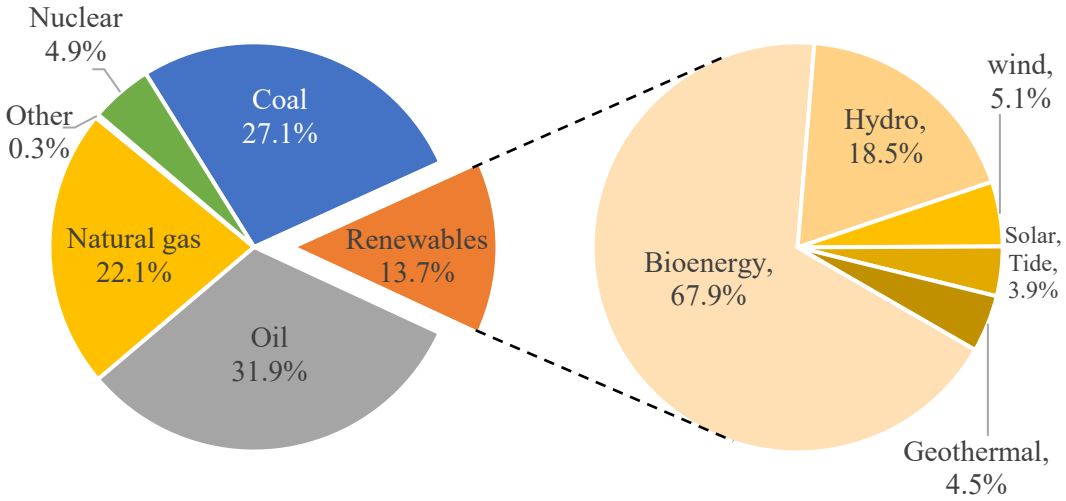

Figure 2.1. Fuel shares in world total primary energy supply (left) and world renewable energy supply (right) in 2017 [2].

2.2. Sewage sludge

Biomass is rich in organic material that comes from natural plants such as agricultural crops and residues, forestry crops and residues, algae, but also animal wastes including manure, municipal

solid waste, and sewage sludge (SS) [12, 13]. Dewatered SS contains sufficient embedded energy around 15-20 MJ/kg of dry SS corresponding to that of lignite and most of the biomass like sawdust, wood pellet, rice straw, etc., thereby being regarded as an attractive energy source [14, 15]. With the proposal and implementation of the concept 'zero waste' in several countries, e.g. China, India, New Zealand, etc, [16], waste-to-energy technologies that simultaneously achieve sustainable SS management and energy supply, attract intensive attention recently [17, 18].

2.2.1. Properties and production of sewage sludge

SS, a complex mixture of organic and inorganic compounds, is a kind of by-product from the wastewater treatment plant. The organic matters of SS vary widely from 22 to 82 wt% with an average of 48 wt% [15], while the lignocellulosic biomass has much higher contents of organic matters of above 75 wt% [19]. Due to a large amount of inorganic solid particles contained in the SS, the inorganic (ash) contents at an average of 44 wt% are much higher than that from the lignocellulosic biomass (around 4 wt%) [15]. And SS has substantially higher nutrients compared to the lignocellulosic biomass, such as nitrogen (7% N), phosphorus (2% P_2O_5), and potassium (0.5% K_2O) [20]. However, there are also significant numbers of microorganisms in the SS, including viral, bacterial, protozoan, fungal, and helminth pathogens [21]. Bibby and Peccia [22] reported that more than 27 kinds of viruses (Adenovirus, Coronavirus, HIV) existing in humans are found in SS. Besides, SS also contains various toxic heavy metals such as Zn, Ni, Cd, Cr, Cu, Pb, etc, [23] and persistent organic pollutants such as dioxins, pesticides, polycyclic aromatic hydrocarbons (PAHs), etc. [24]. Without appropriate disposal and treatment, SS would have a high possibility to pollute the soil, surface water, and groundwater, and pose significant risks of secondary pollution to the environment and human health.

With the growing population and deepening industrialization, a large amount of wastewater is produced. Correspondingly, with the implementation of the continuously strict water environment protection policy, an increasing number of wastewater treatment facilities being constructed result in a soar of SS production. Around 7.2 million dry tonnes of SS are generated in the U.S. annually [14, 25]. In Europe, SS production reached 10.9 and 9.3 million dry tonnes in 2005 and 2010, respectively [26, 27]. The total dry SS production in Australia in 2019 has increased to 0.37 million tonnes, compared to 0.33 million tonnes in 2017 and 0.3 million tonnes in 2010 [28]. From 2013 to 2018, there is a drastic increase in the dry SS production in China with an average annual growth of 12.3%, reaching 11.8 million tonnes in 2018 which is 1.8 times higher than that in 2013 (6.6 million tonnes) [29, 30]. However, the produced SS from the wastewater treatment plant contains around 80% moisture [31]. That means around 36, 47, 2, and 59 million tonnes of dewatered sewage sludge are annually produced and required appropriate treatment and disposal in the U.S., Europe, Australia, and China, respectively. Therefore, the growing and enormous production and complex composition of SS have made the appropriate treatment and disposal be one of the most challenging environmental problems.

2.2.2. Current treatment technologies of sewage sludge

Currently, land application, landfill, and incineration are the three main disposal technologies of SS [14, 26, 28, 32]. Due to the high content of organic matters and nutrients, beneficially use of SS as valuable fertilisers and soil ameliorates for land application has been the principal disposal technology, especially in developed countries. The proportion of SS to the land application is 67%, 41%, 55%, and 14% in Australia, Europe, and the U.S., and China, respectively (Fig. 2.2). To ensure the protection of human health and the environment from the pathogen and heavy metals in SS, several countries have issued their national regulation with the ceiling concentrations of

toxic heavy metals and pathogen reduction guidelines for SS or the soil amended with SS [33-35]. However, no agreement has been reached yet about the adverse effects caused by the land application of SS. Some studies show that none of the heavy metals in the soil amended with SS is over the ceiling concentrations set up by the regulation [36, 37], and the leached heavy metals pose no danger of soil, surface water and groundwater [38, 39]. On the contrary, Islam et al. reported that the accumulation and lability of Cr, Pb, Co, Zn, Cu, Ni, and As significantly increases in the field amended by SS over 25 years, posing a remarkable threat to the groundwater, surface water, and thereby human health [40]. In addition, the heavy metal accumulation in plants exhibits a significant positive correlation with the concentration of heavy metals in the soil amend by SS [41-43]. And the properties of soil, like pH and organic matter content, have negative and positive correlations with the heavy metals in the plant, respectively [40, 41]. Therefore, the persistence, accumulation, and lability of metals in the soils and plants over time and with the change of the soil properties, lead to a rise of the public concern from the land application of SS [36].

A number of problems associated with SS landfill, such as lack of space, offensive odours, flies, and the risks of the surrounding water, soil, and air, resulted in the landfilling of SS being progressively decommissioned [44-46]. In the developed countries, the proportion of SS for landfill gradually decreases, accounting for 4%, 17%, and 30% in Australia, Europe, and the U.S., respectively (Fig. 2.2). Several European countries have banned the landfill of SS [47]. Nevertheless, the landfill is still the most widely used disposal method of SS in China, and up to 63% of SS is disposed of to landfill due to the economical advantages compared to land application and incineration. This trend is also observed in the different members of Europe. For example, 28% of SS is disposed of to landfill in EU-12 (new member states including Poland, Hungary,

Romania, etc.), which is about twofold of that in EU-15 (old member states with better economics including Germany, France, United Kingdom, etc.) [26].

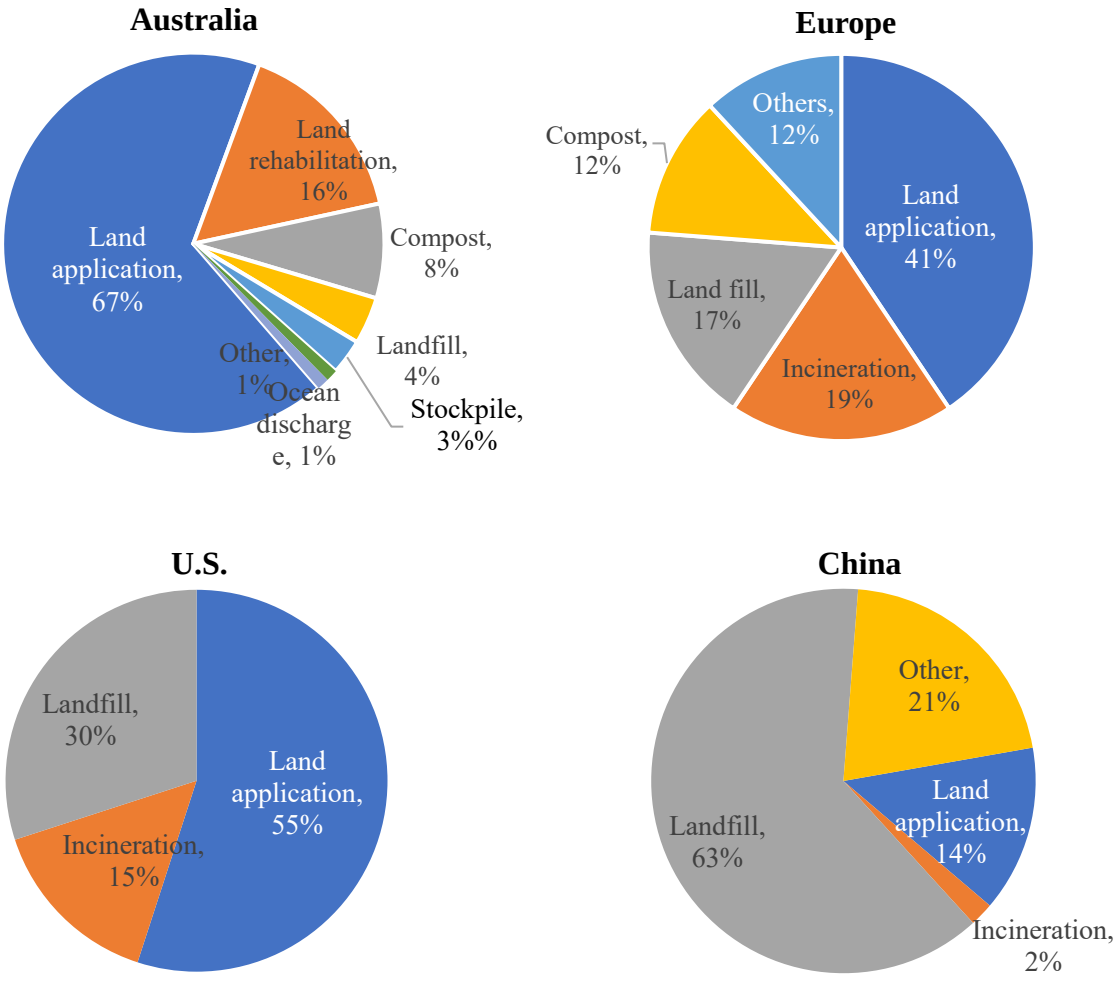

Fig. 2.2. SS disposal methods in Australia [28], Europe [26], U.S. [14], and China [32].

In conclusion, the landfill and land application of SS are becoming less viable and gradually constrained with increasing environmental security and human health concern and regulatory pressure. Therefore, it is urgent to exploit a more environmentally and economically sustainable, effective resource recovery approach for SS treatment [48, 49]. One approach capable of achieving those goals would be thermochemical conversion, e.g. incineration, pyrolysis, gasification, which

is considered as waste-to-energy technologies [50]. Incineration has been widely implemented nowadays, which can not only recover the embedded energy of SS [14], but also minimize the environmental risks of SS, including thermal destruction of toxic organic pathogens and a large reduction of SS volume (around 50-80% of SS). Besides, the generated stabilized ash can be reused to produce ceramic and building materials. The outstanding performance of incineration in the disposal of SS leads to a gradual increase in the percentage of incineration of SS [51], accounting for 19%, 15%, and 2% in Europe, the U.S., and China, respectively (Fig. 2.2). Another emerging thermochemical conversion processes, like pyrolysis and gasification, have not been widely implemented in practice. They still have some key barriers and challenges needed to be addressed prior to their widely practical application.

2.3. Thermochemical conversion process for syngas production

Incineration of SS can generate electricity and heat, while by the means of other emerging thermochemical conversion processes, like pyrolysis and gasification, SS can be converted into value-added chemicals or fuels, such as biochar, bio-oil (tar), and gaseous products [52]. Biochar mostly consists of solid carbon and ash [53], while bio-oil mainly consists of alkanes, alkenes, aromatic compounds, carboxylic acids, fatty acids, aldehydes, ketones, steroids, fatty nitriles and amides, etc [54]. As for the gaseous products, it mainly contains hydrogen (H_2), carbon monoxide (CO), carbon dioxide (CO_2), methane (CH_4) and low molecular weight hydrocarbons. Among all the products, increasing attentions are paid to the production of syngas, a mixture of H_2 and CO, since it has high calorific value and wide application as a platform feedstock for a range of liquid biofuels and value-added chemicals via the Fischer-Tropsch synthesis (FTS) process [55].

2.3.1. Pyrolysis for syngas production

Pyrolysis is the thermal conversion of organic matters in an inert atmosphere, which can be categorized as slow pyrolysis and fast pyrolysis based on operational temperature, heating rate, temperature, and residence time [54]. Slow pyrolysis is characterized by low operating temperature (300-400 °C), slow heating rate, and long residence time (up to several hours), while fast pyrolysis is operated under a higher temperature (450-600 °C), high heating rate (10-200 °C/min), and short residence time (several seconds) [32, 54].

Table 2.1. Thermal behaviour of the pyrolysis of biomass.

Biomass	**Main components and their decomposition temperature range**	**Ref.**
Lignocellulosic biomass	Cellulose: 290-390 °C Hemicellulose: 200-400 °C Lignin: 200-700 °C	[56]
Municipal solid waste	Food residue: 200-600 °C Paper: 200-400 °C Wood and leaf residue: 280-700 °C Plastics: 200-600 °C Textile: 250-400 °C Rubber: 200-500 °C	[57]
Animal waste	Chicken litter: 270-550 °C Cattle litter: 200-600 °C Swine solids: 200-500 °C	[58-60]
Microalgae	Protein: 210-310 °C Lipid: 150-515 °C Carbohydrate: 110-420 °C	[61]
SS	Lipid: 150-290 °C Carbohydrate: 290-410 °C Protein: 360-525 °C	[62]

Generally, most of the lignocellulosic biomass consists of cellulose (30-50%), hemicellulose (20-35%), and lignin (10-27%) [63]. Algae and SS are mainly composed of protein (contents exceed 60%), lipid, and carbohydrates [64]. And animal waste is a complex mixture of the above components. [65, 66]. The pyrolytic thermal behaviour of the different types of biomass is summarised in Table 2.1. The results show that the main pyrolytic process of different types of

biomass occurred at the same temperature range of 200-500 °C, which is fully overlapped with the slow and fast pyrolysis reaction temperature (300-600 °C).

Table 2.2 describes the product distributions of the pyrolysis of different types of biomass. The low operating temperature and inert atmosphere of the pyrolysis result in bio-oil and biochar as the main products with a low gas yield. The yield of bio-oil and biochar obtained from the pyrolysis of biomass are up to 74 wt% and 54 wt%, and gas yields from the pyrolysis of lignocellulosic biomass, municipal solid waste, algae, and SS are in the range of approximately 5-36 wt%, 4-54 wt%, 12-21 wt%, and 3-22 wt%, respectively. Additionally, as the pyrolysis temperature increases, the char yield decreases while the bio-oil and gas yields increase. A short residence time of the fast pyrolysis limits the secondary cracking reaction of bio-oil, thereby leading to a higher bio-oil yield compared to the slow pyrolysis [67-69].

Regarding the gaseous production, the evolution of main gaseous products during the pyrolysis of lignocellulosic biomass, algae, and SS shows a similar trend, which has two distinct stages. Most of the gaseous products, mainly consisting of CO_2, CO, CH_4 and light hydrocarbons (C_2H_4 and C_2H_6), released at a low temperature between 200-500 °C, while H_2 production was mainly observed at high temperatures (>500 °C) [56, 70, 71]. The H_2 production observed at high temperatures (>500 °C), mainly attributes to secondary reactions as CH_4 steam reforming or tar cracking/reforming [56, 68, 72]. It was reported that the formation of CO is mainly attributed to the cracking of carbonyl group rupture of oxygen heterocycles, and dehydrogenation of hydroxyl group [73, 74]. Besides, Maliutina et al. [68] reported that the CO_2 gasification of biochar at a higher temperature than 800 °C also contributes to the CO production. Therefore, the production of H_2 and CO shows an increasing trend with the increasing temperature [68]. As shown in Table 2.3, the purity of H_2 is only 9-18 vol% when the temperature is below 500 °C, while it reaches up

Table 2.2. Product distributions of the pyrolysis of biomass.

Pyrolysis types	Biomass	T (°C)	Products yield (wt%)			Ref.
			Gas	Bio-oil	Biochar	
Lignocellulosic biomass						
SP[a]	Pine wood	300	14	32	54	[75]
		600	26	49	25	
	Bagasse	480	25	26	37	[76]
		680	36	22	28	
FP[b]	Palm kernel shell	600	5	74	21	[68]
		800	17	66	17	
	Wood feed	400	10	66	24	[77]
		550	16	67	17	
	Bagasse	480	14	51	25	
		680	18	40	30	[76]
		680	36	22	28	
Municipal solid waste						
SP	Carpet, paper, plastic etc.	550	34	38	18	[78]
FP	Carpet, paper, plastic etc.	550	54	39	7	[78]
	Tyre	425	4	58	38	
		475	8	57	35	[67]
		575	10	55	35	
Algae						
SP	*Scenedesmus*		12	58	30	
	Defatted Scene.	450	21	45	33	[79]
	Spirulina		15	39	30	
FP	*Chlorella vulgaris*	600	12	46	42	[68]
		800	18	60	22	
SS						
SP	SS	400	12	50	38	[80]
		600	18	52	30	
	SS	475	14	25	55	[81]
		625	19	45	20	
	SS	450	10	37	53	[82]
		850	15	43	42	
FP	SS	400	20	49	31	[82]
		600	22	53	25	
	SS	450	3	45	52	[83]
		600	11	46	43	
	SS	450	10	37	53	[82]
		850	15	43	42	

[a] SP stands for slow pyrolysis.
[b] FP stands for fast pyrolysis.

to 45 vol% at the temperature over 500 °C. Similarly, the purity of CO ranges of 2-14 vol% and 22-55 vol% at the temperature below and above 500 °C, respectively. However, the common

operating temperature of pyrolysis is 300-600 °C, leading to the syngas production from pyrolysis may seem to be much inferior.

Table 2.3. Syngas purity generated from the pyrolysis of biomass.

Pyrolysis types	T (°C)	Syngas purity (vol%)		Ref.
		H_2	CO	
Sugarcane Bagasse				
SP[a]	680	29	38	
FP[b]	480	9	14	[76]
	680	45	21	
Palm kernel shell				
FP	600	20	48	[68]
	800	22	55	
Tyre				
FP	425	18	2	[67]
	475	15	2	
	575	18	2	
Algae (*Chlorella vulgaris*)				
FP	600	9	22	[68]
	800	45	30	
SS				
SP	600	15	25	[84]
	800	23	35	
	1000	30	33	
SP	400	10	9	[85]
	500	25	10	

[a] SP stands for slow pyrolysis.
[b] FP stands for fast pyrolysis.

2.3.2. Gasification for syngas production

Gasification is thermal destruction of organic matters at high temperature (700-1000 °C) under a partial oxygen atmosphere, which favours the generation of gaseous products. The partial oxidant agents can be air, steam, CO_2, or their mixture, the amount of which is lower than that required for the stoichiometric combustion to occur. Gasification can be divided into three main steps, including (1) devolatilisation occurring at a relatively low temperature (300-500 °C); (2) tar cracking and reforming mainly occurring at the temperature over 600 °C; (3) char gasification

mainly occurring at a high temperature (> 700 °C) [86]. Different gasifier agents mainly influence the reactions occurring in the last two steps, thereby yielding different gas compositions during biomass gasification. The important chemical reactions involved in the gasification of biomass are shown in Table 2.4.

Table 2.4. Important chemical reactions involved in the gasification of biomass.

Reaction name	Equation	Equation number
Pyrolysis		
Devolatilisation	$C_xH_yO_z \rightarrow H_2+CO+CO_2+C_mH_n+H_2O+Tar+Char$, $\Delta H_{298K}>0$	Eq.1
Tar cracking/reforming		
Tar reforming	$Tar+H_2O \rightarrow H_2+CO+CO_2+C_mH_n+H_2O$, $\Delta H_{298K}>0$	Eq.2
Tar cracking	$Tar \rightarrow H_2+CO+CO_2+C_mH_n$, $\Delta H_{298K}>0$	Eq.3
Gasification		
Water-gas shift	$CO+H_2O \leftrightharpoons CO_2+H_2$, ΔH_{298K}= -41.2 KJ/mol	Eq.4
Reverse Boudouard	$C+CO_2 \leftrightharpoons 2CO$, ΔH_{298K}= +172.4 KJ/mol	Eq.5
Char reforming-I	$C+H_2O \leftrightharpoons CO+H_2$, ΔH_{298K}= +131 KJ/mol	Eq.6
Char reforming-II	$C+2H_2O \leftrightharpoons CO_2+2H_2$, ΔH_{298K}= +89.8 KJ/mol	Eq.7
Methane reforming	$CH_4+2H_2O \leftrightharpoons CO_2+4H_2$, ΔH_{298K}= +206 KJ/mol	Eq.8
Methanation-I	$2CO+2H_2 \leftrightharpoons CH_4+CO_2$, ΔH_{298K}= -247 KJ/mol	Eq.9
Methanation-II	$C+2H_2 \leftrightharpoons CH_4$, ΔH_{298K}= -72.8 KJ/mol	Eq.10
Combustion		
Char combustion-I	$C+1/2O_2 \leftrightharpoons 2CO$, ΔH_{298K}= -111 KJ/mol	Eq.11
Char combustion-I	$C+O_2 \leftrightharpoons CO_2$, ΔH_{298K}= -394 KJ/mol	Eq.12
CO combustion	$CO+1/2O_2 \leftrightharpoons CO_2$, ΔH_{298K}= -283 KJ/mol	Eq.13
H_2 combustion	$H_2+1/2O_2 \leftrightharpoons H_2O$, ΔH_{298K}= -285.8 KJ/mol	Eq.14
Ca-based reactions		
CaO carbonation	$CaO+CO_2 \leftrightharpoons CaCO_3$, ΔH_{298K}= -178.2 KJ/mol	Eq.15
CaO calcination	$CaCO_3 \leftrightharpoons CaO+CO_2$, ΔH_{298K}= +178.2 KJ/mol	Eq.16

2.3.2.1. Air gasification

Air gasification is the most widely studied and applied since the air is simple and easy to obtain without any extra or complicated process. As shown in Fig. 2.3, the gas evolution from the air and air-steam gasification of biomass reported by Chang et al. [87] could clearly exhibit the performance and character of this process on syngas production. Since the agent air inherently has a high proportion of N_2 (around 78%), the gaseous products from the air and air-steam gasification are typically dominated by N_2 with a low purity of H_2 and CO. Besides, the syngas production is promoted at high temperature, especially above 800 °C. Moreover, the equivalent ratio (ER) is a crucial factor affecting the syngas production. A higher value of ER could promote the oxidization reactions of H_2, CO and char to produce more CO_2 and steam (Eq. 11-14), resulting in a decrease in H_2 and CO production. The air-steam gasification of biomass shows an increase in H_2 and CO_2, while CO and CH_4 slightly decreased, suggesting the occurrence of steam gasification reaction, like water-gas shift reaction (Eq. 4) and methane reforming reaction (Eq. 8) to promote the H_2 and CO_2 production [88].

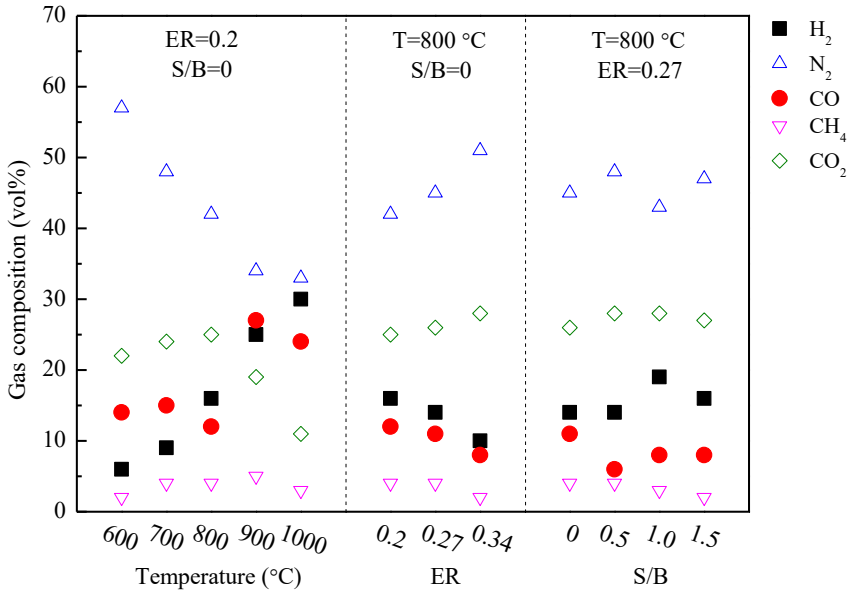

Fig. 2.3. Effluent gas composition from the air and air-steam gasification of biomass as a function of temperatures, ER, and steam to biomass ratios (S/B) [87].

As shown in Table 2.5, the gas products obtained from air gasification of biomass mainly consist of a low yield and purity of H_2 (22-101 mL/$g_{dry\ biomass}$, 2-10 vol%) and CO (55-161 mL/$g_{dry\ biomass}$, 4-18 vol%), while rich in 44-70 vol% N_2. Upon on the air-steam gasification of biomass, higher yield and purity of H_2 (57-127 mL/$g_{dry\ biomass}$, 10-20 vol% H_2) are obtained compared to air gasification, meanwhile with lower yield and purity of CO (29-98 mL/$g_{dry\ biomass}$, 6-8 vol% CO).

Table 2.5. Gas production generated from the air and air-steam gasification of biomass.

Temperature (°C)	ER	S/B	Gas yield (mL/$g_{dry\ biomass}$)				Gas purity (vol%)					Ref.
			H_2	CO	CO_2	CH_4	H_2	CO	CO_2	CH_4	N_2	
Air gasification												
Rice straw												
	0.1		34	151	218	67	4	18	26	8	44	
700	0.2	/	29	143	266	67	3	15	28	7	47	[89]
	0.2		23	161	380	69	2	14	33	6	45	
SS												
	0.2		99	73	144	37	10	7	14	4	61	
750	0.3	/	101	92	188	36	8	7	14	3	65	[90]
	0.4		49	66	218	15	3	4	14	1	75	
SS												
	0.2		22	55	62	5	4	11	13	1	66	
1100	0.2	/	25	63	75	6	4	10	12	1	70	[91]
	0.3		32	80	112	7	4	10	13	1	68	
Air-steam gasification												
SS												
	0.2	0.7	94	29	95	18	18	6	19	4	51	
770	0.1	0.5	108	39	82	22	20	7	16	4	50	
	0.3	0.4	57	36	124	15	11	7	24	3	53	[92]
	0.2	0.3	67	38	97	17	14	8	20	3	53	
SS												
750	0.3	0.5	127	98	189	36	10	8	15	3	61	[90]

2.3.2.2. CO_2 gasification

Under the drive of the beneficial use of CO_2 to produce value-added chemicals and energy, the CO_2 gasification of biomass has been also widely investigated. Taking the CO_2 gasification of lignocellulosic biomass [93] as a sample as shown in Fig. 2.4, the purity of H_2 decreases from 18

to 2 vol% as the percentage of CO_2 introduced into the reactor is increased from 0 to 40% at 900 °C, while the purity of CO increases from 2 to 70 vol%. The presence of CO_2 would promote the reverse Boudouard reaction (Eq. 5) and reverse water-gas shift reaction (Eq. 4) at a high temperature to consume H_2 and produce CO. Thus, a definite H_2 depression and CO enhancement are observed from the CO_2 gasification of biomass with the increasing amount of CO_2 introduced. Also, CO_2 is found to significantly increase the conversion of char residue to volatiles at high gasification temperatures and less than 1% ash remains using CO_2. Similar trends above were observed with municipal solid waste [94] and SS [95] as the feedstock.

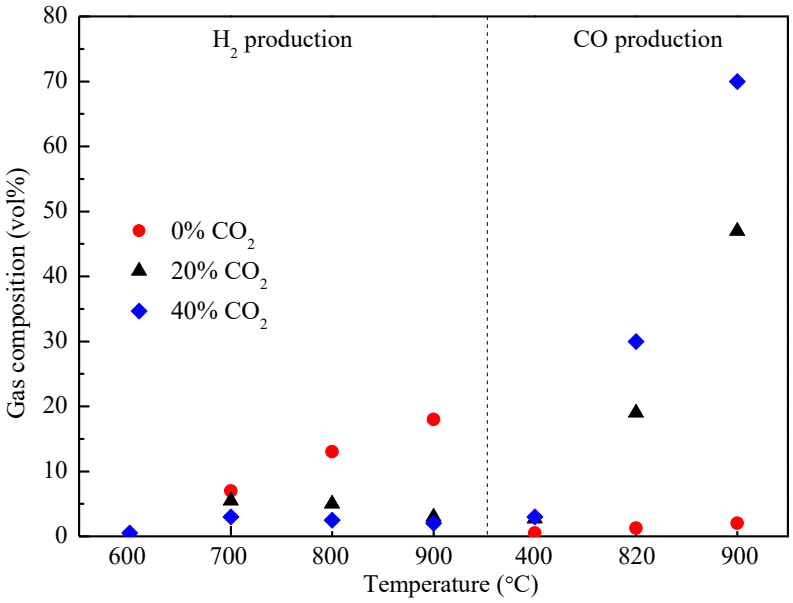

Fig. 2.4. H_2 and CO production of CO_2 gasification of lignocellulosic biomass as a function of the percentage of CO_2 [93].

2.3.2.3. Steam gasification

Steam gasification is considered as one of the most effective techniques for generating H_2 from biomass. Franco et al. [96] reported that the yield of H_2 from steam gasification of Holm-oak significantly increases by 5.6 times compared to the pyrolysis, meanwhile CO_2 yield also increases

by 2.6 times. Zhang et al. [97] also found out that H_2 and CO_2 yield from the steam gasification is higher than those from pyrolysis and oxygen gasification, while the CO and CH_4 yields are lower than those from pyrolysis and oxygen gasification. Besides, a decrease in char and tar yields was observed from the steam gasification of biomass [98]. In the presence of steam, the production of H_2 can be enhanced through steam gasification of tar (Eq. 2), char (Eq. 6, 7), methane (Eq. 8) and water-gas shift reaction (Eq. 4). Nilsson et al. [99] revealed that the reactivity of char with steam (Eq. 6, 7) is roughly three times faster than with CO_2 (Eq. 5) at all temperatures. The steam reforming of char takes preference over reverse Boudouard reaction. Thus, the water-gas shift reaction that consumes CO to produce CO_2 is dominant, leading to a reduction of CO and remarkable enhancement in CO_2 production from steam gasification compared to pyrolysis and air gasification.

The gas production from the steam gasification of sugarcane bagasse reported by Loha et al. [100] is shown in Fig. 2.5 to clarify the performance and characterise of steam gasification on syngas production. It can be seen that the H_2 and CO purity increases with the increasing gasification temperature, since higher temperature favors the endothermic steam gasification and cracking of tar (Eq. 2, 3), char (Eq. 6, 7), methane (Eq. 8) reactions for H_2 and CO production, meanwhile suppress the exothermic water-gas shift reaction that consumes CO and produces CO_2. Regarding the influence of S/B, H_2 and CO_2 purity in the gas increase with higher S/B, while CO and CH_4 decrease. The presence of steam would facilitate the steam reforming reactions, especially methane reforming (Eq. 8) and water-gas shift reactions (Eq. 4) that consume CO and CH_4 to produce H_2 and CO_2. However, several studies have reported that there is a threshold limit of S/B beyond which any increase in S/B would suppress H_2 production [101]. Hu et al. [102] pointed out that

excess steam consumes more energy and thereby results in a decrease in the temperature of the reactor to lower the H_2 production.

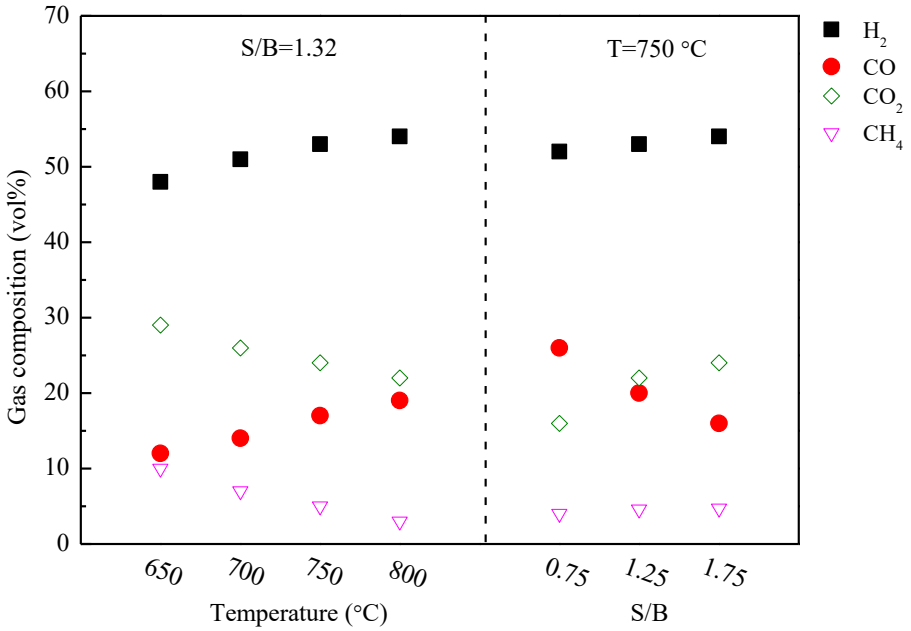

Fig. 2.5. Effluent gas composition from steam gasification of sugarcane bagasse as a function of temperatures and S/B [100].

As shown in Table 2.6, H_2 becomes the most abundant products in the presence of steam, reaching 401-1088 mL/$g_{dry\ biomass}$ of yield and 50-60 vol% of purity, which are significantly higher than those from the air, air-steam and CO_2 gasification of biomass (Table 2.5 and Fig. 2.4). Thus, steam gasification has been perceived as the most attractive pathway for sustainable H_2 production, while the purity of H_2 is still insufficient for directly commercial application. Additionally, CO_2 production is a second only to H_2 with 65-377 mL/ $g_{dry\ biomass}$ of yield and 16-34 vol% of purity. Hence, the process is inevitably problem with undesirable CO_2 generation along with H_2, incurring additional costs and process for gas purity. Moreover, another component of syngas, the yield and purity of CO production from steam gasification are inferior with 73-254 mL/$g_{biomass}$ of yield and 6-26 vol% of purity.

Table 2.6. Gas production generated from the steam gasification of biomass.

Temperature (°C)	S/B	Gas yield (mL/$g_{dry\ biomass}$)				Gas purity (vol%)				Ref.
		H_2	CO	CO_2	CH_4	H_2	CO	CO_2	CH_4	
Oil palm tree										
600		992	106	65	2	56	6	34	2	
700	3.1 [a]	1088	172	93	5	57	9	31	3	[99]
800		960	301	154	12	51	16	26	4	
Sawdust										
	1.1	401	174	209	70	46	20	24	8	
800	1.8	507	159	249	60	51	16	25	6	[100]
	4.7	716	88	377	50	57	7	30	4	
Straw										
	0.5	661	148	273	46	58	13	24	4	
800	0.7	694	108	282	22	61	10	26	2	[101]
	0.9	683	73	315	10	63	7	30	1	
Sugarcane Bagasse										
	0.75					52	26	16	4	
750	1.25			/		53	20	22	4.6	[96]
	1.75					54	16	24	4.7	
SS										
900	14 [b]	494	254	177	62	49	25	18	6	[102]
	3.05	672	247	111	14	49	18	22	6	
900	5.62	728	220	83	8	53	16	20	5	[103]
	7.38	694	227	83	8	52	17	19	5	

[a]. The steam flow rate was set as 3.1 g/min.
[b]. The steam flow rate was set as 14 mL/g/min.

2.3.3. Sorption-enhanced thermochemical conversion process

The sorption-enhanced gasification process was firstly proposed by Gurran et al. [103] in 1967, which was applied for hydrogen-rich gas production from coal. The application of this technology in biomass has gained a lot of attention in recent years. Among the sorption-enhanced steam gasification of biomass, the steam reforming reactions are integrated with a CO_2 sorption reaction in a single step. More specifically, a CO_2 sorbent is used to *in situ* capture of CO_2 as soon as it produced, which can shift the steam reforming reactions, like water-gas shift reactions beyond thermodynamic equilibrium limitations, resulting in enhanced H_2 yield and purity.

2.3.3.1. CO_2 sorbents

A highly efficient CO_2 sorbent, which should possess the properties of thermal stability, high CO_2 sorption capacity, easy regeneration and cost-effectiveness, is one of the key factors for the H_2 rich production from the sorption-enhanced steam gasification process [104]. The natural incurring Ca-based CO_2 sorbent, like, limestone and dolomite, have been demonstrated to have a significant enhancement in H_2 production from sorption-enhanced steam gasification of biomass. It was reported that the H_2 purity increases from 47.6 to 68.2 mol% at 800 °C after the addition of calcined limestone [105]. A similar increase in H_2 purity from 43.6 to 55.5 vol% was obtained from the steam gasification of biomass after the addition of calcined dolomite [106]. Additionally, it was also reported that the Ca-based CO_2 sorbents have a catalytic effect on tar cracking for H_2 production (Eq. 3). Wei et al. [107] presented the influence of sand and dolomite on product yields and gas compositions. The dolomite exhibits a catalytic activity on tar cracking with an obvious increase in gas yield and decreases the tar yield compared to sand, meanwhile, the H_2 purity increases notably in the presence of dolomite. Except for the natural sorbents, the application of some wastes which are rich in CaO for H_2 production from biomass also attracts much more attention. Salaudeen et al. [108] investigated the steam gasification of sawdust with calcined eggshell as a CO_2 sorbent. Increasing calcined eggshell to biomass ratio (CEBR) provides more CaO to capture CO_2 and thereby enhance H_2 production. With the increase of CEBR from 0.5 to 1.0, the H_2 purity increases from 56 to 78 vol%. Weerachanchai et al. [109] compared the gas compositions from the sorption-enhanced steam gasification of larch wood using calcined waste concrete, calcined limestone and silica sand. The calcined waste concrete with 14.8 wt% of CaO gives intermediate amount of H_2 (15.6 mmol/g and 46.9 vol%), compared to calcined limestone (30.2 mmol/g and 63.6 vol%) and silica sand (4.0 mmol/g and 21.8 vol%).

In addition to CaO-based sorbents, other emerging CO_2 sorbents, alkaline ceramic materials and hydrotalcite sorbents have also been proposed as potential candidates for CO_2 adsorption in the sorption-enhanced steam gasification process. Peltzer et al. [110] summarised that alkaline ceramic materials, like Li_2ZrO_3, have superior performance on stable adsorption level over repeated cycles, and easily regenerated even at high CO_2 concentration compared to CaO. Wang et al. [111] investigated the H_2 production from sorption-enhanced steam reforming of glycerol over a $NiO/NiAl_2O_4$ catalyst and K-Li_2ZrO_3 CO_2 sorbent. With the addition of K-Li_2ZrO_3 CO_2 sorbent, the H_2 purity increases from 65% over $NiO/NiAl_2O_4$ to 99.6% over $NiO/NiAl_2O_4$ and K-Li_2ZrO_3. Aceves Olivas et al. [112] reported a 92.2% of H_2 purity from steam gasification of ethanol with Na_2ZrO_3 as a CO_2 sorbent, compared to only 69.6% without the Na_2ZrO_3 sorbent. Hydrotalcite sorbent has the advantages of lower energy consumption of regeneration, thermal stability [113], and is limited its industrial application due to the poor CO_2 sorption capacity and slow reaction kinetics [114]. Wang et al. [115] showed that the H_2 purity enhances from 19 to 33 mol% after the addition of hydrotalcite-based sorbent via sorption-enhanced steam gasification of ethanol. Dewoolkar and Vaidya [116] reported that the H_2 yield increases from 40 to 78% with the increasing Ni-Ca hydrotalcite sorbent mass fraction from 0.1 to 0.25.

2.3.3.2. Performance of Ca-based sorbent on syngas production

Ca-based sorbent (CaO as the main active material) with the advantages of high CO_2 sorption capacity at low CO_2 partial pressure and moderate temperature, low cost and abundance, has been the most widely used CO_2 sorbent in the sorption-enhanced steam gasification of biomass [117]. Regarding the Ca-based sorbent, temperature poses a vital influence on not only the steam reforming reactions, but also the thermodynamic equilibrium between CaO carbonation/calcination reactions (Eq. 15, 16). Kierzkowska et al. [118] plotted the equilibrium

partial pressure of CO_2 ($P_{CO_2}^{eq}$) over CaO using the correlation of Baker [119] as shown in Fig. 2.6. For any given $P_{CO_2}^{eq}$, CaO carbonation takes place when the temperature is lower than the corresponding equilibrium value, while the CaO carbonation is inhibited and $CaCO_3$ calcination occurs with a higher equilibrium value. Han et al. [120] studied the characteristics of CaO carbonation with the increasing temperature at a CO_2 partial pressure of 0.1 atm as shown in Fig. 2.7. It was observed that there are three distinct stages, namely slow carbonation stage (< 480 °C), fast carbonation stage (480-770 °C) and calcination stage (> 770 °C). The temperature is located in the fast carbonation stage could ensure a fast and sufficient CO_2 sorption kinetic and significantly benefit for the H_2 production by moving the water-gas shift reaction (Eq. 4) in the forward direction. When the temperature is located in the calcination stage, the sorption-enhanced effect of CaO becomes negligible, posing less effect on the gas composition.

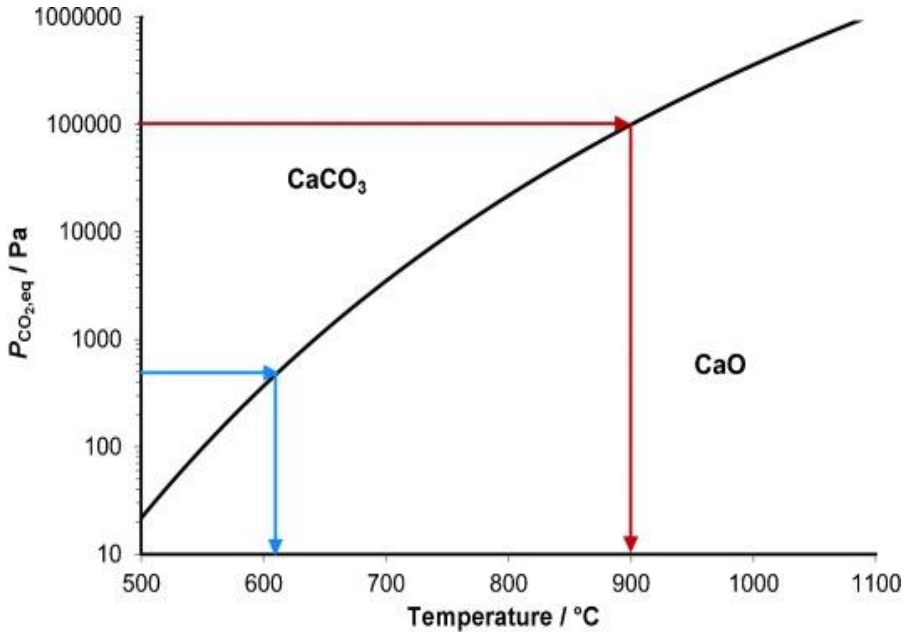

Fig.2.6. Equilibrium partial pressure of CO_2 over CaO [118].

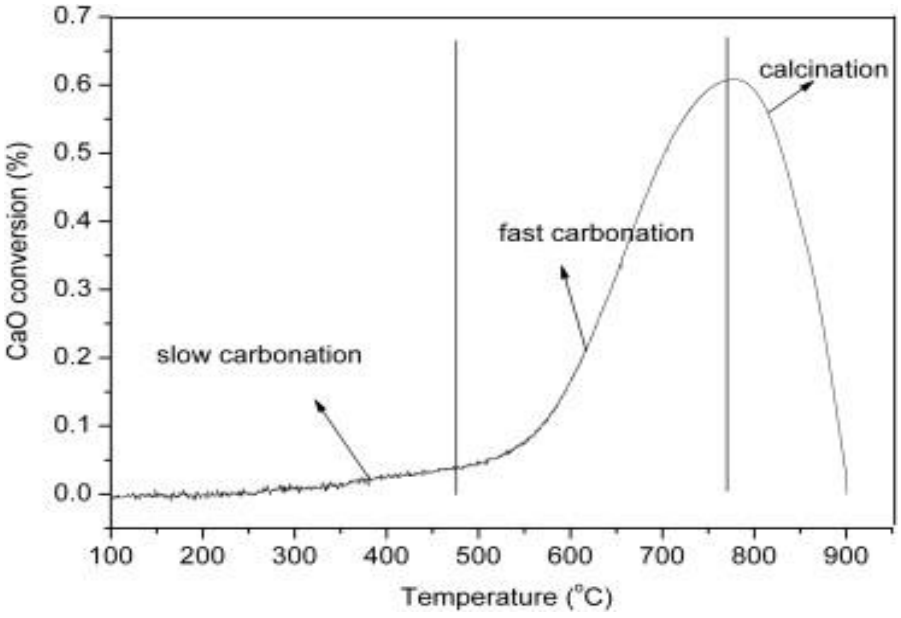

Fig. 2.7. Characteristics of CaO carbonation with the increasing temperature at a CO_2 partial pressure of 0.1 atm [120].

Given this, the influence of temperature on the syngas production from the sorption-enhanced steam gasification of biomass can be clearly illustrated by Fig. 2.8 reported by Zhang et al. [121]. With the increase of temperature, the H_2 yield remarkably enhances from 40 mL/$g_{biomass}$ at 450 °C to 206 mL/$g_{biomass}$ at 850 °C. Nevertheless, the H_2 purity exhibits a trend of initial increase with the temperature, peaking at 550 °C (65 vol%), and then decrease with the temperature. However, the CO and CO_2 purity show an opposite trend, and CH_4 purity mainly decreases with the increasing temperature. At a lower temperature, the CaO carbonation occurs, the H_2 purity increases whereas CO_2 and CO purity diminishes. However, at a higher temperature, the CaO carbonation is inhibited, and thereby the sorption-enhanced effect of CaO is weakened and even disappeared. Meanwhile, the increasing temperature favours the endothermic tar cracking/reforming, reverse Boudouard, char reforming and methane reforming reactions (Eq. 2, 3, 5-8) to facilitate H_2, CO and CO_2 production and consume CH_4, leading to an enhancement in

H_2, CO, CO_2 production and reduction in CH_4. Therefore, at a higher temperature, the H_2 purity diminishes, while CO and CO_2 purity increase. Chen et al. [122] reported a similar trend with the maximum H_2 purity (72.8 vol%) at 700 °C. Hence, there is a compromise between the purity and yield of H_2 when choosing the optimal temperature.

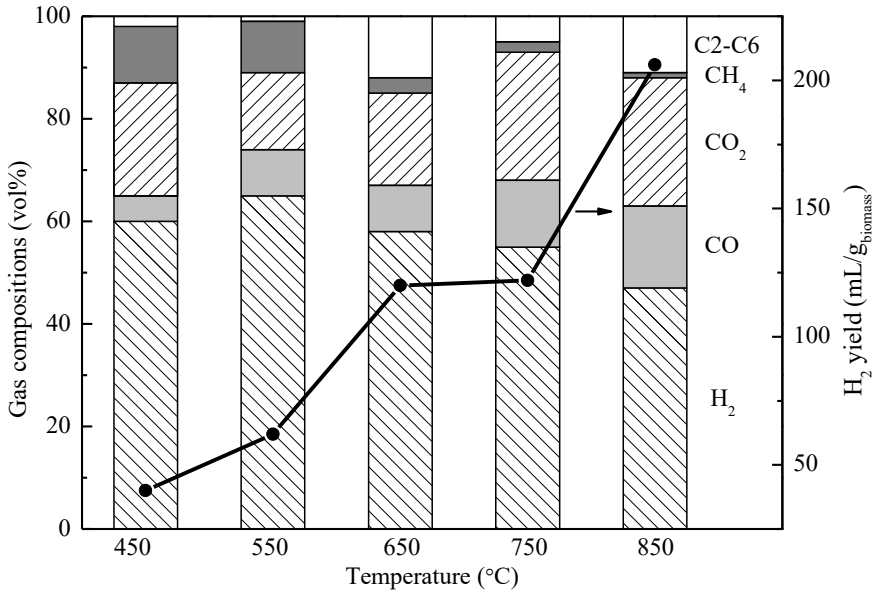

Fig. 2.8. Effluent gas composition and H_2 yield from sorption-enhanced steam gasification of biomass as a function of temperature [121].

The molar ratio of CaO to the carbon in biomass (CaO/C) is another key factor to influence the syngas production. Due to the promoting water-gas shift reaction (Eq. 4) in the presence of CaO, the H_2 production increases with the CaO/C, while the CO production decreases with the CaO/C. Wei et al. [123] reported that the H_2 yield and purity is enhanced from 64.3 mL/$g_{biomass}$ and 28.7 vol% in the absence of CaO to 211.0 mL/$g_{biomass}$ and 61.8 vol% at a CaO/C molar ratio of 2, meanwhile the CO purity declines from 32.0 to 12.1 vol%. However, some studies reported that there exists an optimal value of CaO/C for the highest H_2 production. Hu et al. [102] revealed that the H_2 yield and purity start to decrease when CaO/C is higher than 0.7. The CaO addition has a

significant effect on the heat transfer properties inside the reactor. Zhou et al. [124] reported that CaO addition would slow down the increasing rate of the temperature of the mixture of CaO and biomass compared to that of biomass without CaO. Therefore, there probably exists an optimal CaO/C ratio for H_2 production, since an excess of CaO in the reactor will absorb heat and hinder heat transfer between reactants which leads to the decrease of H_2 production.

2.3.4. Current status and challenges of syngas production from sewage sludge

The syngas production from the air, air-steam, steam, and sorption-enhanced steam gasification of SS is shown in Fig. 2.9. Similar to other types of biomass, it can be seen from Fig. 2.9a that the purity of H_2 is in the range of 6.0-16.4 vol% and 8.2-24.2 vol% from the air and air-steam gasification of SS, respectively. With the addition of steam, the purity of H_2 is increased to 28-53 vol% due to the promoting of steam reforming reactions (Eq. 2, 4, 6-8). In the presence of CO_2 sorbent, the H_2 purity is further enhanced to 59-72 vol% from the sorption-enhanced steam gasification of SS. Despite the enhanced H_2 production, the addition of CaO would produce H_2-rich gas stream at even lower temperature compared to steam and air gasification process. Therefore, SS has the potential to produce high purity clean energy (H_2) using the sorption-enhanced steam gasification process. Besides, there is a significant weight loss after the gasification process, and it was reported that most of the heavy metals are retained in the char [125], which make it easier no matter to recovery the heavy metals or disposal of them. Thereby, the sorption-enhanced steam gasification of SS makes it possible to achieve waste-to-energy and satisfy the environmental criteria of sustainable development and economic and social concerns.

Another important component of the syngas, the CO purity is low, ranging from 5 to 25 vol% (Fig. 2.9b). And no obvious change is observed for the CO purity from air, air-steam, steam and sorption-enhanced steam gasification of SS. Most researches to date focused on H_2 production

from SS, however, effective utilization of carbon in the SS for CO is ignored, and effective approach for the enhanced CO production from SS is still lacking.

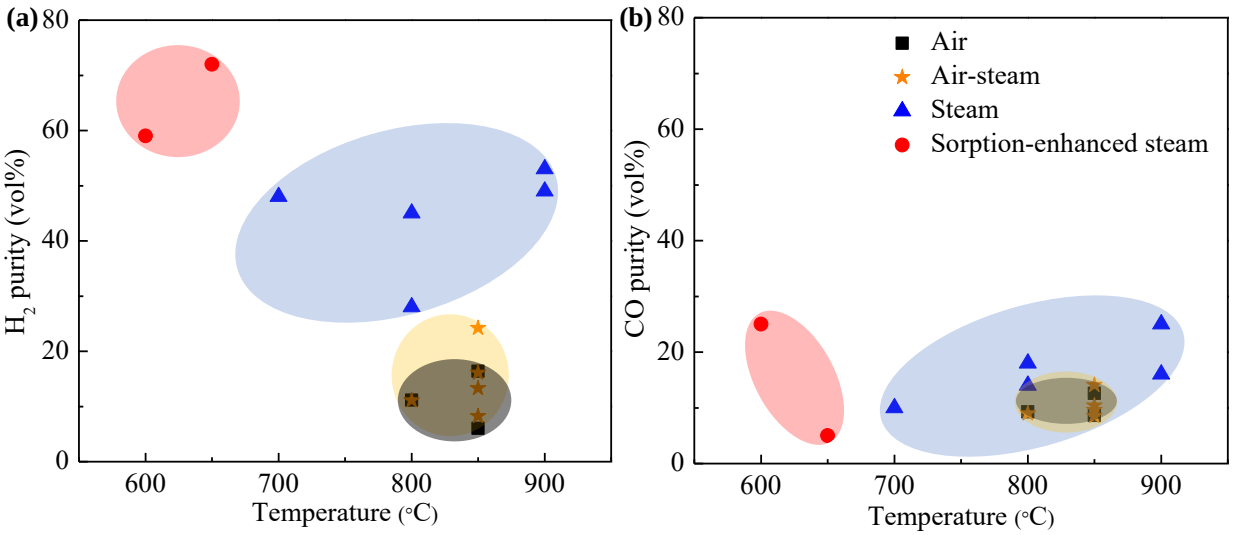

Fig. 2.9. Syngas production from air [90, 91, 95, 126], air-steam [90, 127-130], steam [131-135] and sorption-enhanced steam gasification [122, 136-138] of sewage sludge. (a) H_2 purity; (b) H_2 yield; (c) CO purity; (d) CO yield.

2.4. Tar elimination for syngas production

With the exception of the generation of syngas, tar is also formed accompanying with the syngas during the gasification of biomass, which can be condensed at a lower temperature, then foul, block and corrode the downstream equipment, like pipes, filter, engines, etc [139]. It was reported that the applications of the syngas derived from biomass require a low tar content of less than 0.05 g/Nm^3 [140]. As shown in Table 2.7., the tar content is still far above the required values. Therefore, tar elimination is indispensable for the industrial application of the biomass-derived syngas using gasification technology. Up to now, a lot of work concerning tar elimination using physical and chemical methods has been widely reported [141, 142]. The physical methods including scrubber, filter, cyclone and electrostatic precipitator, have been proven to reduce about

40-99% tar [140]. However, the physical methods only remove the tar from the gaseous products, while there is no energy recovery associated with the physical tar elimination [143]. The chemistry methods mainly containing thermal and catalytic elimination of the tar can not only reduce the tar contents but also enhance the syngas production by converting the tar into syngas.

Table 2.7. Tar contents of the thermochemical conversion of biomass

Biomass types	Thermochemical conversion types	Tar content (g/Nm^3)	Ref.
Black pine	Air	26.8	[88]
	Air-steam	21.2	
Agrol	Steam-oxygen	12.4	[144]
Pine sawdust	Catalytic steam gasification	48	[145]
SS	Air-steam	45.3	[127]
	Pyrolysis	13.1	[133]
	Steam gasification	20.6	

2.4.1. Thermal elimination of tar for syngas production

Thermal elimination of tar means the tar is cracked at a high temperature above 700 °C [146]. Jaramillo-Arango et al. [141] found that the tar yield from the pyrolysis of SS increases with the temperature, reaching a maximum at 600 °C, and then decreases due to the promoting tar reforming/cracking for gas production at a higher temperature. Zhang et al. [84] reported that tar yield slightly decreases between 600 and 700 °C, and then decreases greatly as the temperature increases from 700-1000 °C. de Andrés et al. [128] reported that the tar production from SS with the increasing time from 750 to 850 °C reduced by 65% at a residence time of 7.5 s and 49% at a residence time of 2.5 s. Besides, temperature also poses a crucial influence on tar compositions. The variation in the composition of the tar reported by Jaramillo-Arango et al. [141] shows that oxygenated compounds, aliphatic and aromatic compounds are the major components of the tar derived from SS, which decrease with the temperature, while nitrogen-containing compounds and PAHs increase with the temperature. Similarly, Fuentes-Cano et al. [147] revealed that the rise in

temperature would reduce the content heterocyclic and monoaromatic tar, while increasing the contents of 2-7 rings PAHs. It was concluded that the light tars (heterocyclic and mono-aromatic compounds) are the precursors of heavy tars (2-7 rings PAHs). Furthermore, the higher temperature could lead to a lower yield of tar and a higher yield of gaseous products correspondingly, especially with the steam reforming. Phuphuakrat et al. [148] exhibited a reduction of 78% in the gravimetric tar mass under the thermal cracking at 800 °C. Based on that, the tar elimination efficiency is further promoted to 88% by steam reforming. The H_2 and CO production increases by 143.7% and 42.9% under the thermal cracking at 800 °C. With the steam reforming, the H_2 production increases by 306.3%, while the CO production decreases by 28.9% due to the promoting water-gas shifting reaction (Eq. 4). However, the temperature of thermal cracking needs to be as high as 1000 °C to get complete tar removal [140, 149]. The high temperature requirement incurring abundant energy input makes it hard to eliminate tar thermally alone to get the tar contents meet the requirement for the industrial application of syngas.

2.4.2. Catalytic elimination of tar for syngas production

Contrary to thermal cracking of tar, the addition of catalyst would achieve high tar elimination efficiency at a lower temperature. Abu El-Rub et al. [150] showed that the conversion efficiency of phenol is only 6.0 wt% at 700 °C, while it is enhanced to 91 wt% at 700 °C with the presence of Ni catalysts. Furthermore, catalytic elimination of tar is an attractive and sustainable method in dual aspects of eliminating tar efficiently and simultaneously producing syngas. Various types of catalysts such as alkali metals [151, 152], noble metal-based catalysts [153-155], nickel-based catalysts [156-158], have been developed for tar elimination during the gasification of biomass. Umeki et al. [151] studied the tar and soot production from the gasification of pine sawdust impregnating with aqueous K_2CO_3 solution. The results indicated that K could promote the

decomposition of light tar (1-2 rings aromatic compounds) and inhibit the formation of PAHs. Among the noble metals, Guan et al. [159] claimed that Rh is found to be significantly more active than others with a selectivity order of Rh > Pt > Pd > Ru ≈ Ni. Ammendola et al. [160] also disclosed that the noble $Rh/LaCoO_3/Al_2O_3$ catalyst can completely convert the tar as well as the light hydrocarbons with a limited coke formation, being far more active than the Ni/Al_2O_3, dolomite, and olivine. Although noble metal catalysts perform excellent catalytic active and good resistance toward deactivation and sintering, their high cost and limited availability restrict their large-scale industrial applications.

Ni-based catalysts have attracted much attention due to the high activity, low-cost and easy regeneration. Ni has been proved to have a significant capacity for C-C, C-H, and C-O bond cleavage. Zhu et al. [161] exhibited the highest activity of Ni/AC (activated carbon) for cleavage of C-O bond compared to Co/AC and Cu/AC. Prats et al. [162] found that Ni clusters dispersed on the surface of TiC are able to capture and dissociate the C-H bond of methane at room temperature, and C-H bond scission energy barriers become smaller than the CH_4 adsorption energies and can be as low as 0.18 eV. Given this, Ni-based catalysts are widely applied for the purpose of dry reforming of methane [163, 164], water-gas shift reaction [165, 166] for syngas production. Also, the C-C, C-H, and C-O bonds are the important linkages in the structure of tar, and thereby the cleavage of those bonds is conducive to the cracking/reforming of tar and light hydrocarbons for syngas production. Choi et al. [142] reported 97% of tar removal efficiency with the addition of Ni/AC. And the addition of Ni poses an increment in H_2 purity from 11.8 to 29.2 vol%, and an enhancement in the CO purity from 9.1 to 15.9 vol%. Moreover, the Ni-based catalysts had the ability to reduce gaseous by-products, like, NO_x, NH_3 emission during the gasification of biomass,

especially SS with high N contents. A significant reduction in NH_3 content in the produced gas from 1926 to 259 ppm from the gasification of SS with the addition of Ni/AC [142].

However, the rapid deactivation deriving from carbon deposition and thermal sintering is the shortcoming of the Ni-based catalysts. Much effort has been devoted to improving Ni catalysts performance on the selection of the type support [167-171] and subsequent modifiers [172-174]. The support plays a key role on catalyst performance, since it can promote the secondary reactions of coke to inhibit coke deposition and the strong metal-support interaction enhancing Ni dispersion and minimizing Ni sintering [168, 175]. A wide range of Ni support, like Al_2O_3, CeO_2, SiO_2, ZrO_2, MgO, TiO_2, dolomite, has been proposed for the tar elimination. Santamaria et al. [167] compared the influence of support on Ni catalysts performance in the in-line steam reforming of tar derived from biomass fast pyrolysis. The tar elimination efficiency and H_2 selectivity are found in the following order: $Ni/Al_2O_3 \approx Ni/ZrO_2 > Ni/MgO > Ni/TiO_2 > Ni/SiO_2$. The Ni/Al_2O_3 and Ni/ZrO_2 catalysts show the best catalytic activity with 98% of tar removal efficiency, which is related to the suitable physical properties of the support favouring a proper metal dispersion. The low Ni dispersion in the Ni/TiO_2 catalyst leads a poor activity on the tar removal efficiency. Although Ni/SiO_2 catalyst has a high surface area and Ni dispersion, its microporous structure hinders the access of tar bulky molecules to Ni activity sites leading to the lowest tar elimination efficiency. Miyazawa et al. [168] demonstrated that Ni/Al_2O_3 exhibits the highest tar removal efficiency with the highest H_2/CO ratio in the generated syngas from no matter the oxygen or steam gasification of tar derived from biomass. The order of the catalytic performance at 550 °C is as follows: $Ni/Al_2O_3 > Ni/ZrO_2 > Ni/TiO_2 > Ni/CeO_2 > Ni/MgO >$ no catalyst. While Ni/CeO_2 shows a smaller amount of coke than other catalysts since it can promote the reaction of carbon with O_2 and steam. The experimental results conducted by Furusawa et al. [169] concluded that Al_2O_3 supported metal

(Ni and Pt) catalysts show better catalytic performances on the steam reforming of naphthalene/benzene than CeO_2, MgO, ZrO_2, TiO_2 supported catalysts. Wu and Williams [170] also claimed that a typical and suitable support for Ni catalysts is Al_2O_3, because of its chemical and physical stability and high mechanical properties. Besides, the Ni/ Al_2O_3 catalyst prepared by co-precipitation shows a higher catalytic performance on the tar elimination and gas production compared to the Ni/Al_2O_3, Ni/ZSM-5, Ni/CeO_2/Al_2O_3, Ni/CeO_2, Ni/MgO catalysts prepared by the impregnation method, which can be explained that co-precipitation allows catalyst with a big metallic area and high thermal stability of metallic phase [176].

Various modifiers, like noble metals (Ce, Ru, Co, Pb) [172, 177-179], alkali (Na, K, Mg, Ca) [173, 174, 180, 181] have also been studied to improve catalytic activity, coking resistance, and stability of Ni-based catalyst. Among all the modifiers, CaO is becoming an appealing one in the steam reforming of biomass-derived tar and light hydrocarbons in view of its bi-functional property. In the bi-functional Ni/CaO catalyst, the Ni species is associated with the steam reforming of tar and light hydrocarbons and CaO species possess the sorption property, both of which are contributed to the syngas production. Wu et al. [174] prepared Ni-CaO-Al_2O_3 multifunctional catalysts using the co-precipitation method showing higher H_2 concentration and larger CO_2 adsorption ability in 10 reaction-desorption cycles in comparison with the mixture of CaO adsorbent and Ni/Al_2O_3 catalyst. And this Ni-CaO-Al_2O_3 catalyst was recommended to be widely applied for many other sorption-enhanced processes for syngas production. Ashok et al. [182] compared the catalytic activity of NiO-CaO-Al_2O_3 (Ni-Ca-Al), NiO-CaO (Ni-Ca) and NiO-Al_2O_3 (Ni-Al) prepared by the co-precipitation method on the steam reforming of toluene as a model compound of tar. The Ni-Ca-Al catalyst has higher H_2 production and lower CO_2 production compared to the Ni-Ca and Ni-Al catalysts, suggesting a synergy between the Ni and CaO. Also, the Ni-Ca-Al catalyst possesses

lower amount of carbon formation rate (2.5 mg/g/h) as compared to the carbon formation rate of Ni-Ca (130.4 mg/g/h) and Ni-Al (45.3 mg/g/h). Nahil et al. [183] reported that the addition of CaO to the Ni-Mg-Al catalyst leads to an increase in H_2 production and selectivity due to the promoting of the water-gas shift reaction by *in situ* CO_2 capture. The catalyst deactivation and sintering due to the carbon deposition are significantly decreased with the addition of CaO. Besides, the Ni-Mg-Al-CaO catalyst shows a comparatively stable CO_2 adsorption capacity even after 20 cycles. Xu et al. [184] designed an ordered mesoporous NiO-CaO-Al_2O_3 with advantageous textural properties and superior thermal stabilities, which exhibits excellent catalytic activities and long catalytic stabilities on the dry reforming of CH_4. Besides, the modification of Ca among the mesoporous skeletons also improve the catalytic performance as well as suppressing carbon deposition by enhancing the chemisorbed activation of the CO_2. In conclusion, the above-mentioned results indicate that bi-functional Ni-CaO-Al_2O_3 catalyst is an appealing candidate for the sorption-enhanced process, posing dual roles in tar cracking/reforming for gas production and promoting H_2 production with the *in situ* CO_2 capture.

2.4.3. Biochar for syngas production

Biochar is another product of the thermochemical conversion of biomass, the applications of which are diverse, ranging from heat and power production [185], environmental decontamination [186], soil amendment [187] and animal husbandry [188], or building materials [189]. Besides, the biomass-derived char has the potential for syngas production mainly in the following two aspects [190].

Vassilev et al. [191] presented a comprehensive review on the composition of biomass ash, showing that the main components in biochar are alkali and alkaline-earth metals, like SiO_2, CaO,

K_2O, P_2O_5, Al_2O_3 and MgO. And a porous biochar is obtained as the gases devolatilize from the solid biomass during pyrolysis. Somerville and Jahanshahi [192] described that the porosity of biochar increases with pyrolysis temperature, increasing from 50% at 300 °C to 70% at 850 °C. Similarly, the surface area of biochar significantly enhances with the temperature. Chen et al. [193] discovered that the surface area of pine needle is extremely low (0.65 m^2/g). With increasing pyrolytic temperature to 400 °C, the removal and destruction of -OH, aliphatic C-O, ester C=O groups and aliphatic alkyl lead to an enhancement of surface area to 112.4 m^2/g. The further removal of aromatic CO- and phenolic -OH linked to aromatic cores boosts the surface area to 490.8 m^2/g at 700 °C. Raw biomass is typically acidic or basic with pH-values ranging from 5 to 7.5. Biochar is typically alkaline with pH-values of 9-12 [194]. Due to the alkali and alkaline-earth metals, high porosity, surface area and pH value, biochar has been proved to have a promoting effect on the tar cracking/reforming for syngas production (Eq. 2, 3). Park et al. [179] studied tar production from fir wood by pyrolysis at 500 °C and then pass through the second reactor with different temperature or biochar particles. The tar yield is reduced from 24.8% by pyrolysis to 13.7% by thermal cracking at 800 °C, and further to 7.7% with the biochar in the reactor at 800 °C. Besides, the syngas yields are increased correspondingly. The CO yield shows the largest increase from 7.7 wt% by pyrolysis to 18.0 wt% by thermal cracking at 800 °C, and further to 25 wt% with the biochar at 800 °C. The H_2 yield increases from 0.04 wt% by pyrolysis to 0.5 wt% by thermal cracking at 800 °C, and further to 1.0 wt% with biochar at 800 °C.

Moreover, biochar derived from lignocellulosic biomass features rich carbon. The carbon contents could reach as high as 95% with increasing pyrolytic temperature above 700 °C, whereas the oxygen and hydrogen contents decrease due to the dehydration, deoxygenation and depolymerization of the biomass [195]. The carbon-rich biochar has been demonstrated to be

gasified by CO_2 for CO production via reverse Boudouard reaction (Eq. 5), which has attracted wide attention. It has the potential to be used to mitigate the accumulation of CO_2 in the atmosphere or as a post-treatment technique to improve the quality of exhaust/flue gas [190]. Regarding the char derived from SS, the carbon contents are low, only ranging 0.6-6.4% reported by Oh et al. [196] and 20.2-30.7% reported by Ahmad et al. [195], due to high ash contents in SS. However, SS-derived char shows high reactivity with CO_2. Gupta et al. [197] also claimed that CO_2 gasification of biomass-derived char is influenced by char morphology and inorganic content, later being the major factor. Scott et al. [198] compared the CO_2 gasification rate of three types of chars (SS, car tyres, coal). The highest reactivity of char with CO_2 is derived from SS, which is attributed to the SS-derived char containing large amounts of alkali and alkaline-earth metals to catalyse the gasification of carbon by CO_2.

2.5. Summary

This chapter presents the literature review that rapid growth in generation and hazardous components of SS pose a significant challenge to conventional disposal and treatment approaches considering the land shortage and environmental concerns. Sorption-enhanced thermochemical conversion, regarded as a waste-to-energy technology, can achieve the transformation of SS into high yield and purity H_2 as a promising alternative to combat the increasing environmental issue facing SS management. However, the conventional sorption-enhanced thermochemical conversion only aims to enhance H_2 production. Another important component of the syngas, CO, has not received much attention from the sorption-enhanced thermochemical conversion process, and effective approach for the enhancement in CO production is still lacking. Additionally, a certain amount of tar is also produced along with the syngas from the sorption-enhanced thermochemical conversion process, restricting the application of the generated syngas. The bi-functional Ni-

CaO/Al_2O_3 catalyst and biochar have been reviewed to be capable of tar elimination and enhancement in syngas production. The next chapters will discuss the results on the development of a novel two-stage sorption-enhanced process to enhance the CO production under the premise of high H_2 production, and further maximise the syngas yield and improve the syngas quality.

References

1. Dudley, B., *BP Statistical Review of World Energy*. 2019, BP Statistical Review: London, UK.
2. *Renewables information overview*. 2019, Internation Energy Agency.
3. Panwar, N.L., S.C. Kaushik, and S. Kothari, *Role of renewable energy sources in environmental protection: A review.* Renewable and Sustainable Energy Reviews, 2011. **15**(3): p. 1513-1524.
4. Demirbas, A., *Potential applications of renewable energy sources, biomass combustion problems in boiler power systems and combustion related environmental issues.* Progress in Energy and Combustion Science, 2005. **31**(2): p. 171-192.
5. Burke, M.J. and J.C. Stephens, *Political power and renewable energy futures: A critical review.* Energy Research & Social Science, 2018. **35**: p. 78-93.
6. Kuang, Y., et al., *A review of renewable energy utilization in islands.* Renewable and Sustainable Energy Reviews, 2016. **59**: p. 504-513.
7. Connolly, D., H. Lund, and B.V. Mathiesen, *Smart Energy Europe: The technical and economic impact of one potential 100% renewable energy scenario for the European Union.* Renewable and Sustainable Energy Reviews, 2016. **60**: p. 1634-1653.

8. Cutz, L., et al., *Switching to efficient technologies in traditional biomass intensive countries: The resultant change in emissions.* Energy, 2017. **126**: p. 513-526.

9. Masera, O.R., et al., *Environmental burden of traditional bioenergy use.* Annual Review of Environment and Resources, 2015. **40**(1): p. 121-150.

10. Quaschning, V., *Understanding renewable energy systems*. 2016: Routledge.

11. Sikarwar, V., et al., *An overview of advances in biomass gasification.* Energy & Environmental Science, 2016. **9**(10).

12. Vassilev, S.V., et al., *An overview of the chemical composition of biomass.* Fuel, 2010. **89**(5): p. 913-933.

13. Hamzeh, Y., et al., *Current and potential capabilities of biomass for green energy in Iran.* Renewable and Sustainable Energy Reviews, 2011. **15**(9): p. 4934-4938.

14. Peccia, J. and P. Westerhoff, *We should expect more out of our sewage sludge.* Environmental Science & Technology, 2015. **49**(14): p. 8271-8276.

15. Syed-Hassan, S.S.A., et al., *Thermochemical processing of sewage sludge to energy and fuel: Fundamentals, challenges and considerations.* Renewable and Sustainable Energy Reviews, 2017. **80**: p. 888-913.

16. Song, Q., J. Li, and X. Zeng, *Minimizing the increasing solid waste through zero waste strategy.* Journal of Cleaner Production, 2015. **104**: p. 199-210.

17. Cucchiella, F., I. D'Adamo, and M. Gastaldi, *Sustainable waste management: Waste to energy plant as an alternative to landfill.* Energy Conversion and Management, 2017. **131**: p. 18-31.

18. Yi, S., Y.-C. Jang, and A.K. An, *Potential for energy recovery and greenhouse gas reduction through waste-to-energy technologies.* Journal of Cleaner Production, 2018. **176**: p. 503-511.

19. Vassilev, S.V., et al., *An overview of the organic and inorganic phase composition of biomass.* Fuel, 2012. **94**(1): p. 1-33.

20. Alloway, B.J. and A.P. Jackson, *The behaviour of heavy metals in sewage sludge-amended soils.* Science of The Total Environment, 1991. **100**: p. 151-176.

21. Straub, T.M., I.L. Pepper, and C.P. Gerba, *Hazards from pathogenic microorganisms in land-disposed sewage sludge.* Reviews of Environmental Contamination and Toxicology, 1993: p. 55-91.

22. Bibby, K. and J. Peccia, *Identification of viral pathogen diversity in sewage sludge by metagenome analysis.* Environmental Science & Technology, 2013. **47**(4): p. 1945-1951.

23. Fytili, D. and A. Zabaniotou, *Utilization of sewage sludge in EU application of old and new methods—A review.* Renewable and Sustainable Energy Reviews, 2008. **12**(1): p. 116-140.

24. Chen, J., et al., *Nationwide reconnaissance of five parabens, triclosan, triclocarban and its transformation products in sewage sludge from China.* Journal of Hazardous Materials, 2019. **365**: p. 502-510.

25. *A national biosolids regulation, quality, end use & disposal survey*. 2007, North East Biosolids and Residuals Association (NEBRA).

26. Kelessidis, A. and A.S. Stasinakis, *Comparative study of the methods used for treatment and final disposal of sewage sludge in European countries.* Waste Management, 2012. **32**(6): p. 1186-1195.

27. Eurostat. *Sewage sludge production and disposal*. [cited 2020 Apr 20].

28. *Australian Biosolids Statistics*. Australian & New Zealand Biosolids Partnership.

29. *China Urban-Rural Construction Statistical Yearbook*. 2013, Ministry of Housing and Urban-Rural Development of the People's Republic of China (MOHURD).

30. *China Urban-Rural Construction Statistical Yearbook*. 2018, Ministry of Housing and Urban-Rural Development of the People's Republic of China (MOHURD).

31. He, C., et al., *Hydrothermal gasification of sewage sludge and model compounds for renewable hydrogen production: A review.* Renewable and Sustainable Energy Reviews, 2014. **39**: p. 1127-1142.

32. Raheem, A., et al., *Opportunities and challenges in sustainable treatment and resource reuse of sewage sludge: A review.* Chemical Engineering Journal, 2018. **337**: p. 616-641.

33. EPA, U.S., *Land Application of Sewage Sludge: A Guide for Land Appliers on the Requirements of the Federal Standard for the Use or Disposal of Sewage Sludge, 40 CFR Part 503 (EPA/831-B-93−002b)*. 1994: Washington, DC.

34. *National water quality management strategy, guidlines for sewerage systems biosolids management*. 2004, Australian National Resource Management Ministerial Council: Canberra, Australia.

35. *EUR-Lex Council Directive 86/278/EEC. Council directive of 12 June 1986 on the protection of the environment, and in particular of the soil, when the sewage sludge is used in Agriculture* Official Journal of the European Communities, 1986. **181**: p. 6-12.

36. Zufiaurre, R., et al., *Speciation of metals in sewage sludge for agricultural uses.* Analyst, 1998. **123**(2): p. 255-259.

37. Collivignarelli, M.C., A. Abbà, and I. Benigna, *The reuse of biosolids on agricultural land: Critical issues and perspective.* Water Environment Research, 2020. **92**(1): p. 11-25.

38. Toribio, M. and J. Romanyà, *Leaching of heavy metals (Cu, Ni and Zn) and organic matter after sewage sludge application to Mediterranean forest soils.* Science of the Total Environment, 2006. **363**(1-3): p. 11-21.

39. Thaís, C., et al., *Leaching of heavy metals in soils conditioned with biosolids from sewage sludge.* Floresta e Ambiente, 2019. **26**(spe1).

40. Islam, K., et al., *Biosolid impact on heavy metal accumulation and lability in soiln under alternate-year no-till corn-soybean rotation.* Water, Air, & Soil Pollution, 2013. **224**(3): p. 1-10.

41. Eid, E., et al., *Prediction models for evaluating the uptake of heavy metals by cucumbers (Cucumis sativus L.) grown in agricultural soils amended with sewage sludge.* Environmental Monitoring and Assessment, 2018. **190**(9): p. 1-12.

42. Chatterjee, C. and B.K. Dube, *Impact of pollutant elements on vegetables growing in sewage-sludge-treated soils.* Journal of Plant Nutrition, 2005. **28**(10): p. 1811-1820.

43. Singh, R.P. and M. Agrawal, *Effects of sewage sludge amendment on heavy metal accumulation and consequent responses of Beta vulgaris plants.* Chemosphere, 2007. **67**(11): p. 2229-2240.

44. Deng, Y. and J.D. Englehardt, *Treatment of landfill leachate by the Fenton process.* Water Research, 2006. **40**(20): p. 3683-3694.

45. Renou, S., et al., *Landfill leachate treatment: Review and opportunity.* Journal of Hazardous Materials, 2008. **150**(3): p. 468-493.

46. Allen, M.R., A. Braithwaite, and C.C. Hills, *Trace organic compounds in landfill gas at seven U.K. waste disposal sites.* Environmental Science & Technology, 1997. **31**(4): p. 1054-1061.

47. *Landfill Taxes and Bans*. Confederation of European Waste-to-Energy Plants (CEWEP).

48. Malerius, O. and J. Werther, *Modeling the adsorption of mercury in the flue gas of sewage sludge incineration.* Chemical Engineering Journal, 2003. **96**(1): p. 197-205.

49. Lin, H. and X. Ma, *Simulation of co-incineration of sewage sludge with municipal solid waste in a grate furnace incinerator.* Waste Management, 2012. **32**(3): p. 561-567.

50. Samolada, M.C. and A.A. Zabaniotou, *Comparative assessment of municipal sewage sludge incineration, gasification and pyrolysis for a sustainable sludge-to-energy management in Greece.* Waste Management, 2014. **34**(2): p. 411-420.

51. Werther, J. and T. Ogada, *Sewage sludge combustion.* Progress in Energy and Combustion Science, 1999. **25**(1): p. 55-116.

52. Zhang, L., C. Xu, and P. Champagne, *Overview of recent advances in thermo-chemical conversion of biomass.* Energy Conversion and Management, 2010. **51**(5): p. 969-982.

53. Manara, P. and A. Zabaniotou, *Towards sewage sludge based biofuels via thermochemical conversion – A review.* Renewable and Sustainable Energy Reviews, 2012. **16**(5): p. 2566-2582.

54. Fonts, I., et al., *Sewage sludge pyrolysis for liquid production: A review.* Renewable and Sustainable Energy Reviews, 2012. **16**(5): p. 2781-2805.

55. Schulz, H., *Short history and present trends of Fischer–Tropsch synthesis.* Applied Catalysis A: General, 1999. **186**(1): p. 3-12.

56. Sanchez-Silva, L., et al., *Thermogravimetric–mass spectrometric analysis of lignocellulosic and marine biomass pyrolysis.* Bioresource Technology, 2012. **109**: p. 163-172.

57. Zhou, H., et al., *Classification of municipal solid waste components for thermal conversion in waste-to-energy research.* Fuel, 2015. **145**: p. 151-157.

58. Kim, S.-S. and F.A. Agblevor, *Pyrolysis characteristics and kinetics of chicken litter.* Waste Management, 2007. **27**(1): p. 135-140.

59. Ngo, T.-A., J. Kim, and S.-S. Kim, *Characteristics and kinetics of cattle litter pyrolysis in a tubing reactor.* Bioresource Technology, 2010. **101**(1, Supplement): p. S104-S108.

60. Ro, K.S., K.B. Cantrell, and P.G. Hunt, *High-temperature pyrolysis of blended animal manures for producing renewable energy and value-added biochar.* Industrial & Engineering Chemistry Research, 2010. **49**(20): p. 10125-10131.

61. Bach, Q.-V. and W.-H. Chen, *A comprehensive study on pyrolysis kinetics of microalgal biomass.* Energy Conversion and Management, 2017. **131**: p. 109-116.

62. Alvarez, J., et al., *Fast co-pyrolysis of sewage sludge and lignocellulosic biomass in a conical spouted bed reactor.* Fuel, 2015. **159**: p. 810-818.

63. Zhou, C.-H., et al., *Catalytic conversion of lignocellulosic biomass to fine chemicals and fuels.* Chemical Society Reviews, 2011. **40**(11): p. 5588-5617.

64. Shuping, Z., et al., *Pyrolysis characteristics and kinetics of the marine microalgae Dunaliella tertiolecta using thermogravimetric analyzer.* Bioresource Technology, 2010. **101**(1): p. 359-365.

65. Sipra, A.T., N. Gao, and H. Sarwar, *Municipal solid waste (MSW) pyrolysis for bio-fuel production: A review of effects of MSW components and catalysts.* Fuel Processing Technology, 2018. **175**: p. 131-147.

66. Kamarudin, S.K., et al., *Production of methanol from biomass waste via pyrolysis.* Bioresource Technology, 2013. **129**: p. 463-468.

67. Lopez, G., et al., *Waste truck-tyre processing by flash pyrolysis in a conical spouted bed reactor.* Energy Conversion and Management, 2017. **142**: p. 523-532.

68. Maliutina, K., et al., *Comparative study on flash pyrolysis characteristics of microalgal and lignocellulosic biomass in entrained-flow reactor.* Energy Conversion and Management, 2017. **151**: p. 426-438.

69. Zhao, B., et al., *Hydrogen production from biomass combining pyrolysis and the secondary decomposition.* International Journal of Hydrogen Energy, 2010. **35**(7): p. 2606-2611.

70. Magdziarz, A. and S. Werle, *Analysis of the combustion and pyrolysis of dried sewage sludge by TGA and MS.* Waste Management, 2014. **34**(1): p. 174-179.

71. López-González, D., et al., *Pyrolysis of three different types of microalgae: Kinetic and evolved gas analysis.* Energy, 2014. **73**: p. 33-43.

72. Widyawati, M., et al., *Hydrogen synthesis from biomass pyrolysis with in situ carbon dioxide capture using calcium oxide.* International Journal of Hydrogen Energy, 2011. **36**(8): p. 4800-4813.

73. Mohammed, M.A.A., et al., *Hydrogen rich gas from oil palm biomass as a potential source of renewable energy in Malaysia.* Renewable and Sustainable Energy Reviews, 2011. **15**(2): p. 1258-1270.

74. Raheem, A., et al., *Thermogravimetric study of Chlorella vulgaris for syngas production.* Algal Research, 2015. **12**: p. 52-59.

75. Williams, P.T. and S. Besler, *The influence of temperature and heating rate on the slow pyrolysis of biomass.* Renewable Energy, 1996. **7**(3): p. 233-250.

76. Al Arni, S., *Comparison of slow and fast pyrolysis for converting biomass into fuel.* Renewable Energy, 2018. **124**: p. 197-201.

77. Horne, P.A. and P.T. Williams, *Influence of temperature on the products from the flash pyrolysis of biomass.* Fuel, 1996. **75**(9): p. 1051-1059.

78. Velghe, I., et al., *Study of the pyrolysis of municipal solid waste for the production of valuable products.* Journal of Analytical and Applied Pyrolysis, 2011. **92**(2): p. 366-375.

79. Vardon, D.R., et al., *Thermochemical conversion of raw and defatted algal biomass via hydrothermal liquefaction and slow pyrolysis.* Bioresource Technology, 2012. **109**: p. 178-187.

80. Barry, D., et al., *Pyrolysis as an economical and ecological treatment option for municipal sewage sludge.* Biomass and Bioenergy, 2019. **122**: p. 472-480.

81. Trinh, T.N., et al., *Influence of the pyrolysis temperature on sewage sludge product distribution, bio-oil, and char properties.* Energy & Fuels, 2013. **27**(3): p. 1419-1427.

82. Inguanzo, M., et al., *On the pyrolysis of sewage sludge: the influence of pyrolysis conditions on solid, liquid and gas fractions.* Journal of Analytical and Applied Pyrolysis, 2002. **63**(1): p. 209-222.

83. Alvarez, J., et al., *Characterization of the bio-oil obtained by fast pyrolysis of sewage sludge in a conical spouted bed reactor.* Fuel Processing Technology, 2016. **149**: p. 169-175.

84. Zhang, B., et al., *Mechanism of wet sewage sludge pyrolysis in a tubular furnace.* International Journal of Hydrogen Energy, 2011. **36**(1): p. 355-363.

85. Tomasi Morgano, M., et al., *Screw pyrolysis technology for sewage sludge treatment.* Waste Management, 2018. **73**: p. 487-495.

86. Florin, N.H. and A.T. Harris, *Enhanced hydrogen production from biomass with in situ carbon dioxide capture using calcium oxide sorbents.* Chemical Engineering Science, 2008. **63**(2): p. 287-316.

87. Chang, A.C.C., et al., *Biomass gasification for hydrogen production.* International Journal of Hydrogen Energy, 2011. **36**(21): p. 14252-14260.

88. Kihedu, J.H., R. Yoshiie, and I. Naruse, *Performance indicators for air and air-steam auto-thermal updraft gasification of biomass in packed bed reactor.* Fuel Processing Technology, 2016. **141**: p. 93-98.

89. Liu, L., et al., *Experimental study of biomass gasification with oxygen-enriched air in fluidized bed gasifier.* Science of The Total Environment, 2018. **626**: p. 423-433.

90. de Andrés, J.M., A. Narros, and M.E. Rodríguez, *Air-steam gasification of sewage sludge in a bubbling bed reactor: Effect of alumina as a primary catalyst.* Fuel Processing Technology, 2011. **92**(3): p. 433-440.

91. Seggiani, M., et al., *Cogasification of sewage sludge in an updraft gasifier.* Fuel, 2012. **93**: p. 486-491.

92. Gil-Lalaguna, N., et al., *Air–steam gasification of sewage sludge in a fluidized bed. Influence of some operating conditions.* Chemical Engineering Journal, 2014. **248**: p. 373-382.

93. Butterman, H.C. and M.J. Castaldi, *CO_2 as a carbon neutral fuel source via enhanced biomass gasification.* Environmental Science & Technology, 2009. **43**(23): p. 9030-9037.

94. Zheng, X., et al., *CO_2 gasification of municipal solid waste in a drop-tube reactor: experimental study and thermodynamic analysis of syngas.* Energy & Fuels, 2018. **32**(4): p. 5302-5312.

95. Dogru, M., A. Midilli, and C.R. Howarth, *Gasification of sewage sludge using a throated downdraft gasifier and uncertainty analysis.* Fuel Processing Technology, 2002. **75**(1): p. 55-82.

96. Franco, C., et al., *The study of reactions influencing the biomass steam gasification process.* Fuel, 2003. **82**(7): p. 835-842.

97. Zhang, Y., et al., *Tar destruction and coke formation during rapid pyrolysis and gasification of biomass in a drop-tube furnace.* Fuel, 2010. **89**(2): p. 302-309.

98. Herguido, J., J. Corella, and J. Gonzalez-Saiz, *Steam gasification of lignocellulosic residues in a fluidized bed at a small pilot scale: Effect of the type of feedstock.* Industrial & Engineering Chemistry Research, 1992. **31**(5): p. 1274-1282.

99. Nilsson, S., A. Gómez-Barea, and D.F. Cano, *Gasification reactivity of char from dried sewage sludge in a fluidized bed.* Fuel, 2012. **92**(1): p. 346-353.

100. Loha, C., P.K. Chatterjee, and H. Chattopadhyay, *Performance of fluidized bed steam gasification of biomass-Modeling and experiment.* Energy Conversion and Management, 2011. **52**(3): p. 1583-1588.

101. Sharma, S. and P.N. Sheth, *Air-steam biomass gasification: Experiments, modeling and simulation.* Energy Conversion and Management, 2016. **110**: p. 307-318.

102. Hu, M., et al., *Hydrogen-rich gas production by the gasification of wet MSW (municipal solid waste) coupled with carbon dioxide capture.* Energy, 2015. **90**: p. 857-863.

103. Curran, G.P., C.E. Fink, and E. Gorin, *CO_2 Acceptor Gasification Process: Studies of acceptor properties*, in *Fuel Gasification*. 1967, American Chemical Society. p. 141-165.

104. Shokrollahi Yancheshmeh, M., H.R. Radfarnia, and M.C. Iliuta, *High temperature CO_2 sorbents and their application for hydrogen production by sorption enhanced steam reforming process.* Chemical Engineering Journal, 2016. **283**: p. 420-444.

105. Wei, L., et al., *Hydrogen production in steam gasification of biomass with CaO as a CO_2 absorbent.* Energy & Fuels, 2008. **22**(3): p. 1997-2004.

106. Rapagnà, S., et al., *Steam-gasification of biomass in a fluidised-bed of olivine particles.* Biomass and Bioenergy, 2000. **19**(3): p. 187-197.

107. Wei, L., et al., *Steam gasification of biomass for hydrogen-rich gas in a free-fall reactor.* International Journal of Hydrogen Energy, 2007. **32**(1): p. 24-31.

108. Salaudeen, S.A., et al., *Hydrogen-rich gas stream from steam gasification of biomass: Eggshell as a CO_2 sorbent.* Energy & Fuels, 2020. **34**(4): p. 4828-4836.

109. Weerachanchai, P., M. Horio, and C. Tangsathitkulchai, *Effects of gasifying conditions and bed materials on fluidized bed steam gasification of wood biomass.* Bioresource Technology, 2009. **100**(3): p. 1419-1427.

110. Peltzer, D., et al., *Characterization of potassium doped Li_2ZrO_3 based CO_2 sorbents: Stability properties and CO_2 desorption kinetics.* Chemical Engineering Journal, 2018. **336**: p. 1-11.

111. Wang, C., et al., *Sorption-Enhanced Steam Reforming of Glycerol for Hydrogen Production over a $NiO/NiAl_2O_4$ Catalyst and Li_2ZrO_3-Based Sorbent.* Energy & Fuels, 2015. **29**(11): p. 7408-7418.

112. Aceves Olivas, D.Y., et al., *Enhanced ethanol steam reforming by CO_2 absorption using CaO, CaO*MgO or Na_2ZrO_3.* International Journal of Hydrogen Energy, 2014. **39**(29): p. 16595-16607.

113. Dou, B., et al., *Solid sorbents for in-situ CO_2 removal during sorption-enhanced steam reforming process: A review.* Renewable and Sustainable Energy Reviews, 2016. **53**: p. 536-546.

114. Ding, Y. and E. Alpay, *Equilibria and kinetics of CO_2 adsorption on hydrotalcite adsorbent.* Chemical Engineering Science, 2000. **55**(17): p. 3461-3474.

115. Wang, S., et al., *Prediction of sorption-enhanced reforming process on hydrotalcite sorbent in a fluidized bed reactor.* Energy Conversion and Management, 2019. **180**: p. 924-930.

116. Dewoolkar, K.D. and P.D. Vaidya, *Improved hydrogen production by sorption-enhanced steam methane reforming over hydrotalcite- and calcium-based hybrid materials.* Energy & Fuels, 2015. **29**(6): p. 3870-3878.

117. Gil, M.V., et al., *Production of fuel-cell grade H_2 by sorption enhanced steam reforming of acetic acid as a model compound of biomass-derived bio-oil.* Applied Catalysis B: Environmental, 2016. **184**: p. 64-76.

118. Kierzkowska, A.M., R. Pacciani, and C.R. Müller, *CaO‐based CO_2 sorbents: From fundamentals to the development of new, highly effective materials.* Chemsuschem, 2013. **6**: p. 1130-1148.

119. Baker, E.H., *87. The calcium oxide-carbon dioxide system in the pressure range 1-300 atmospheres.* Journal of the Chemical Society (Resumed), 1962(0): p. 464-470.

120. Han, L., et al., *Hydrogen production via CaO sorption enhanced anaerobic gasification of sawdust in a bubbling fluidized bed.* International Journal of Hydrogen Energy, 2011. **36**(8): p. 4820-4829.

121. Zhang, B., et al., *Hydrogen-rich gas production from wet biomass steam gasification with CaO/MgO.* International Journal of Hydrogen Energy, 2015. **40**(29): p. 8816-8823.

122. Chen, S., et al., *Steam gasification of sewage sludge with CaO as CO_2 sorbent for hydrogen-rich syngas production.* Biomass and Bioenergy, 2017. **107**: p. 52-62.

123. Wei, L., et al., *Absorption-enhanced steam gasification of biomass for hydrogen production: Effect of calcium oxide addition on steam gasification of pyrolytic volatiles.* International Journal of Hydrogen Energy, 2014. **39**(28): p. 15416-15423.

124. Zhou, C., et al., *Effect of calcium oxide on high-temperature steam gasification of municipal solid waste.* Fuel, 2014. **122**: p. 36-46.

125. Gao, N., et al., *Continuous pyrolysis of sewage sludge in a screw-feeding reactor: Products characterization and ecological risk assessment of heavy metals.* Energy & Fuels, 2017. **31**(5): p. 5063-5072.

126. Manyà, J.J., et al., *Air gasification of dried sewage sludge in a fluidized bed: Effect of the operating conditions and in-bed use of alumina.* Energy & Fuels, 2005. **19**(2): p. 629-636.

127. Gil-Lalaguna, N., et al., *Air-steam gasification of sewage sludge in a fluidized bed. Influence of some operating conditions.* Chemical Engineering Journal, 2014. **248**: p. 373-382.

128. de Andrés, J.M., et al., *Characterisation of tar from sewage sludge gasification. Influence of gasifying conditions: Temperature, throughput, steam and use of primary catalysts.* Fuel, 2016. **180**: p. 116-126.

129. Roche, E., et al., *Air and air-steam gasification of sewage sludge. The influence of dolomite and throughput in tar production and composition.* Fuel, 2014. **115**: p. 54-61.

130. García, G., et al., *Influence of feedstock composition in fluidised bed co-gasification of mixtures of lignite, bituminous coal and sewage sludge.* Chemical Engineering Journal, 2013. **222**: p. 345-352.

131. Nipattummakul, N., et al., *Hydrogen and syngas production from sewage sludge via steam gasification.* International Journal of Hydrogen Energy, 2010. **35**(21): p. 11738-11745.

132. Peng, L., et al., *Co-gasification of wet sewage sludge and forestry waste in situ steam agent.* Bioresource Technology, 2012. **114**: p. 698-702.

133. Chun, Y.N., D.W. Ji, and K. Yoshikawa, *Pyrolysis and gasification characterization of sewage sludge for high quality gas and char production.* Journal of Mechanical Science and Technology, 2013. **27**(1): p. 263-272.

134. Nipattummakul, N., et al., *High temperature steam gasification of wastewater sludge.* Applied Energy, 2010. **87**(12): p. 3729-3734.

135. Schweitzer, D., et al., *Steam gasification of wood pellets, sewage sludge and manure: Gasification performance and concentration of impurities.* Biomass and Bioenergy, 2018. **111**: p. 308-319.

136. Zhang, Q., et al., *Effect of Fe/Ca-based composite conditioners on syngas production during different sludge gasification stages: Devolatilization, volatiles homogeneous*

reforming and heterogeneous catalyzing. International Journal of Hydrogen Energy, 2017. **42**(49): p. 29150-29158.

137. Liu, H., et al., *Co-production of clean syngas and ash adsorbent during sewage sludge gasification: Synergistic effect of Fenton peroxidation and CaO conditioning.* Applied Energy, 2016. **179**: p. 1062-1068.

138. Zhang, Q. and J. Kano, *A new approach for hydrogen generation from sewage sludge.* Bioresource Technology, 2016. **201**: p. 191-194.

139. Watson, J., et al., *Gasification of biowaste: A critical review and outlooks.* Renewable and Sustainable Energy Reviews, 2018. **83**: p. 1-17.

140. Han, J. and H. Kim, *The reduction and control technology of tar during biomass gasification/pyrolysis: An overview.* Renewable and Sustainable Energy Reviews, 2008. **12**(2): p. 397-416.

141. Jaramillo-Arango, A., et al., *Product compositions from sewage sludge pyrolysis in a fluidized bed and correlations with temperature.* Journal of Analytical and Applied Pyrolysis, 2016. **121**: p. 287-296.

142. Choi, Y.-K., M.-H. Cho, and J.-S. Kim, *Air gasification of dried sewage sludge in a two-stage gasifier. Part 4: Application of additives including Ni-impregnated activated carbon for the production of a tar-free and H_2-rich producer gas with a low NH_3 content.* International Journal of Hydrogen Energy, 2016. **41**(3): p. 1460-1467.

143. Chen, H., T. Namioka, and K. Yoshikawa, *Characteristics of tar, NOx precursors and their absorption performance with different scrubbing solvents during the pyrolysis of sewage sludge.* Applied Energy, 2011. **88**(12): p. 5032-5041.

144. Meng, X., et al., *Biomass gasification in a 100 kWth steam-oxygen blown circulating fluidized bed gasifier: Effects of operational conditions on product gas distribution and tar formation.* Biomass and Bioenergy, 2011. **35**(7): p. 2910-2924.

145. Cortazar, M., et al., *Advantages of confining the fountain in a conical spouted bed reactor for biomass steam gasification.* Energy, 2018. **153**: p. 455-463.

146. Anis, S. and Z.A. Zainal, *Tar reduction in biomass producer gas via mechanical, catalytic and thermal methods: A review.* Renewable and Sustainable Energy Reviews, 2011. **15**(5): p. 2355-2377.

147. Fuentes-Cano, D., et al., *The influence of temperature and steam on the yields of tar and light hydrocarbon compounds during devolatilization of dried sewage sludge in a fluidized bed.* Fuel, 2013. **108**: p. 341-350.

148. Phuphuakrat, T., T. Namioka, and K. Yoshikawa, *Tar removal from biomass pyrolysis gas in two-step function of decomposition and adsorption.* Applied Energy, 2010. **87**(7): p. 2203-2211.

149. Schmidt, S., et al., *Catalytic tar removal from bio syngas-Catalyst development and kinetic studies.* Catalysis Today, 2011. **175**(1): p. 442-449.

150. Abu El-Rub, Z., E.A. Bramer, and G. Brem, *Experimental comparison of biomass chars with other catalysts for tar reduction.* Fuel, 2008. **87**(10): p. 2243-2252.

151. Umeki, K., et al., *Reduction of tar and soot formation from entrained-flow gasification of woody biomass by alkali impregnation.* Energy & Fuels, 2017. **31**(5): p. 5104-5110.

152. Pushp, M., et al., *Influence of bed material, additives, and operational conditions on alkali metal and tar concentrations in fluidized bed gasification of biomass.* Energy & Fuels, 2018. **32**(6): p. 6797-6806.

153. Polychronopoulou, K., J.L.G. Fierro, and A.M. Efstathiou, *The phenol steam reforming reaction over MgO-based supported Rh catalysts.* Journal of Catalysis, 2004. **228**(2): p. 417-432.

154. Savuto, E., et al., *Steam reforming of tar model compounds over Ni/Mayenite catalysts: effect of Ce addition.* Fuel, 2018. **224**: p. 676-686.

155. Hoang, T.M.C., et al., *Investigation of Ce-Zr oxide-supported Ni catalysts in the steam reforming of meta-Cresol as a model component for bio-derived tar.* ChemCatChem, 2015. **7**(3): p. 468-478.

156. Kimura, T., et al., *Development of Ni catalysts for tar removal by steam gasification of biomass.* Applied Catalysis B: Environmental, 2006. **68**(3): p. 160-170.

157. Artetxe, M., et al., *Steam reforming of different biomass tar model compounds over Ni/Al_2O_3 catalysts.* Energy Conversion and Management, 2017. **136**: p. 119-126.

158. Ren, J., et al., *Layered uniformly delocalized electronic structure of carbon supported Ni catalyst for catalytic reforming of toluene and biomass tar.* Energy Conversion and Management, 2019. **183**: p. 182-192.

159. Guan, G., et al., *Catalytic steam reforming of biomass tar: Prospects and challenges.* Renewable and Sustainable Energy Reviews, 2016. **58**: p. 450-461.

160. Ammendola, P., et al., *Dual bed reactor for the study of catalytic biomass tars conversion.* Experimental Thermal and Fluid Science, 2010. **34**(3): p. 269-274.

161. Zhu, C., et al., *Mechanism of Ni-catalyzed selective CO cleavage of lignin model compound benzyl phenyl ether under mild conditions.* Journal of the Energy Institute, 2019. **92**(1): p. 74-81.

162. Prats, H., et al., *Room temperature methane capture and activation by Ni clusters supported on TiC(001): Effects of metal-carbide interactions on the cleavage of the C-H bond.* Journal of the American Chemical Society, 2019. **141**(13): p. 5303-5313.

163. Sokolov, S., et al., *Stable low-temperature dry reforming of methane over mesoporous La_2O_3-ZrO_2 supported Ni catalyst.* Applied Catalysis B: Environmental, 2012. **113-114**: p. 19-30.

164. Sun, N., et al., *Effect of pore structure on Ni catalyst for CO_2 reforming of CH_4.* Energy & Environmental Science, 2010. **3**(3): p. 366.

165. Xu, M., et al., *TiO_{2-x}-modified Ni nanocatalyst with tunable metal-support interaction for water-gas shift reaction.* ACS Catalysis, 2017. **7**(11): p. 7600-7609.

166. Xu, M., et al., *Insights into interfacial synergistic catalysis over Ni@TiO_{2-x} catalyst toward water-gas shift reaction.* Journal of the American Chemical Society, 2018. **140**(36): p. 11241-11251.

167. Santamaria, L., et al., *Influence of the support on Ni catalysts performance in the in-line steam reforming of biomass fast pyrolysis derived volatiles.* Applied Catalysis B: Environmental, 2018. **229**: p. 105-113.

168. Miyazawa, T., et al., *Catalytic performance of supported Ni catalysts in partial oxidation and steam reforming of tar derived from the pyrolysis of wood biomass.* Catalysis Today, 2006. **115**(1): p. 254-262.

169. Furusawa, T., et al., *Steam reforming of naphthalene/benzene with various types of Pt- and Ni-based catalysts for hydrogen production.* Fuel, 2013. **103**: p. 111-121.

170. Wu, C. and P.T. Williams, *Hydrogen production by steam gasification of polypropylene with various nickel catalysts.* Applied Catalysis B: Environmental, 2009. **87**(3): p. 152-161.

171. Garbarino, G., et al., *Steam reforming of ethanol-phenol mixture on Ni/Al_2O_3: Effect of Ni loading and sulphur deactivation.* Applied Catalysis B: Environmental, 2013. **129**: p. 460-472.

172. Wang, N., et al., *Facile route for synthesizing ordered mesoporous Ni-Ce-Al oxide materials and their catalytic performance for methane dry reforming to hydrogen and syngas.* ACS Catalysis, 2013. **3**(7): p. 1638-1651.

173. Li, D., et al., *Steam reforming of tar from pyrolysis of biomass over Ni/Mg/Al catalysts prepared from hydrotalcite-like precursors.* Applied Catalysis B: Environmental, 2011. **102**(3): p. 528-538.

174. Wu, G., et al., *Sorption enhanced steam reforming of ethanol on $Ni-CaO-Al_2O_3$ multifunctional catalysts derived from hydrotalcite-like compounds.* Energy & Environmental Science, 2012. **5**(10): p. 8942-8949.

175. Seyedeyn Azad, F., et al., *Production of hydrogen via steam reforming of bio-oil over Ni-based catalysts: Effect of support.* Chemical Engineering Journal, 2012. **180**: p. 145-150.

176. García, L., et al., *Catalytic steam gasification of pine sawdust. Effect of catalyst weight/biomass flow rate and steam/biomass ratios on gas production and composition.* Energy & Fuels, 1999. **13**(4): p. 851-859.

177. Wang, L., et al., *Catalytic performance and characterization of Ni-Co catalysts for the steam reforming of biomass tar to synthesis gas.* Fuel, 2013. **112**: p. 654-661.

178. Chen, J., et al., *Promoting effect of trace Pd on hydrotalcite-derived Ni/Mg/Al catalyst in oxidative steam reforming of biomass tar.* Applied Catalysis B: Environmental, 2015. **179**: p. 412-421.

179. Oh, G., et al., *Ni/Ru-Mn/Al_2O_3 catalysts for steam reforming of toluene as model biomass tar.* Renewable Energy, 2016. **86**: p. 841-847.

180. Kuchonthara, P., et al., *Catalytic steam reforming of biomass-derived tar for hydrogen production with K_2CO_3/NiO/γ-Al_2O_3 catalyst.* Korean Journal of Chemical Engineering, 2012. **29**(11): p. 1525-1530.

181. Fang, Z., et al., *Liquefaction and gasification of cellulose with Na_2CO_3 and Ni in subcritical water at 350 °C.* Industrial & Engineering Chemistry Research, 2004. **43**(10): p. 2454-2463.

182. Ashok, J., et al., *Bi-functional hydrotalcite-derived NiO-CaO-Al_2O_3 catalysts for steam reforming of biomass and/or tar model compound at low steam-to-carbon conditions.* Applied Catalysis B: Environmental, 2015. **172-173**: p. 116-128.

183. Nahil, M.A., et al., *Novel bi-functional Ni-Mg-Al-CaO catalyst for catalytic gasification of biomass for hydrogen production with in situ CO_2 adsorption.* RSC Advances, 2013. **3**(16): p. 5583.

184. Xu, L., H. Song, and L. Chou, *One-pot synthesis of ordered mesoporous NiO-CaO-Al_2O_3 composite oxides for catalyzing CO_2 reforming of CH_4.* ACS Catalysis, 2012. **2**(7): p. 1331-1342.

185. Ji, C., et al., *Environmental and economic assessment of crop residue competitive utilization for biochar, briquette fuel and combined heat and power generation.* Journal of Cleaner Production, 2018. **192**: p. 916-923.

186. Kołodyńska, D., J. Krukowska, and P. Thomas, *Comparison of sorption and desorption studies of heavy metal ions from biochar and commercial active carbon.* Chemical Engineering Journal, 2017. **307**: p. 353-363.

187. Shaaban, M., et al., *A concise review of biochar application to agricultural soils to improve soil conditions and fight pollution.* Journal of Environmental Management, 2018. **228**: p. 429-440.

188. Man, K.Y., et al., *Use of biochar as feed supplements for animal farming.* Critical Reviews in Environmental Science and Technology, 2020: p. 1-31.

189. Yang, S., et al., *Biochar-red clay composites for energy efficiency as eco-friendly building materials: Thermal and mechanical performance.* Journal of Hazardous Materials, 2019. **373**: p. 844-855.

190. Lahijani, P., et al., *Conversion of the greenhouse gas CO_2 to the fuel gas CO via the Boudouard reaction: A review.* Renewable and Sustainable Energy Reviews, 2015. **41**: p. 615-632.

191. Vassilev, S.V., et al., *An overview of the composition and application of biomass ash. Part 1. Phase-mineral and chemical composition and classification.* Fuel, 2013. **105**: p. 40-76.

192. Somerville, M. and S. Jahanshahi, *The effect of temperature and compression during pyrolysis on the density of charcoal made from Australian eucalypt wood.* Renewable Energy, 2015. **80**: p. 471-478.

193. Chen, B., D. Zhou, and L. Zhu, *Transitional adsorption and partition of nonpolar and polar aromatic contaminants by biochars of pine needles with different pyrolytic temperatures.* Environmental Science & Technology, 2008. **42**(14): p. 5137-5143.

194. Weber, K. and P. Quicker, *Properties of biochar.* Fuel, 2018. **217**: p. 240-261.

195. Ahmad, M., et al., *Biochar as a sorbent for contaminant management in soil and water: A review.* Chemosphere, 2014. **99**: p. 19-33.

196. Oh, T.-K., et al., *Effect of pH conditions on actual and apparent fluoride adsorption by biochar in aqueous phase.* Water, Air, & Soil Pollution, 2012. **223**(7): p. 3729-3738.

197. Gupta, A., S.K. Thengane, and S. Mahajani, *CO_2 gasification of char from lignocellulosic garden waste: Experimental and kinetic study.* Bioresource Technology, 2018. **263**: p. 180-191.

198. Scott, S.A., et al., *The rate of gasification by CO_2 of chars from waste.* Proceedings of the Combustion Institute, 2005. **30**(2): p. 2151-2159.

Chapter 3 Sorption-enhanced thermochemical conversion of sewage sludge to syngas with intensified carbon utilization

Published as: Yang, X., Tian, S., Kan, T., Zhu, Y., Xu, H., Strezov, V., Nelson, P., Jiang, Y. (2019) Sorption-enhanced thermochemical conversion of sewage sludge to syngas with intensified carbon utilization, *Applied Energy*, Vol. 254, 113663, https://doi.org/10.1016/j.apenergy.2019.113663.

3.1. Introduction

Developing renewable energy is an effective solution to the energy crisis and climate change, and contributes 32% of the reduction in anthropogenic CO_2 emissions to limit global warming to well below 2 °C [1]. Given its abundant availability and low dependence on geographical and climatic conditions [2, 3], biomass has played an important role in the development of global renewable energy. It is projected that the share of biomass-derived electricity will reach 12% of the total electricity derived from renewable energy in 2040, increasing by more than 30% as compared to the 2013 level [4]. In addition to electricity generation in the power sector, biomass can also be converted to a wide range of end-use fuels and value-added chemicals [5], offering a choice of renewable energy products via various approaches for dedicated conversion.

Thermochemical conversion would be one efficient way to transform biomass into biochar [6, 7], liquid fuel [8], and syngas [9, 10]. Among these products, syngas, which consists mainly of H_2 and CO, has gained increasing interest due to its high calorific value and wide application as a platform feedstock for the production of a variety of liquid biofuels via the Fischer-Tropsch synthesis process [11-13]. Recently, sewage sludge, a kind of municipal solid waste generated in large quantities during wastewater treatment, has been recognized as a promising source of biomass, given its high content of organics and increasing annual generation [14-16]. Thermochemical conversion of sewage sludge to syngas is attracting increasing attention, since it could not only make use of the bioenergy contained in the sewage sludge, but also lead to an effective minimization of this hazardous waste in an environmentally benign and sustainable manner [17].

Considering that H_2 is carbon-free energy and is versatile in the chemical industry, most attention so far has been paid to obtaining H_2 with regard to syngas production from sewage sludge. Recovering the H_2-containing pyrolytic gas as a byproduct has been considered during the pyrolysis of sewage sludge to produce biochar or liquid fuel [18-20]. However, the yield of H_2 is quite low because the inert atmosphere applied for pyrolysis is unfavourable for the production of gaseous components [20]. In order to promote the yield of H_2, the gasification technique that has been widely investigated for biomass conversion was applied to sewage sludge. Such a technique is based on thermal treatment of organic matters with an oxidizing agent, including air [21, 22], steam [17], and oxygen [23]. Among these agents, steam has been proved to be the most effective to gasify biomass for H_2 production [24], while the gasification with air or oxygen leads to a lowered H_2 purity [10]. As for steam gasification of sewage sludge, Nipattummakul et al. [17] concluded that the yield of H_2 could be improved with an increasing steam-to-sludge ratio, since H_2 is directly produced through the steam reforming reactions, especially the water-gas shift (WGS) reaction (Eq. 1).

$$CO+H_2O \leftrightharpoons CO_2+H_2\ ,\ \Delta H_{298\ K} = -41.2\ kJ/mol \qquad (1)$$

However, the WGS reaction would inevitably result in the generation of CO_2 along with H_2, limiting the purity of H_2 in the gas stream obtained to 40-50 vol% [25]. Recently, steam gasification of sewage sludge or other biomass enhanced with CO_2 sorption was proposed to further improve the H_2 yield and purity. In this process, a CO_2 sorbent, typically CaO, is employed to *in situ* capture the CO_2 released directly from the biomass matrix and generated due to the steam reforming reactions of CO or light hydrocarbons, driving the whole biomass conversion process to the direction of producing more H_2 [26-28]. The purity of H_2 in the gas stream obtained after

the sorption-enhanced steam gasification of biomass can be increased to as high as 70-80 vo% [29, 30].

Technically, H_2 production from sewage sludge can be substantially improved by steam gasification enhanced with CO_2 sorption. However, the improvement in H_2 production mainly comes from the hydrogen in the steam rather than that in the sewage sludge. Furthermore, this is realized at the cost of the utilization efficiency of carbon, which is the most abundant element in the sewage sludge. Here, in order to intensify the carbon utilization of sewage sludge, we propose a novel two-stage sorption-enhanced (TSSE) thermochemical conversion process, where the production of H_2 and CO is separated and CO-rich syngas is obtained through manipulating the CaO-based CO_2 carrying cycle for capture and conversion of the carbon in sewage sludge. In this chapter, the technical feasibility of the proposed process was experimentally demonstrated, the key factors influencing the syngas production and carbon utilization of sewage sludge were investigated, and the mechanism for intensification of carbon utilization was clarified.

3.2. Experimental section

3.2.1. Sample preparation

The sewage sludge used in this chapter was obtained prior to anaerobic digestion from a municipal wastewater treatment plant in Sydney, Australia. The moisture content of the raw sewage sludge as received was 95.6%, and the proximate and ultimate analysis of the sewage sludge after dewatering at 105 ℃ for 16 h are shown in Table 3.1. The contents of volatile organics and the main elements, including C, H, N, and S, in the dewatered sewage sludge accorded with the typical values as reported in previous studies [14].

The sewage sludge pellets blended with different amounts of CaO were prepared using the following method. A calculated amount of CaO (Reagent grade, Sigma-Aldrich) was mixed with the sewage sludge under magnetic stirring for 3 h at room temperature. Then, the resulting slurry was dried at 105 ℃ for 16 h, followed by grinding, pressing, and sieving to obtain SS-CaO pellets (0.85-1.00 mm) ready for tests. For convenience, the SS-CaO pellets prepared were notated as SS (without the addition of CaO), Ca/SS-1:9, Ca/SS-3:7, Ca/SS-1:1, Ca/SS-7:3, and Ca/SS-9:1, in which x:y indicates the mass ratio of CaO to sludge (dry basis).

Table 3.1. Ultimate and proximate analysis of the sewage sludge after dewatering.

Proximate Analysis [a]	**(wt%, dry basis)**	**Ultimate analysis** [b]	**(wt%, dry ash free basis)**
Moisture	13.6	C	47.1
Volatile matter	60.1	H	7.7
Ash	21.8	N	8.8
Fixed carbon	4.5		

[a] The proximate analysis was conducted using a thermogravimetric analyzer (TGA, TGA/DSC 1, Mettler Toledo).
[b] The ultimate analysis was conducted using an elemental analyzer (Vario EL III, Elementar).

3.2.2. Test of the prepared SS-CaO pellets

Temperature-programmed decomposition (TPD) of SS and Ca/SS-1:1 was performed using a thermogravimetric analyzer (TGA, TGA/DSC 1, Mettler Toledo). Approximately 30 mg of the sample was placed in a 70 μL alumina pan and heated from room temperature to 1000 °C at a rate of 10 °C/min under a N_2 flow of 100 mL/min. A fourier transform infrared (FT-IR) spectrometer (Nicolet 6700, Thermo Scientific) was connected to the TGA to simultaneously monitor the change in gas composition in the reaction atmosphere, and the FT-IR spectra were recorded every 0.52 min with a 4 cm^{-1} resolution and 32 scans in the range of 4000-600 cm^{-1}. The H_2 in the

atmosphere was monitored every 1.5 min using a gas chromatograph (GC, 7890B, Agilent) equipped with a 5A molecular sieve column and a thermal conductivity detector (TCD).

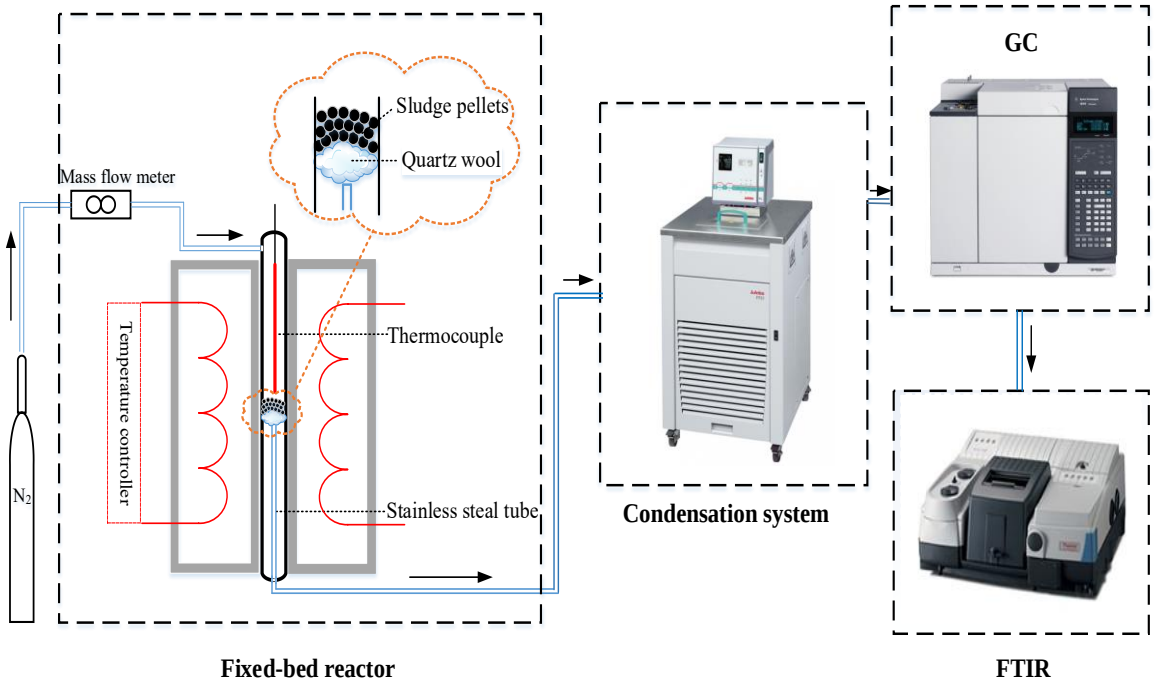

Fig. 3.1. Illustration of the experimental setup used for thermochemical conversion of sewage sludge in this chapter.

Thermochemical conversion tests of the prepared SS-CaO pellets were carried out in a fixed-bed reactor with a stainless steel tube (inner diameter: 6 mm) at atmospheric pressure, and the whole experimental setup is illustrated in Fig. 3.1. During the temperature-programmed isothermal pyrolysis of SS and Ca/SS-1:1, 0.25 g of SS or 0.50 g of Ca/SS-1:1 was loaded on the quartz wool supported in the tube. Then, The loaded sample was heated from room temperature to 350 °C at a rate of 30 °C/min and held for 30 min, and then heated to 950 °C at a rate of 30 °C/min with the temperature held for 30 min every 100 °C under a N_2 flow of 15 mL/min. During syngas production tests of the SS-CaO pellets in the proposed TSSE thermochemical conversion process, an appropriate amount of the SS-CaO pellet sample was loaded in the tube. Under a N_2 flow of 10

mL/min, the sample was heated to and kept at 550 °C for 30 min to produce H_2; after that, the remaining sample was heated to and kept at 750 °C for another 30 min to produce CO. During the experiment, the condensation gas (tar) was condensed and collected in the condensation system. The concentrations of H_2 and CO in the effluent gas from the fixed-bed reactor were monitored on-line by a 7890B GC, while CO_2, CH_4, C_2H_4, and C_2H_6 in the effluent gas were detected on-line by a Nicolet 6700 FT-IR spectrometer. The data acquisition interval for both GC and FT-IR was every 1.5 min.

3.2.3. Sample characterization

FT-IR spectra of the freshly prepared SS and Ca/SS-1:1, as well as the residues after isothermal pyrolysis at different temperatures, that were mixed with KBr powder in a mass ratio of 1:200, were recorded by a Nicolet 6700 FT-IR spectrometer with a 4 cm^{-1} resolution and 32 scans in the range of 4000-600 cm^{-1}. Powder X-ray diffraction (XRD) was performed to identify the crystal phase in the sludge residues after pyrolysis using an X-ray diffractometer (X'Pert PRO, PANalytical) with Cu Kα radiation in the 2θ range of 10–80°. The carbon and hydrogen contents of the freshly prepared SS-CaO pellets and their residues after pyrolysis were determined using an elemental analyzer (Vario EL III, Elementar). The percentage of residual sludge was expressed as the mass fraction of the solid sample after N_2-TPD with the initial solid sample.

The remaining carbon (η_C) in the sludge residues of SS and Ca/SS-1:1 after isothermal pyrolysis at different temperatures is calculated according to the following Eq. 2:

$$\eta_C\ (\%) = \frac{C_R}{C} \times 100\% \qquad (2)$$

where C_R is the mass percentage of the carbon remaining in the sludge residues of SS or Ca/SS-1:1 after pyrolysis at a certain temperature, %; C is the mass percentage of the total carbon in the freshly prepared SS or Ca/SS-1:1, %.

The utilization efficiency of carbon in the sludge to CO (η_{CO}) is calculated according to the following Eq. 3:

$$\eta_{CO}\,(\%) = \frac{12 \times Y_{CO}}{22.4 \times C \times 1000} \times 100\% \qquad (3)$$

where Y_{CO} is the yield of CO, NmL/$g_{dry\ SS}$; C is the mass percentage of the total carbon in the freshly prepared SS-CaO pellets, %.

The utilization efficiency of hydrogen in the freshly prepared SS-CaO pellets to H_2 is calculated according to the following Eq. 4:

$$\eta_{H_2}\,(\%) = \frac{2 \times Y_{H_2}}{22.4 \times H \times 1000} \times 100\% \qquad (4)$$

where Y_{H2} is the yield of H_2, NmL/$g_{dry\ SS}$; H is the mass percentage of the total hydrogen in the freshly prepared sludge pellets, %.

3.3. Results and discussion

3.3.1. Investigation of the process integration scheme

Process integration of the sludge pyrolysis and the CaO-based CO_2 carrying cycle is studied by comparison of the thermochemical behaviour of SS and Ca/SS-1:1 during the temperature-programmed decomposition in a N_2 atmosphere (N_2-TPD) as shown in Fig. 3.2. The freshly prepared SS is pyrolyzed following four stages. As shown in Fig. 3.2a, the weight loss below 185 °C results largely from the removal of moisture in the sludge matrix. The largest weight loss

(~52.2%), accompanied by the appearance of CO_2, H_2O, and light hydrocarbons in the reaction atmosphere, is observed in the temperature region of 185 °C-550 °C. This is due to devolatilization of the sludge [31], during which we could notice that a considerable proportion of the carbon in the sludge is released in the form of CO_2. Most of the H_2 is generated from 550 °C to 800 °C due to cracking of the sludge tar [32], and the generation of CO is not notable until the temperature was over 850 °C.

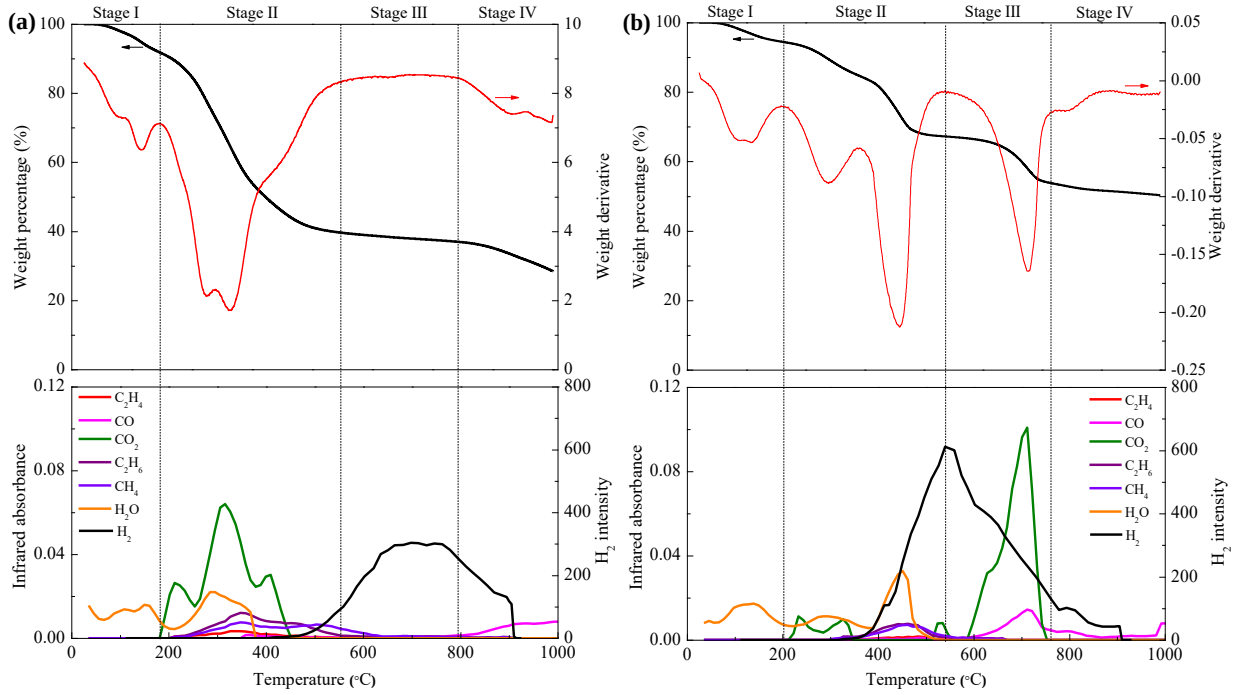

Fig. 3.2. N_2-TPD profiles of the freshly prepared (a) SS and (b) Ca/SS-1:1.

It should be noted that the CaO is converted into $Ca(OH)_2$ in the sewage sludge slurry during the SS-CaO pellets preparation. Upon introduction of CaO into the sludge matrix, the thermochemical behaviour of the as-derived mixture (Ca/SS-1:1) exhibits a significant difference as compared to that of SS. It is clearly observed in Fig. 3.2b that the strong CO_2 peak disappears in stage II, while a sharp H_2O peak appears at ~450 °C, a temperature which is appreciably lower than that for

$Ca(OH)_2$ decomposition [33]. This is attributed to the carbonation reaction between $Ca(OH)_2$ and the CO_2 released due to sludge pyrolysis (Eq. 5). There is a notable weight loss in stage III (Fig. 3.2b), which is accompanied by the appearance of the CO_2 and CO peaks. This indicates the occurrence of $CaCO_3$ decomposition and reverse Boudouard (Eq. 6) reactions in this temperature region. It can be concluded that $Ca(OH)_2$ works as a CO_2 carrier in the sludge matrix, capturing the CO_2 generated during sludge pyrolysis and releasing it to gasify the pyrolysis-derived sludge char for CO production at higher temperatures. It is worth mentioning that 22.1% of the sludge components remain after N_2-TPD of Ca/SS-1:1, which is appreciably lower than that of SS (28.5%) and close to the content of ash in the sludge (21.8%). In addition, it is shown in Fig. 3.2 that the generation of both H_2 and CO shifts to lower temperatures when $Ca(OH)_2$ participates in the sludge pyrolysis. Thus, these observations clearly reveal that H_2 and CO production could be significantly enhanced on account of integrating the CaO-based CO_2 carrying cycle into sludge pyrolysis.

$$Ca(OH)_2 + CO_2 \rightarrow CaCO_3 + H_2O,\ \Delta H_{298\,K} = -69.0\ kJ/mol \quad (5)$$

$$C + CO_2 \leftrightharpoons 2CO,\ \Delta H_{298\,K} = +172.4\ kJ/mol \quad (6)$$

Transformation of the Ca species during N_2-TPD of Ca/SS-1:1 is revealed in Fig. 3.3. The only Ca species identified in the freshly prepared Ca/SS-1:1 is $Ca(OH)_2$, which is formed through the hydration reaction between CaO and H_2O in the sludge slurry during sample preparation, and starts to capture CO_2 through the carbonation reaction at ~350 °C. The identification of $CaCO_3$ in the sludge residues after pyrolysis at 450 °C supports the occurrence of the carbonation reaction of $Ca(OH)_2$ (Eq. 5) in Fig. 3.2b. It is shown in Fig. 3.3 that the $CaCO_3$ phase, formed by carbonation of $Ca(OH)_2$ below 500 °C [34, 35] and CaO at higher temperatures [36], could be identified in the

temperature range of 350 °C to 650 °C. This indicates that the temperature regions where the sludge releases CO_2 due to pyrolysis (Fig. 3.2a) and $Ca(OH)_2$ or CaO captures CO_2 due to carbonation could fully overlap, which is an important basis for the efficient operation of the proposed process to intensify the carbon utilization of sludge.

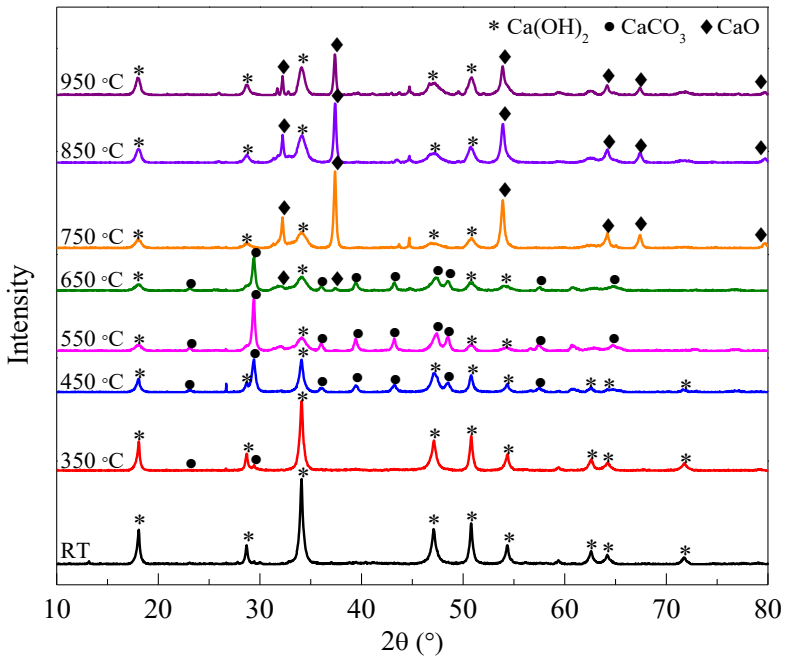

Fig. 3.3. XRD patterns of the freshly prepared Ca/SS-1:1 and its corresponding residues after isothermal pyrolysis at various temperatures.

The influence of the presence of Ca species on the pyrolysis characteristics of the sludge during N_2-TPD was further investigated by analyzing the change in the FT-IR spectra as shown in Fig. 3.4. In the freshly prepared SS, the bands related to the stretching vibrations of O–H (~3400 cm^{-1}), $–CH_2–$ (~2925 and 2850 cm^{-1}), $–CH_3$ (~2960 and 1440 cm^{-1}), C=O (~1650 cm^{-1}), COO^- (~1400 cm^{-1}), and Si–O–Si (~1030 cm^{-1}); and the bending vibration of N–H (~1560 cm^{-1}) are identified [37, 38]. The most significant change in the FT-IR spectra regarding SS is the gradual disappearance of the $–CH_2$, $–CH_3$, C=O, and COO^- bands as the temperature increases from 350

to 550 °C. This indicates the destruction of aliphatic chains and carbonyl groups in the sludge matrix, and therefore results in the generation and release of CO_2, CO, and light hydrocarbons as shown in Fig. 3.2a. No evident bands, except Si–O–Si, are observed in Fig. 3.4a after 650 °C, revealing that the sample is largely mineralized. With regard to Ca/SS-1:1, there are no new bands identified in the spectra except the ones indicating Ca species, viz., $Ca(OH)_2$ (~3640 cm^{-1}) and $CaCO_3$ (~1415 and 870 cm^{-1}) [39], whose change in the spectra is in line with the XRD analysis in Fig. 3.3. The change in the bands related to O–H, $–CH_2–$, $–CH_3$, C=O, $COO^–$, and N–H in the spectra regarding Ca/SS-1:1 do not differ much when compared to those regarding SS. However, the Si–O–Si band become stronger as the temperature increased, indicative of an enhanced mineralization effect. This observation is supported by the weight loss analysis in Fig. 3.2.

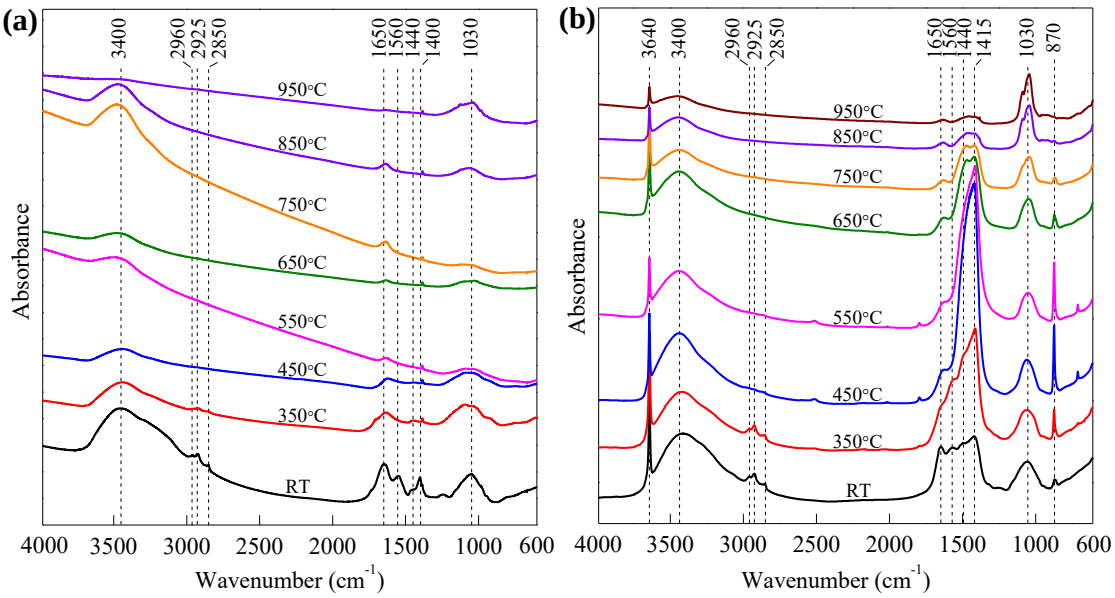

Fig. 3.4. FT-IR spectra of the freshly prepared (a) SS and (b) Ca/SS-1:1, and their corresponding residues after isothermal pyrolysis at various temperatures.

3.3.2. Production of syngas with separated H_2- and CO-rich streams

Temperature-programmed isothermal pyrolysis of SS and Ca/SS-1:1 at selected temperatures was performed to further compare their syngas production characteristics (Fig. 3.5). With regard to H_2 production, the temperature-dependence of yield exhibits different characteristics between SS and Ca/SS-1:1. Without the addition of CaO (SS), the production of H_2 lasts for a wide temperature range from 550 °C to 950 °C. This is in line with the results in Fig. 3.2a and the conclusions from other studies that a sufficiently high temperature is required to achieve an acceptable yield of H_2 from sludge [10]. However, almost 85% of the total yield of H_2 from Ca/SS-1:1 is attributed to the pyrolysis of sludge at temperatures between 450 °C and 650 °C, where carbonation of $Ca(OH)_2$ or CaO to capture the CO_2 released due to sludge pyrolysis occurs as discussed above. In fact, the increase in the total H_2 yield from 68.1 $NmL/g_{dry\ SS}$ for SS to 107.5 $NmL/g_{dry\ SS}$ for Ca/SS-1:1 (Fig. 3.6) comes from the enhancement in H_2 production in this temperature range, indicating that the occurrence of the $Ca(OH)_2$ or CaO carbonation reaction would facilitate H_2 production from sludge at lower temperatures. This is probably due to the sorption-enhanced steam gasification effect that promotes the WGS reaction (Eq. 1) via capture of CO_2 by $Ca(OH)_2$ or CaO [40]. In addition, the enhanced H_2 production would also be associated with the catalytic effect of CaO on tar cracking [32, 41].

The production of CO from sludge is more sensitive to temperature than that of H_2, since it is intensively generated within 850-950 °C for SS and 650-750 °C for Ca/SS-1:1. The sludge would need to be pyrolyzed at elevated temperatures, higher than 850 °C, if the production of CO is required. However, with the addition of CaO, CO is produced during sludge pyrolysis at a temperature of as low as 650 °C. This is determined by the thermodynamics of the CaO-based CO_2 carrying cycle, where the CO_2 captured at lower temperatures starts to be released due to $CaCO_3$ decomposition at such a temperature (Figs. 3.3 and 3.4) [36]. Thus, it is conceivable that the

intensive release of CO_2 at temperatures between 650 °C and 750 °C drove the reverse Boudouard reaction with sludge char for CO production. In addition to the facilitation in CO production, the

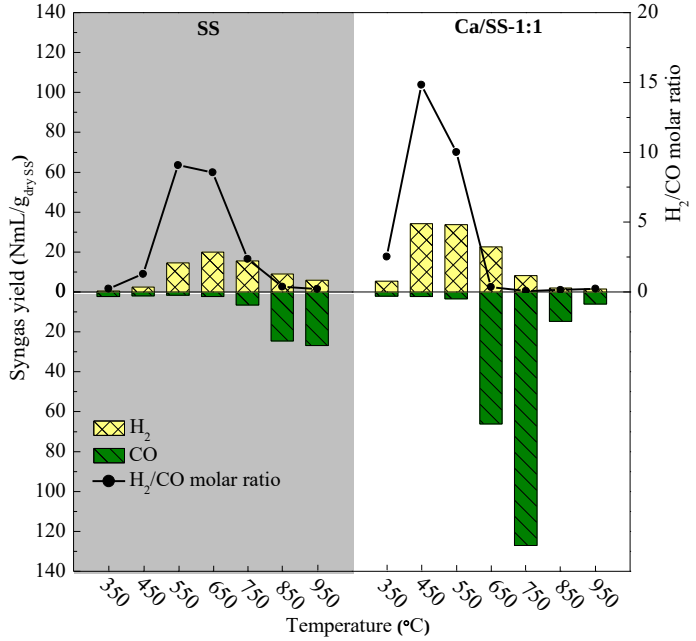

Fig. 3.5. Yields of H_2 and CO during temperature-programmed isothermal pyrolysis of SS and Ca/SS-1:1, respectively, at selected temperatures.

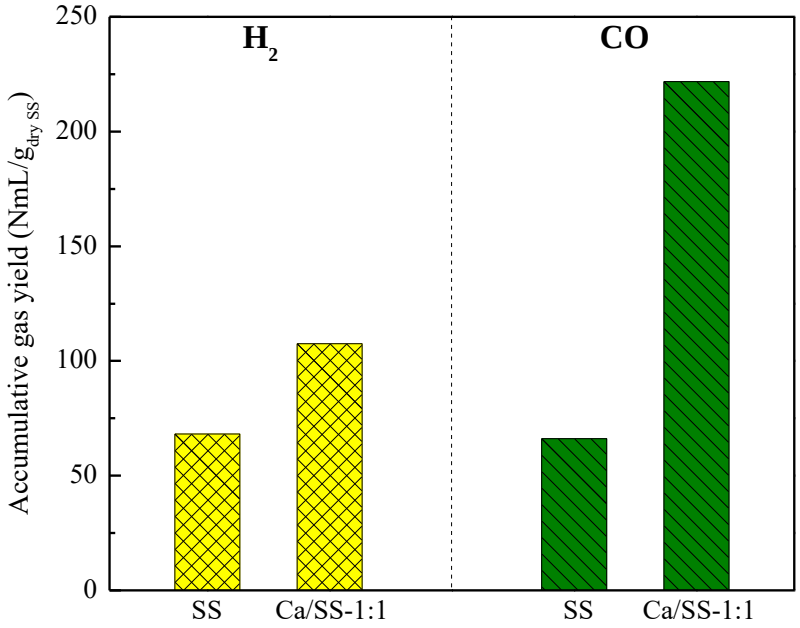

Fig. 3.6. The total yield of H_2 and CO during the temperature-programmed isothermal pyrolysis of SS and Ca/SS-1:1 from 350 °C to 950 °C.

total yield of CO from Ca/SS-1:1 (221.8 NmL/$g_{dry\ SS}$) is more than 3 times that from SS (66.1 NmL/$g_{dry\ SS}$) as shown in Fig. 3.6. It is clear that the significant increase in CO yield resulted from the utilization of CO_2 released during sludge pyrolysis which is captured by $Ca(OH)_2$ or CaO and converted into CO via the reverse Boudouard reaction (Eq. 6) with sludge char.

The H_2/CO molar ratio in the syngas produced from Ca/SS-1:1 is higher than that from SS at temperatures below 550 °C, and lower than that from SS at temperatures above 650 °C. This means that the integration of the CaO-based CO_2 carrying cycle into sludge pyrolysis improves the selectivity to H_2 production at lower temperatures and to CO production at higher temperatures. The selectivity of both H_2 to CO at 550 °C and CO to H_2 at 750 °C is over 10:1 (molar ratio) for Ca/SS-1:1 as shown in Fig. 3.5, offering an opportunity to control the H_2/CO molar ratio in the syngas produced by performing the pyrolysis in sequence at selected temperatures. In fact, this is an important consideration when we proposed the TSSE thermochemical conversion process in this chapter.

Fig. 3.7 exhibits the performance of syngas production from SS-CaO pellets using the proposed TSSE pyrolysis process at various mass ratios of CaO to sludge (dry basis). The temperatures are determined as 550 °C and 750 °C, which were proved to be optimal for the production of H_2 and CO, respectively, in Fig. 3.5. During the H_2 production stage at 550 °C, the yield of H_2 increases with the CaO/sludge mass ratio, and reaches 171.8 NmL/$g_{dry\ SS}$ at a CaO/sludge mass ratio of 9:1, almost 9 times as high as the yield without the addition of CaO (Fig. 3.7a). In addition to the find in previous studies that the presence of CaO could promote tar cracking to increase H_2 production [32, 41], we would like to explain the role of CaO in the H_2 production stage according to Le Chatelier's principle in this chapter. Considering that Ca species would exist in the form of

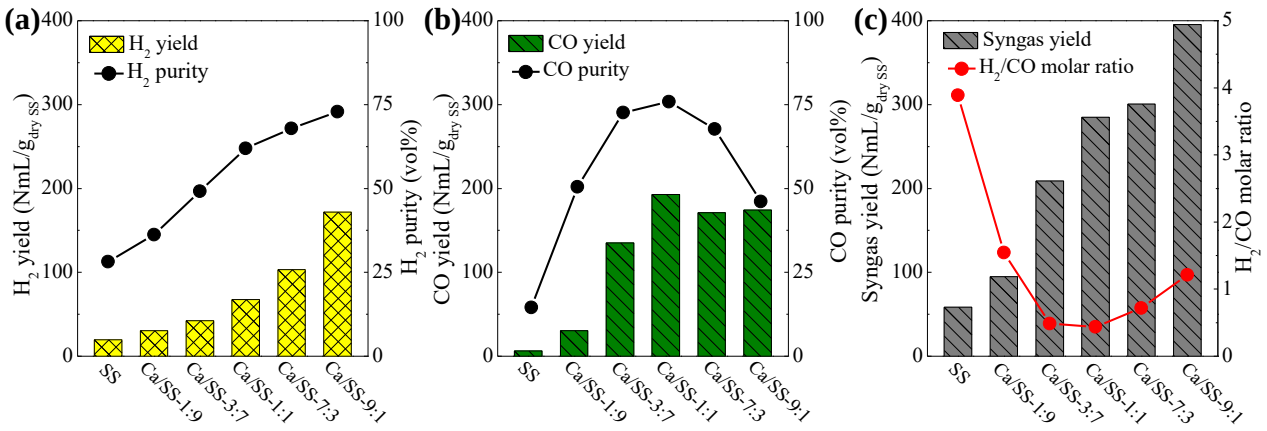

Fig. 3.7. Syngas production performance of sewage sludge in the proposed TSSE pyrolysis process: (a) H_2 yield and purity generated at the first stage; (b) CO yield and purity generated at the second stage; (c) syngas yield and the CO/H_2 molar ratio, as a function of the mass ratio of CaO to sewage sludge. Experimental conditions: 550 °C for the first stage, 750 °C for the second stage.

$Ca(OH)_2$ in the sludge matrix at temperatures below 550 °C [33][34], it is actually $Ca(OH)_2$ that captures the CO_2 released from sludge and provides steam as a hydrogen feedstock through the carbonation reaction (Eq. 5), shifting the equilibrium of the WGS reaction (Eq. 1) forward to H_2 production. Hence, as is shown in the global reaction (Eq. 7), more H_2 would be produced with higher $Ca(OH)_2$ contents in the sludge, resulting in higher H_2 concentrations in the gas stream obtained after pyrolysis at 550 °C. This explanation can be supported by the time evolution of the CO_2 release rate at this stage (Fig. 3.8). It was clearly observed in Fig. 3.8 that less CO_2 is released from each gram of the dry sewage sludge with a higher CaO/sludge mass ratio in the H_2 production stage, indicating that more CO_2 is captured by $Ca(OH)_2$ to promote the WGS reaction.

$$Ca(OH)_2 + CO \rightarrow CaCO_3 + H_2\ ,\ \Delta H_{298\,K} = -110.2\ kJ/mol \qquad (7)$$

Unlike the situation in the H_2 production stage, the yield of CO during the CO production stage at 750 °C do not keep increasing with the mass ratio of CaO to sludge after the yield and the

concentration of CO reaching 192.8 NmL/$g_{dry\ SS}$ and 75.8 vol%, respectively, at a CaO/sludge mass ratio of 1:1. This is not surprising when we realize that the excess $Ca(OH)_2$ which did not participate in the capture and release of CO_2, would not benefit the reverse Boudouard reaction for CO production in this stage. From this point of view, the recommended mass ratio of CaO to SS would be 1:1 for syngas production using the proposed TSSE pyrolysis process, during which gas streams with a high purity of H_2 and CO, respectively, could be obtained from the two stages. Typically, 209.0-300.5 NmL/$g_{dry\ ss}$ of the CO-rich syngas with a H_2/CO molar ratio of 0.4-0.7 is produced from SS-CaO pellets through the TSSE pyrolysis process proposed in this chapter.

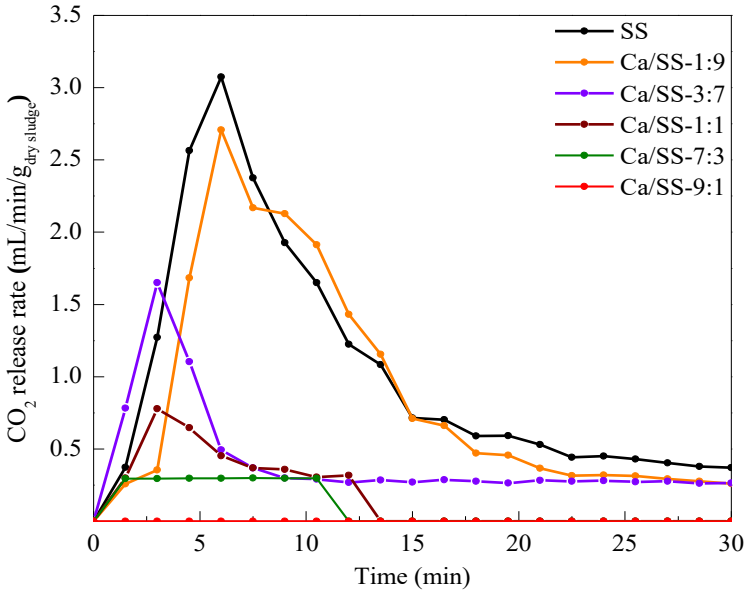

Fig. 3.8. CO_2 release rate of different sludge samples as a function of time during the first stage for H_2 production at 550 °C.

3.3.3. Improvement in carbon utilization efficiency

The utilization efficiency of carbon in the sludge during the proposed TSSE pyrolysis process, relying on the CaO-based CO_2 carrying cycle, was studied by analyzing the change in the remaining carbon (Eq. 2) and the accumulative conversion of sludge carbon into CO (Eq. 3) in

Fig. 3.9. The remaining carbon in the SS residues significantly decreases to less than 40% after the isothermal pyrolysis at 450 °C, and experiences a marginal decrease as the temperature increases. After the isothermal pyrolysis at 950 °C, still 25.2% of the carbon remains as sludge chars in the residues. The significant loss of carbon observed at ~450 °C is due to the devolatilization of sludge as discussed above in Fig. 3.2a, resulting in the release of sludge carbon in the form of tars [42] and carbon-containing gases (CO, CO_2, and light hydrocarbons). However, in the presence of $Ca(OH)_2$ (Ca/SS-1:1), the amount of remaining carbon is higher than that in the pyrolysis residues of SS under 600 °C, which results from the capture of CO_2 released from the sludge and storage of it in the form of $CaCO_3$. After 600 °C, the remaining carbon in the Ca/SS-1:1 residues becomes lower than that in the SS residues, which is accompanied by the significantly higher accumulative conversion of sludge carbon into CO of Ca/SS-1:1 as compared to SS. The largest difference in both the remaining carbon and the accumulative conversion of sludge carbon into CO were observed at 750 °C, indicating an efficient integration of $CaCO_3$ decomposition and reverse Boudouard reactions at this temperature. Hence, the mechanism that the CaO-based CO_2 carrying cycle enhances the carbon utilization efficiency can be concluded as the gasification of sludge carbon into CO at temperatures of ~750 °C using the CO_2 released from sludge at lower temperatures.

The elemental availability of the proposed TSSE pyrolysis process was further explored by comparing the conversion of the carbon in the sludge into CO (Eq. 3) and of the total hydrogen in the sample into H_2 (Eq. 4) at various CaO/sludge mass ratios (Fig. 3.10). The hydrogen conversion is less than 8%, and do not gradually increase as the yield of H_2 do (Fig. 3.7a) with increasing CaO/sludge mass ratios. This reveals that the hydrogen availability is not sensitive to the CaO/sludge mass ratio, albeit more steam is introduced, through the decomposition of $Ca(OH)_2$,

for H_2 production as the addition of CaO increased in the SS-CaO samples (Table 3.2). However, the conversion of carbon is much higher than that of hydrogen when the CaO/sludge mass ratio is over 3:7, and could reach a conversion efficiency of as high as 20.4% at the CaO/sludge mass ratio of 1:1. When the syngas production performance of Ca/SS-1:1 is further compared with that reported in other studies (Table 3.3), it can be observed that the H_2 yield in this study is higher than that from pyrolysis of sewage sludge reported in most of the other studies, and comparable with the yield of H_2 produced from pyrolysis of other biomass. Regardless of the biomass used, the yield of H_2 could be significantly improved upon introduction of steam, albeit sewage sludge appears to be a less competitive candidate for H_2 production via steam gasification as compared with other biomass. However, the yield of CO in this study is remarkably higher than those from pyrolysis or steam gasification of sewage sludge and other biomass, revealing clearly that the TSSE thermochemical conversion process proposed in this study can realize a significantly improved utilization of carbon in the biomass, in the form of CO, in comparison to other conventional processes.

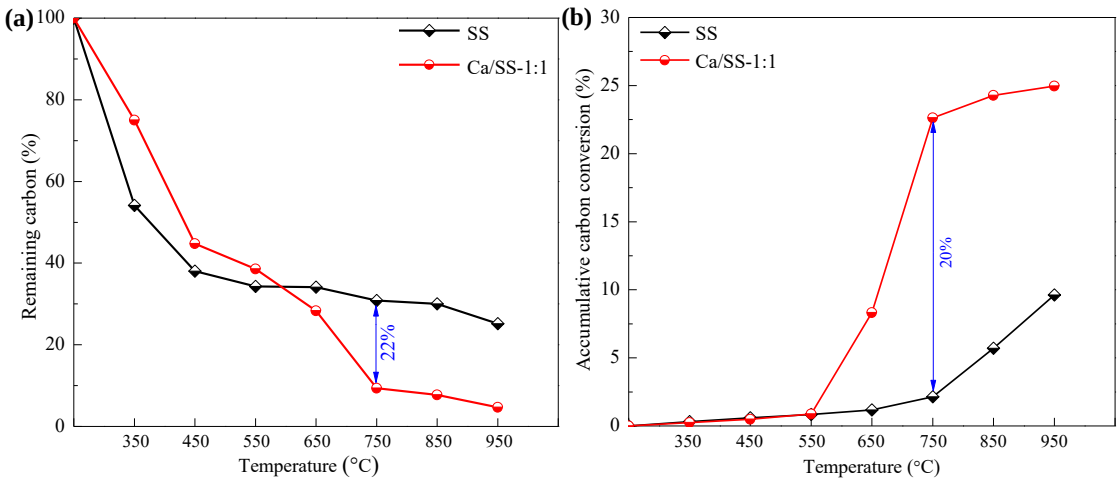

Fig. 3.9. The (a) remaining carbon in the sludge residues and (b) accumulative conversion of sludge carbon into CO after the temperature-programmed isothermal pyrolysis at various temperatures.

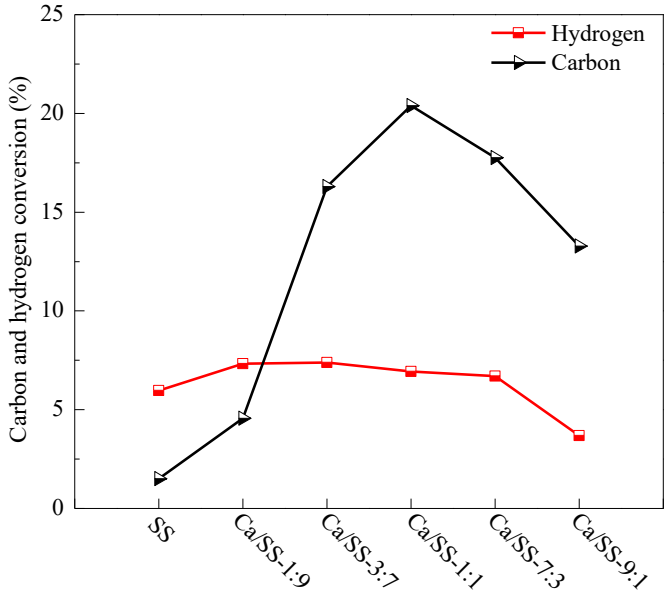

Fig. 3.10. Total utilization efficiency of carbon in the sludge to CO and hydrogen in the sample to H_2 during the proposed TSSE pyrolysis process.

Table 3.2. The molar ratio of bonded water in $Ca(OH)_2$ to carbon in the freshly prepared SS-CaO samples.

Sample	Water/carbon molar ratio
SS	0
Ca/SS-1:9	0.1
Ca/SS-3:7	0.2
Ca/SS-1:1	0.5
Ca/SS-7:3	1.1

Table 3.3. Summary of syngas production via sorption-enhanced thermochemical conversion of biomass

Biomass	Technique [a]	CaO dosage	Temperature (°C)	H_2 yield ($mL/g_{dry\ basis}$)	CO yield ($mL/g_{dry\ basis}$)	Ref.
Southern pine bark	SG	1 [b]	600	850	80	[43]
Japanese oak	SG	2 [c]	600	500 [g]	-	[44]
Pine tree	SG	0.5 [c]	700	210 [g]	-	[45]
Sawdust	P	2 [d]	850 [e]	90	75	[46]
SS	SG	0.43 [d]	600	130 [g]	80 [g]	[47]
SS	SG	0.7 [c]	650	125	-	[48]
SS	P	0.43 [d]	600	40	20	[49]
SS	**P**	**1 [d]**	**550/750 [f]**	**87 [g]**	**198 [g]**	**This chapter**

[a]. SG and P are short for steam gasification and pyrolysis, respectively.
[b]. The molar ratio of CaO to biomass.
[c]. The molar ratio of Ca to carbon in the biomass.
[d]. The mass ratio of CaO to biomass.
[e]. The sample was heated at a rate of 40 °C/min to 850 °C.
[f]. The sample was treated in sequence at 550 °C and 750 °C.
[g]. The value was expressed in the normal volume per gram of biomass in dry basis, $NmL/g_{dry\ basis}$.

3.3.4. Operation mechanism of the proposed TSSE thermochemical conversion process

Based on the discussions above, we can summarize the operation mechanism of the proposed TSSE thermochemical conversion process for syngas production from sewage sludge as follows (Fig. 3.11). The first stage operated at temperatures below 600 °C is based on the conventional thermochemical biomass conversion process integrated with CaO. In which, $Ca(OH)_2$ provides steam to reform CO and the light hydrocarbons generated due to sludge devolatilization, producing H_2 and CO_2. The CO_2 generated, due to both the steam reforming reactions and the sludge devolatilization, is captured by $Ca(OH)_2$ or CaO and stored in the sludge matrix in the form of $CaCO_3$, which drives the pyrolysis of sludge towards the direction in favour of H_2 production. Although H_2 production is enhanced due to the sorption of CO_2 by CaO, quantities of carbon

remain in the sludge residues, in the form of $CaCO_3$ and char, without an effective utilization. Therefore, a second-stage operated at a higher temperature of 700-800 °C is introduced into the thermochemical conversion process to intensify the carbon utilization efficiency. In this stage, the stored CO_2 is released due to $CaCO_3$ decomposition and *in situ* gasifies sludge char to produce CO via the reverse Boudouard reaction (Eq. 6). Therefore, compared to the conventional thermochemical H_2 production enhanced by CaO, the proposed two-stage process has the following two advantages: (1) carbon utilization of the sewage sludge is intensified by producing CO from the byproducts, viz., CO_2 and char, during pyrolysis; (2) separate collection of the gas streams rich in H_2 and CO, respectively, can be achieved through the two stages, making it possible to adjust the molar ratio of CO to H_2 in the syngas produced for a downstream synthesis of chemicals or fuels.

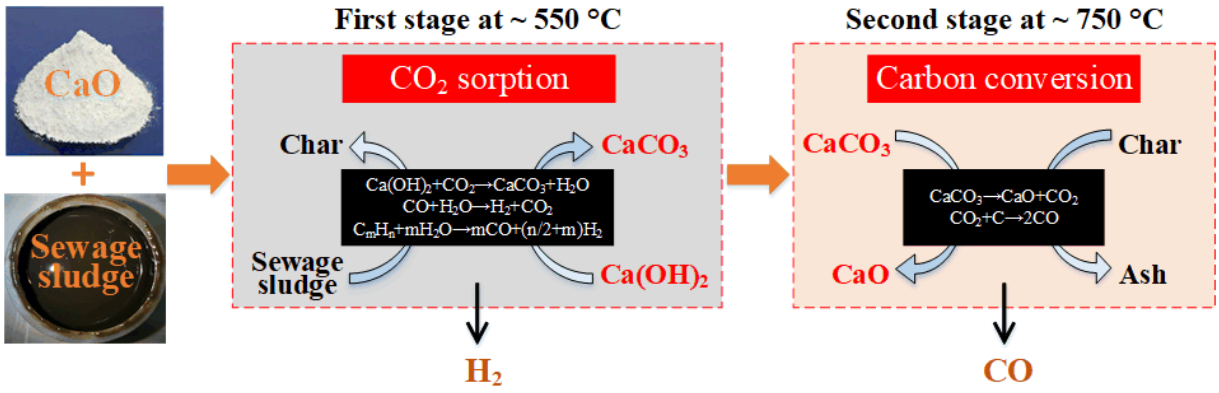

Fig. 3.11. Process integration mechanism of the TSSE thermochemical conversion of sewage sludge.

Nonetheless, there is still room for further improvement of the proposed TSSE thermochemical conversion process considering its practical application. On one hand, the process requires to be operated at a high CaO-to-sludge mass ratio of around 1:1. However, considering that the sludge ash after the second stage is rich in free CaO (Fig. 3.12), the actual usage of lime could be substantially reduced by recycling portions of the CaO-rich sludge ash as a substitute of the fresh

limestone. Furthermore, the spent CaO, which is sintered and diluted with the ash components of sludge after several recycling cycles, would be potentially suitable as raw materials for the cement industry [50]. On the other hand, CO_2 could still be detected in the gas streams obtained at both stages (Fig. 3.13). Alternatively, highly efficient and cost-effective CaO-based CO_2 sorbents could be employed to improve the CO_2 capture performance during the first stage, while the fluidized-bed reactor mode deserves to be explored to promote the CO_2 gasification of char during the second stage. In addition, incorporation of steam gasification into the first stage is an approach worth studying to further improve the yield and purity of the syngas produced from sewage sludge through the TSSE thermochemical conversion process proposed.

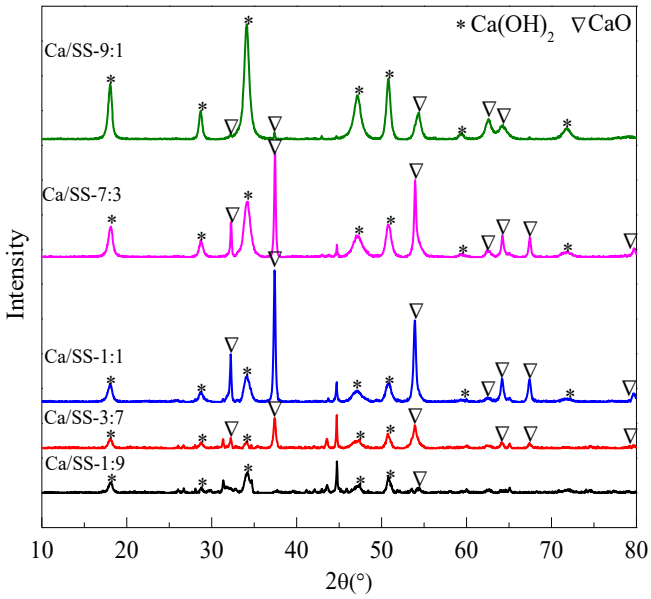

Fig. 3.12. XRD patterns of the corresponding residues after the TSSE thermochemical conversion of different SS-CaO pellets prepared.

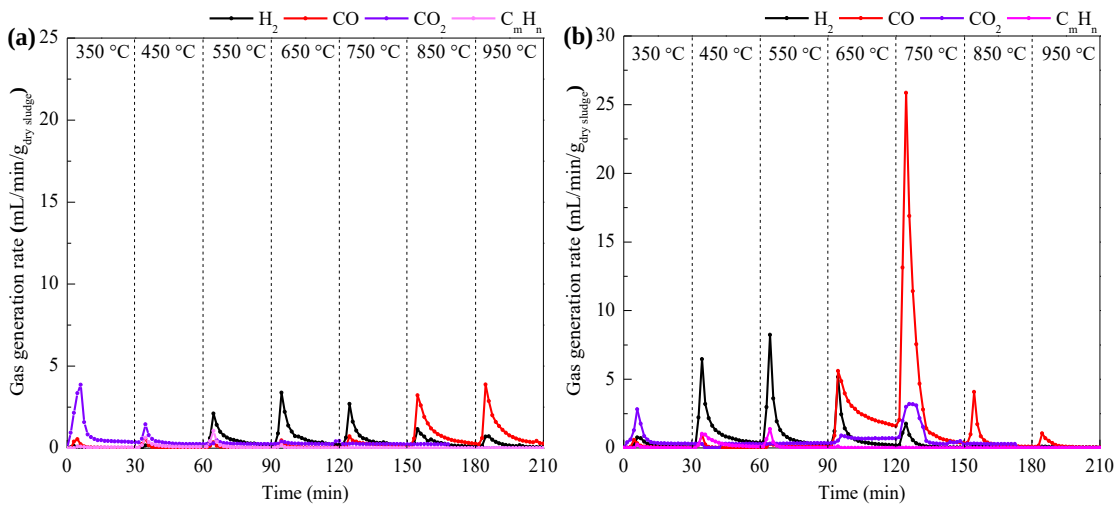

Fig. 3.13. Time evolution of the gas generation rate during the temperature-programmed isothermal pyrolysis of (a) SS and (b) Ca/SS-1:1. C_mH_n represents CH_4, C_2H_6, and C_2H_4.

3.4. Conclusion

A novel TSSE thermochemical conversion process is proposed in this chapter to effectively convert sewage sludge into syngas. On account of integrating the CaO-based CO_2 carrying cycle into the conventional thermochemical conversion of sewage sludge, the CO_2 generated from sewage sludge is captured and stored in the form of $CaCO_3$ at a temperature of ~550 °C, and is then released at a higher temperature of ~750 °C to gasify the char for CO production. This two-stage process has been experimentally demonstrated to improve thermochemical syngas production in the following two aspects: (1) producing syngas with separated H_2- and CO-rich streams, and (2) improving the utilization efficiency of carbon in sewage sludge.

Temperature and the CaO/SS mass ratio are key factors influencing the performance of the proposed TSSE thermochemical conversion process for syngas production from sewage sludge. At low temperatures of ~550 °C, a high selectivity of H_2 to CO is achieved in the syngas produced, leading to the acquisition of a H_2-rich gas stream; while at higher temperatures of ~750 °C, a high selectivity of CO to H_2 leads to the acquisition of a CO-rich gas stream. The inherent separation

of H_2 and CO during syngas production offers a chance to adjust the CO/H_2 molar ratio for a downstream synthesis of chemicals or fuels. Importantly, as much as 20.4% of the carbon in the sewage sludge could be utilized in the form of CO through the proposed process, resulting in a remarkably higher yield of CO than other biomass conversion processes currently reported for thermochemical syngas production.

References

1. *20 years of carbon capture and storage: Accelerating future deployment*. 2016, Internation Energy Agency.
2. Xu, D., et al., *A novel chemical looping partial oxidation process for thermochemical conversion of biomass to syngas.* Applied Energy, 2018. **222**: p. 119-131.
3. Sikarwar, V., et al., *An overview of advances in biomass gasification.* Energy & Environmental Science, 2016. **9**(10).
4. *World Energy Outlook 2015*. 2015, Internation Energy Agency.
5. Kuo, Y.-T., G.A. Almansa, and B.J. Vreugdenhil, *Catalytic aromatization of ethylene in syngas from biomass to enhance economic sustainability of gas production.* Applied Energy, 2018. **215**: p. 21-30.
6. Tripathi, M., J.N. Sahu, and P. Ganesan, *Effect of process parameters on production of biochar from biomass waste through pyrolysis: A review.* Renewable and Sustainable Energy Reviews, 2016. **55**: p. 467-481.
7. Li, J., et al., *Biochar from microwave pyrolysis of biomass: A review.* Biomass and Bioenergy, 2016. **94**: p. 228-244.

8. Li, C. and K. Suzuki, *Tar property, analysis, reforming mechanism and model for biomass gasification-An overview.* Renewable and Sustainable Energy Reviews, 2009. **13**(3): p. 594-604.

9. Yao, Z., et al., *Biomass gasification for syngas and biochar co-production: Energy application and economic evaluation.* Applied Energy, 2018. **209**: p. 43-55.

10. Tian, S., et al., *Calcium-looping reforming of methane realizes in situ CO utilization with improved energy efficiency.* Science advances, 2019. **5**(4): p. eaav5077.

11. Sansaniwal, S.K., et al., *Recent advances in the development of biomass gasification technology: A comprehensive review.* Renewable and Sustainable Energy Reviews, 2017. **72**: p. 363-384.

12. Beller, M., et al., *Progress in hydroformylation and carbonylation*. 1995. p. 17-85.

13. Dry, M.E., *The Fischer-Tropsch process: 1950-2000.* Catalysis Today, 2002. **71**(3-4): p. 227-241.

14. Syed-Hassan, S.S.A., et al., *Thermochemical processing of sewage sludge to energy and fuel: Fundamentals, challenges and considerations.* Renewable and Sustainable Energy Reviews, 2017. **80**: p. 888-913.

15. He, C., et al., *Hydrothermal gasification of sewage sludge and model compounds for renewable hydrogen production: A review.* Renewable and Sustainable Energy Reviews, 2014. **39**: p. 1127-1142.

16. Yang, G., G. Zhang, and H. Wang, *Current state of sludge production, management, treatment and disposal in China.* Water Research, 2015. **78**: p. 60-73.

17. Nipattummakul, N., et al., *High temperature steam gasification of wastewater sludge.* Applied Energy, 2010. **87**(12): p. 3729-3734.

18. Fonts, I., et al., *Study of the pyrolysis liquids obtained from different sewage sludge.* Journal of Analytical and Applied Pyrolysis, 2009. **85**(1): p. 184-191.

19. Zhang, B., et al., *Mechanism of wet sewage sludge pyrolysis in a tubular furnace.* International Journal of Hydrogen Energy, 2011. **36**(1): p. 355-363.

20. Alvarez, J., et al., *Sewage sludge valorization by flash pyrolysis in a conical spouted bed reactor.* Chemical Engineering Journal, 2015. **273**: p. 173-183.

21. Manyà, J.J., et al., *Air gasification of dried sewage sludge in a fluidized bed: Effect of the operating conditions and in-bed use of alumina.* Energy & Fuels, 2005. **19**(2): p. 629-636.

22. Mun, T.-Y., J.-W. Kim, and J.-S. Kim, *Air gasification of dried sewage sludge in a two-stage gasifier: Part 1. The effects and reusability of additives on the removal of tar and hydrogen production.* International Journal of Hydrogen Energy, 2013. **38**(13): p. 5226-5234.

23. Maroño, M., J.M. Sánchez, and E. Ruiz, *Hydrogen-rich gas production from oxygen pressurized gasification of biomass using a Fe-Cr water gas shift catalyst.* International Journal of Hydrogen Energy, 2010. **35**(1): p. 37-45.

24. Choi, Y.-K., M.-H. Cho, and J.-S. Kim, *Steam/oxygen gasification of dried sewage sludge in a two-stage gasifier: Effects of the steam to fuel ratio and ash of the activated carbon on the production of hydrogen and tar removal.* Energy, 2015. **91**: p. 160-167.

25. Florin, N.H. and A.T. Harris, *Enhanced hydrogen production from biomass with in situ carbon dioxide capture using calcium oxide sorbents.* Chemical Engineering Science, 2008. **63**(2): p. 287-316.

26. Sikarwar, V.S., et al., *Equilibrium modeling of sorption-enhanced cogasification of sewage sludge and wood for hydrogen-rich gas production with in situ carbon dioxide capture.* Industrial & Engineering Chemistry Research, 2017. **56**(20): p. 5993-6001.

27. Broda, M., et al., *High-purity hydrogen via the sorption-enhanced steam methane reforming reaction over a synthetic CaO-based sorbent and a Ni catalyst.* Environmental science & technology, 2013. **47**(11): p. 6007-6014.

28. Han, L., et al., *H_2 rich gas production via pressurized fluidized bed gasification of sawdust with in situ CO_2 capture.* Applied Energy, 2013. **109**: p. 36-43.

29. Zhang, L., et al., *Pyrolysis behavior of biomass with different Ca-based additives.* RSC Advances, 2014. **4**(74): p. 39145-39155.

30. Chen, S., et al., *Steam gasification of sewage sludge with CaO as CO_2 sorbent for hydrogen-rich syngas production.* Biomass and Bioenergy, 2017. **107**: p. 52-62.

31. Kan, T., V. Strezov, and T. Evans, *Effect of the heating rate on the thermochemical behavior and biofuel properties of sewage sludge pyrolysis.* Energy & Fuels, 2016. **30**(3): p. 1564-1570.

32. Widyawati, M., et al., *Hydrogen synthesis from biomass pyrolysis with in situ carbon dioxide capture using calcium oxide.* International Journal of Hydrogen Energy, 2011. **36**(8): p. 4800-4813.

33. Halstead, P.E. and A.E. Moore, *769. The thermal dissociation of calcium hydroxide.* Journal of the Chemical Society (Resumed), 1957(0): p. 3873-3875.

34. Tian, S. and J. Jiang, *Sequestration of flue gas CO_2 by direct gas-solid carbonation of air pollution control system residues.* Environmental Science & Technology, 2012. **46**(24): p. 13545-13551.

35. Tian, S., et al., *Direct gas–solid carbonation kinetics of steel slag and the contribution to in situ sequestration of flue gas CO_2 in steel‐making plants.* ChemSusChem, 2013. **6**(12): p. 2348-2355.

36. Tian, S., et al., *Highly efficient CO_2 capture with simultaneous iron and CaO recycling for the iron and steel industry.* Green Chemistry, 2016. **18**(14): p. 4022-4031.

37. He, C., A. Giannis, and J.-Y. Wang, *Conversion of sewage sludge to clean solid fuel using hydrothermal carbonization: Hydrochar fuel characteristics and combustion behavior.* Applied Energy, 2013. **111**: p. 257-266.

38. Hlavsová, A., et al., *The effects of varying CaO content and rehydration treatment on the composition, yield, and evolution of gaseous products from the pyrolysis of sewage sludge.* Journal of Analytical and Applied Pyrolysis, 2014. **108**: p. 160-169.

39. Cizer, Ö., et al., *Phase and morphology evolution of calcium carbonate precipitated by carbonation of hydrated lime.* Journal of Materials Science, 2012. **47**(16): p. 6151-6165.

40. Liu, H., et al., *Enhancement of hydrogen production in steam gasification of sewage sludge by reusing the calcium in lime-conditioned sludge.* International Journal of Hydrogen Energy, 2013. **38**(3): p. 1332-1341.

41. Yongbin, J., H. Jiejie, and W. Yang, *Effects of calcium oxide on the cracking of coal tar in the freeboard of a fluidized bed.* Energy & Fuels, 2004. **18**(6): p. 1625-1632.

42. Liu, H., et al., *Dual role of conditioner CaO in product distributions and sulfur transformation during sewage sludge pyrolysis.* Fuel, 2014. **134**: p. 514.

43. Mahishi, M.R. and D.Y. Goswami, *An experimental study of hydrogen production by gasification of biomass in the presence of a CO_2 sorbent.* International Journal of Hydrogen Energy, 2007. **32**(14): p. 2803-2808.

44. Hanaoka, T., et al., *Hydrogen production from woody biomass by steam gasification using a CO_2 sorbent.* Biomass and Bioenergy, 2005. **28**(1): p. 63-68.

45. Guoxin, H. and H. Hao, *Hydrogen rich fuel gas production by gasification of wet biomass using a CO_2 sorbent.* Biomass and Bioenergy, 2009. **33**(5): p. 899-906.

46. Ji, G., et al., *Enhanced hydrogen production from sawdust decomposition using hybrid-functional Ni-CaO-Ca_2SiO_4 materials.* Environmental Science & Technology, 2017. **51**(19): p. 11484.

47. Liu, H., et al., *Co-production of clean syngas and ash adsorbent during sewage sludge gasification: Synergistic effect of Fenton peroxidation and CaO conditioning.* Applied Energy, 2016. **179**: p. 1062-1068.

48. Hu, M., et al., *Hydrogen-rich gas production by the gasification of wet MSW (municipal solid waste) coupled with carbon dioxide capture.* Energy, 2015. **90**: p. 857-863.

49. Zhang, Q., et al., *Effect of Fe/Ca-based composite conditioners on syngas production during different sludge gasification stages: Devolatilization, volatiles homogeneous reforming and heterogeneous catalyzing.* International Journal of Hydrogen Energy, 2017. **42**(49): p. 29150-29158.

50. Dean, C.C., D. Dugwell, and P.S. Fennell, *Investigation into potential synergy between power generation, cement manufacture and CO_2 abatement using the calcium looping cycle.* Energy & Environmental Science, 2011. **4**(6): p. 2050-2053.

Chapter 4 Tunable syngas production from two-stage sorption-enhanced steam gasification of sewage sludge

Published as: Yang, X., Kan, T., Kheradmand, A., Xu, H., Strezov, V., Yu, A., Jiang, Y. (2021) Tunable syngas production from two-stage sorption-enhanced steam gasification of sewage sludge, *Chemical Engineering Journal,* Vol. 404, 126069, https://doi.org/10.1016/j.cej.2020.126069.

4.1. Introduction

The global fuel and chemical production predominantly originate from petroleum crude oil. With the depleting reserves and rising prices of crude oil, producing fuels from renew chemical feedstocks is imperative. Syngas, a variable composition mixture of hydrogen (H_2) and carbon monoxide (CO), has been cited as an essential precursor to a wide range of high value-added fuels and chemicals via well-established industrial processes such as Fischer-Tropsch synthesis (FTS) process [1-3]. The conventional production of syngas is based on partial oxidation with steam and oxygen from non-renewable fossil fuels (e.g. coal and natural gas), which could increase the consumption of fossil fuels and aggravate the energy crisis [4-6]. Syngas production from renewable biomass is an alternative, sustainable and carbon-neutral approach to combat the energy crisis [7]. To date, syngas production based on the thermochemical conversion of biomass has become increasingly interesting [8, 9].

Different synthetic products and FTS operation modes demand various H_2/CO usage ratios in the syngas. For example, a H_2/CO ratio of 1 is desired for hydroformylation process [10, 11], whereas a H_2/CO ratio of 2 is typically optimal for the synthesis of methanol, paraffins, olefins and oxygenates via FTS process [12]. For cobalt catalysts, the H_2/CO usage ratio ranges between 2.06 and 2.16, while iron-based catalysts would facilitate the water-gas shift (WGS) reaction and thereby reducing the H_2/CO usage ratio ranging from 0.5-2 [13]. Tunable H_2/CO ratio in syngas could easily meet any demand usage ratios for the downstream synthesis process, avoiding extra steps to adjust the H_2/CO ratio and thereby maximising the conversion efficiency of syngas into

downstream synthetic liquid fuels and value-added chemicals. Thus, it is critical to precisely control the H_2/CO ratio in the syngas, making it a versatile and flexible platform feedstock for industrial applications [14].

It is still challenging for conventional thermochemical conversion of biomass to produce syngas with tunable H_2/CO ratio. Firstly, H_2 and CO are produced together via the conventional thermochemical conversion processes. Secondly, the conventional biomass-derived syngas always consists of a high purity of H_2 production while a poor CO production. Different types of processes have been studied to pursue high yield and high purity of H_2, such as steam gasification [15, 16], hydrothermal gasification [17], sorption-enhanced steam gasification [18, 19] and catalytic gasification [20, 21]. A high H_2 purity of 97 mol% is produced from the sorption-enhanced chemical looping reforming of waste cooking oil in a packed-bed reactor reported by Pimenidou et al. [22]. The H_2 purity could reach up to 70-80% from the sorption-enhanced steam gasification [19, 23], hydrothermal gasification [24] and pyrolysis with on-line steam reforming [25] of biomass. However, high-purity H_2 is often accompanied by a relatively low purity of CO from the thermochemical conversion of biomass. For example, a CO purity of 26% and 11.4% were obtained from the steam gasification of wood [18] and supercritical water gasification of sewage sludge [24], respectively. Hence, additional steps are usually needed to adjust the H_2/CO ratio in the syngas to meet the requirements, which makes the overall process more complex and expensive [26].

The novel proposed two-stage sorption-enhanced (TSSE) pyrolysis process shown in Chapter 3, achieved a separate production of the unprecedentedly high purity of H_2 and CO at different stages from sewage sludge (SS), which is a promising option for SS treatment. These findings showed that the TSSE pyrolysis of SS could produce a CO-rich syngas mixture with a H_2/CO ratio of 0.4.

Considering steam is the most efficient partial-oxidation atmosphere for H_2 production [27], the present work investigates the incorporation of steam gasification into the first stage to further adjust the H_2 and CO production through the TSSE steam gasification process, and then to broaden the H_2/CO ratio in the syngas produced from SS. This work presents a new process to control and tune the H_2/CO ratio in the biomass-derived syngas, which is of significant interest to the downstream synthesis of chemicals and fuels from an industrial perspective. Besides, there is no report on the performance characterization of the novel TSSE thermochemical conversion including pyrolysis and steam gasification process. A clear understanding of the underlying mechanism of the novel TSSE thermochemical conversion process would be greatly beneficial to the subsequent optimization for further improving the yield and purity of H_2 and CO production from biomass. Therefore, studies on the performance characterization in terms of specific product distributions, tar compositions, and elemental utilization in the TSSE thermochemical conversion process are also conducted in this chapter.

4.2. Material and methods

4.2.1. Sample preparation

The SS used in this chapter was obtained prior to anaerobic digestion from a municipal wastewater treatment plant in Sydney, Australia. The ultimate and proximate analysis of the SS and the preparation method of SS and CaO (SS-CaO) pellets were shown in Section 3.2.1 in Chapter 3. The prepared SS-CaO pellets were notated as Ca/SS-1:9, Ca/SS-1:4, Ca/SS-3:7, Ca/SS-2:3, and Ca/SS-1:1, in which x:y indicates the mass ratio of CaO to SS (CaO/SS, dry basis).

4.2.2. Experimental procedures

The TSSE steam gasification of SS was performed in a fixed-bed reactor at atmospheric pressure, and the diagram of the experimental setup is shown in Fig. 4.1. The SS-CaO pellets were loaded

on the quartz wool supported in a stainless-steel tube (length: 300 mm; inner diameter: 6 mm) and heated by an electric furnace. A nitrogen flow of 15 mL/min was used as the carrier gas during the experiment, and a constant flow pump and a preheater were employed to introduce steam into the reactor. The detailed procedures are as follows: (1) heating the loaded SS-CaO pellets from room temperature to 550°C at a rate of 30 °C/min and keeping at 550 °C for 45 min, as the first stage process; (2) subsequently, heating the remained sample from 550 °C to 750 °C at a rate of 30 °C/min and keeping at 750 °C for another 45 min, as the second stage process. Steam was introduced into the reactor for the first 30 min at the first stage. The corresponding introduced steam to SS-embedded carbon molar ratio (S/C) was 0.5, 1, 1.5 and 2, respectively. No steam was introduced into the reactor for the TSSE pyrolysis of Ca/SS-3:7. During the experiment, the condensable gas (tar and steam) released from the fixed-bed reactor was condensed and collected in a condensation tube, which was put into a dewar flask containing a mixture of dry ice and ethylene glycol with a cooling bath temperature of -15 °C. The incondensable gas was monitored on-line using a comprehensive two-dimensional gas chromatograph (GC, 7890B, Agilent) equipped with two columns and two thermal conductivity detectors (TCDs). The H_2, N_2, CH_4, CO, and CO_2 were initially separated on the first-dimensional column (PoraPLOT Q), and the first column effluent of H_2, N_2, CH_4, CO was then injected into the second-dimensional column (HP-Molesieve) for further separation. The data acquisition interval for GC was every 2 min.

4.2.3. Sample characterisation

The qualitative and quantitative analyses of the organic compounds in the condensable tar were conducted by a gas chromatography-mass spectrometer (GC-MS) (Agilent) with an HP-5MS column (30 m×250 μm×0.25 μm). Prior to the tar analysis, the steam condensed with the tar was

dehydrated using anhydrous sodium sulfate. The electron ionization mode was used at an electron energy of 70 eV.

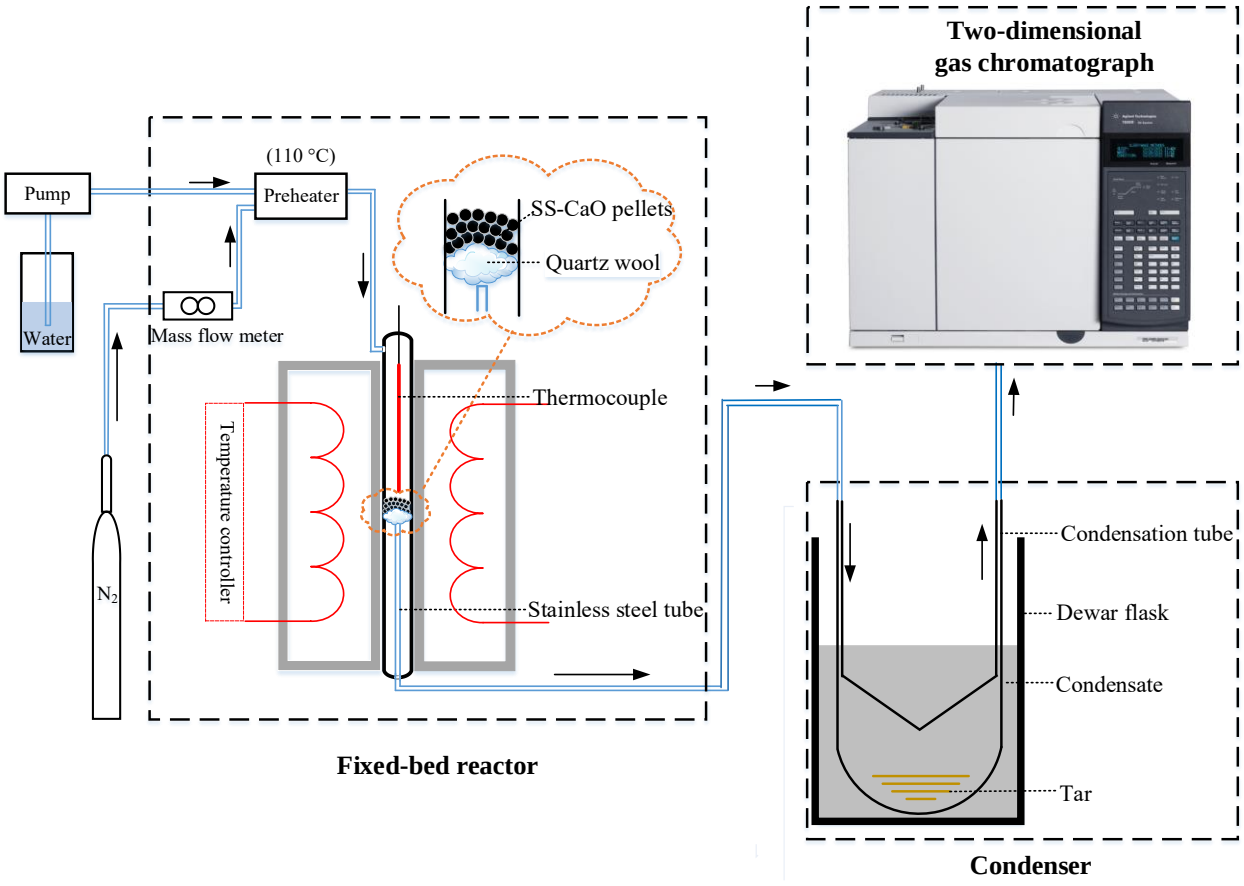

Fig. 4.1. Illustration of the experimental setup for the TSSE steam gasification of SS used in this chapter.

The distributions of char and tar at 550 °C (first stage) and 750 °C (second stage) are expressed in mass fractions of char and tar obtained after each stage in the initial sum of SS and steam, respectively, while the percentage of gas was calculated by the difference between total and the fractions of char and tar. For each case, the mass of char and tar were gained as the weight differences of solid sample and condenser before and after the TSSE thermochemical conversion of Ca/SS-3:7, respectively. Regarding the yield of char, the mass of CaO was excluded as CaO has no potential to be converted into tar or gas. Since the water could take part in the reactions for

syngas production and it was condensed together with the liquid tar, the mass of water was included in the yield of tar.

The contents of carbon and hydrogen in the fresh Ca/SS-3:7 and its residual chars were determined using Vario MICRO cube elemental analyser (Elementar Analysensyteme GmbH, Germany). The carbon and hydrogen in the gas were calculated by Eq. 1 and 2, respectively.

The proportion of carbon in the fresh Ca/SS-3:7 converted into gas was expressed as gas-C and calculated according to the following Eq. 1:

$$\text{Gas-C}(\%)=\frac{12\times(Y_{CO}+Y_{CO_2}+Y_{CH_4})}{22.4\times C\times 1000}\times 100\% \qquad (1)$$

where Y is the yield of CO, CO_2, and CH_4, NmL/$g_{dry\ SS}$; C is the mass percentage of the total carbon in the freshly prepared Ca/SS-3:7, %.

The proportion of hydrogen in the total hydrogen fed into the system including the hydrogen contents of fresh Ca/SS-3:7 and added steam converted into gas was express as gas-H, which was calculated according to the following Eq. 2:

$$\text{Gas-H}(\%)=\frac{2\times Y_{H_2}+4\times Y_{CH_4}}{22.4\times H\times 1000}\times 100\% \qquad (2)$$

where Y is the yield of H_2 and CH_4, NmL/$g_{dry\ SS}$; H is the mass percentage of the total hydrogen in the freshly prepared Ca/SS-3:7 and added steam, %.

The quantity of $CaCO_3$ in the residual char of Ca/SS-3:7 was determined based on the reference intensity ratio (RIR) method [28] using an X-ray diffractometer (X'Pert PRO, PANalytical) with the Cu Kα radiation in the 2θ range of 10-80°. A known weight fraction of corundum (Al_2O_3) as an internal standard was used. The content of $CaCO_3$ in the residual char of Ca/SS-3:7 was calculated by the following Eq.3.

$$X_{cal}=\frac{I_{cal}}{I_{cor}}\cdot\frac{X_{cor}}{K_{cal,cor}}\cdot\frac{1}{1-X_{cor}} \qquad (3)$$

Where x is the weight fraction, and I is the intensity of the strongest line of phase, and the subscripts *cal* and *cor* are phase $CaCO_3$ and the standard phase Al_2O_3, respectively. The value $K_{cal,cor}$ is determined by taking the ratio of the strongest line of phase $CaCO_3$ to the intensity of the strongest line of phase Al_2O_3 in a 50:50 mixture by weight.

4.3. Results and discussion

4.3.1. Tunable H_2/CO ratios in the syngas from the TSSE steam gasification of SS

The syngas production generated from the TSSE steam gasification of SS with various mass ratios of CaO to SS at S/C-1 is shown in Fig. 4.2. At the first stage, CO_2 is the predominant component in the effluent gas stream obtained from the bare SS (Fig. 4.3a). Upon the addition of CaO, an increase in H_2 production is observed at the first stage (Fig. 4.2a), which is attributed to the catalytic effect of CaO on the tar-steam reforming and cracking for H_2 production. Besides, the addition of CaO could *in situ* capture CO_2 to promote the WGS reaction (Eq. 4) thus achieving a higher H_2 production. However, the yield of H_2 at the first stage does not keep increasing with the CaO/SS ratios when the CaO/SS ratio is over 3:7. It was reported that the excess of CaO and addition of steam would absorb large amounts of heat and hinder heat transfer to reduce the activity of WGS reaction (Eq. 4) leading to the decrease of H_2 production at the first stage [29]. The purity of H_2 increases with the CaO/SS ratios and H_2 becomes the predominant component of the effluent gas stream when the CaO/SS ratio is over 1:4. As shown in Fig. 4.3, the CO_2 production decreases with the increasing CaO contents, and the flow rate of CO_2 is almost negligible at the first stage when the CaO/SS ratio is over 3:7, leading to the highest H_2 purity of 81.6 vol% from the Ca/SS-1:1 at the first stage (Fig. 4.2a).

$$CO+H_2O \leftrightharpoons CO_2 + H_2 \text{ , } \Delta H_{298\,K} = -41.2 \text{ kJ/mol} \qquad (4)$$

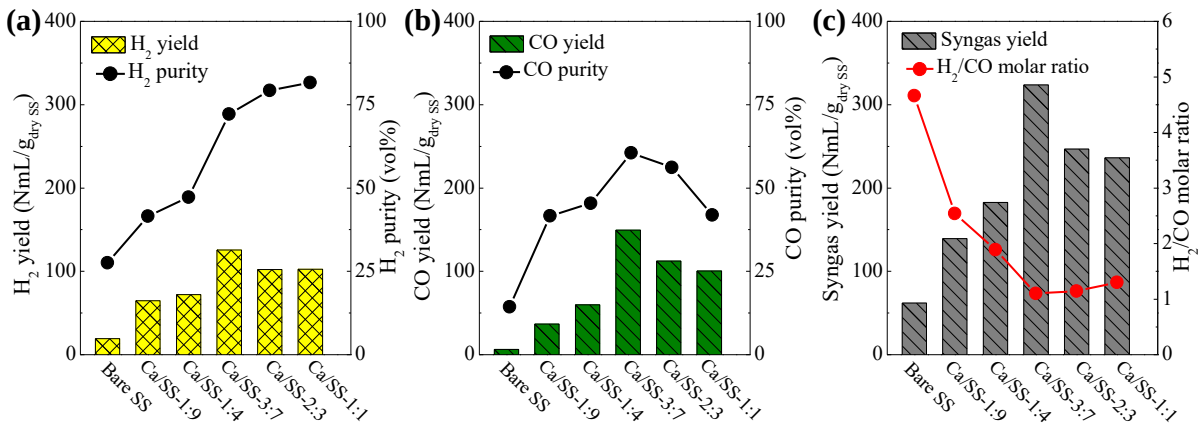

Fig. 4.2. H_2 and CO production obtained from the TSSE steam gasification of SS as a function of the CaO/SS mass ratio: (a) H_2 yield and purity generated at the first stage; (b) CO yield and purity generated at the second stage; c) total syngas (H_2+CO) yield and H_2/CO molar ratio. Experimental conditions: S/C-1, 550 °C for the first stage, 750 °C for the second stage.

At the second stage, H_2 dominates the effluent gas stream generated from the bare SS (Fig. 4.3a). Upon the addition of CaO, the yield and purity of CO gradually increase with the CaO contents reaching maximum over the Ca/SS-3:7 (Fig. 4.2b). Since no steam was introduced at the second stage resulting in negligible steam gasification of char, the increasing CO production is due to the increased amount of CO_2 captured with the CaO contents at the first stage and released at the second stage to gasify the char for CO production via the reverse Boudouard reaction (Eq. 5). Similar to the H_2 production, the yield and purity of CO decrease when the CaO/SS ratio is over 3:7, which might be caused by the negative effect of excess CaO on the heat transfer in the reactor, thereby reducing the activity of the reverse Boudouard reaction (Eq. 5) [29]. Besides, a high CO_2 purity is released at the second stage, resulting in a lower CO purity of 41.9 vol% from Ca/SS-1:1 at the second stage (Fig. 4.2b).

$$C + CO_2 \leftrightharpoons 2CO,\ \Delta H_{298\,K} = +172.4\ kJ/mol \qquad (5)$$

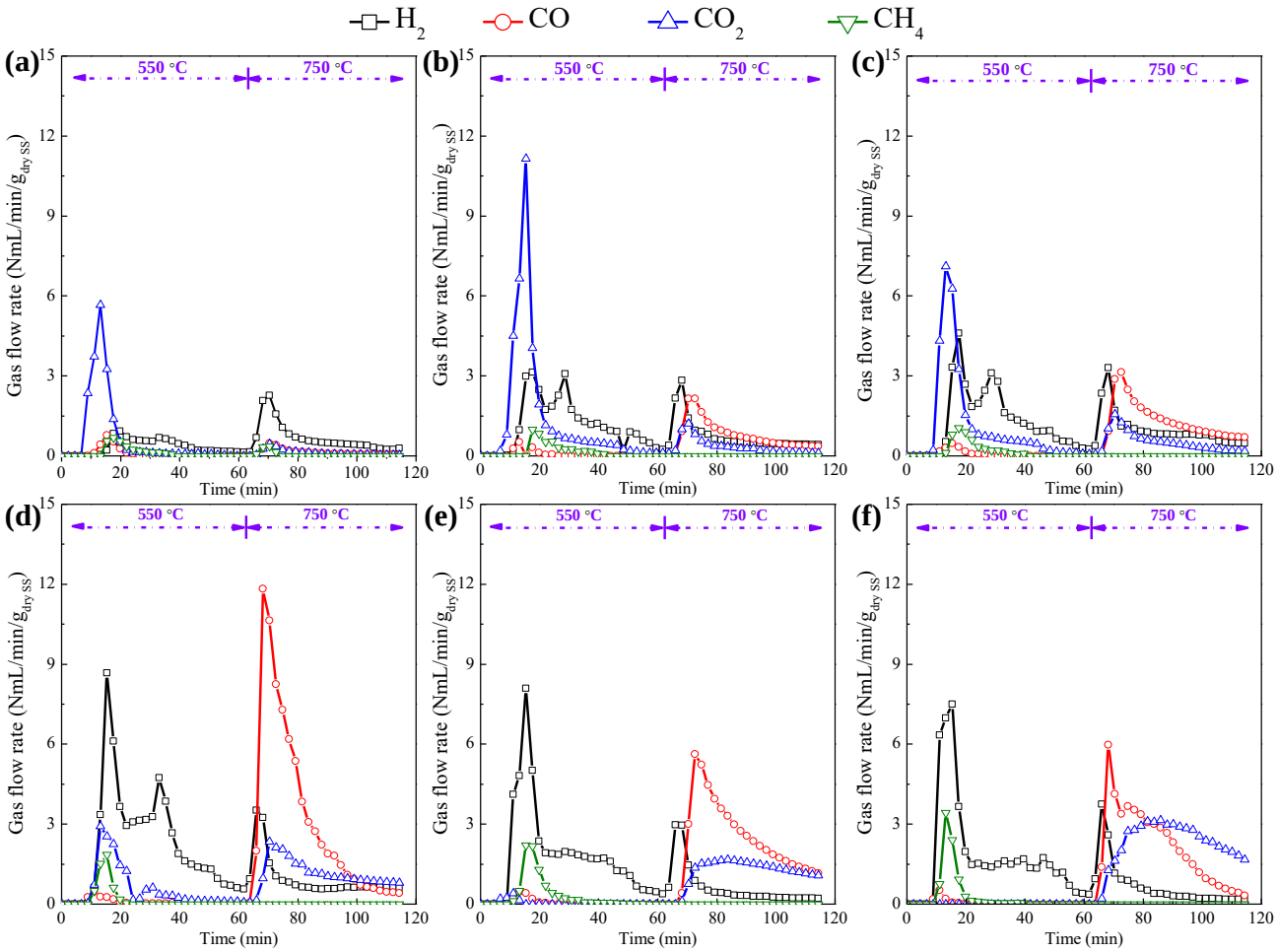

Fig. 4.3. The gas flow rate produced from the TSSE steam gasification of SS as a function of the CaO/SS mass ratio: (a) bare SS; (b) Ca/SS-1:9; (c) Ca/SS-1:4; (d) Ca/SS-3:7; (e) Ca/SS-2:3; (f) Ca/SS-1:1. Experimental conditions: S/C-1, 550 °C for the first stage, 750 °C for the second stage.

In summary, the addition of CaO could increase the selectivity of H_2 at the first stage and CO at the second stage. The syngas production peaks at 323.8 NmL/$g_{dry\ SS}$ produced from the TSSE steam gasification of Ca/SS-3:7, with 72.2 vol% of H_2 at the first stage and 60.5 vol% of CO at the second stage (Fig. 4.2), indicating that there is a threshold limit value for CaO contents. Compared to the H_2 production from the TSSE pyrolysis shown in Chapter 3, the H_2 production from the TSSE steam gasification in the present work is greatly enhanced (Fig. 4.2a). More specifically, the H_2 yield of Ca/SS-3:7 reaches 125.7 NmL/$g_{dry\ SS}$ at S/C-1, which is around 3 times higher than that of

42.5 NmL/$g_{dry\ SS}$ from the TSSE pyrolysis (Fig. 3.4, Chapter 3). It is apparent that at the first stage the peak flow rate of H_2 increases dramatically and remains for about 50 min at the first stage of the TSSE steam gasification (Fig. 4.3d), while in the TSSE pyrolysis the H_2 flow rate peaks in 16 min, and then rapidly drops to a very low level (Fig. 4.4). The enhancement in H_2 purity from 49.2 to 72.2 vol% is also observed at the first stage with the addition of steam. The presence of steam could promote the WGS reaction (Eq. 4) for enhanced H_2 production. Hence, not only a higher yield of H_2 but also a higher purity of H_2 could be obtained upon the addition of steam at the first stage. For the CO production at the second stage, there is only a slight difference in the yield of CO from the steam gasification and pyrolysis, while the addition of steam reduces the purity of CO due to a higher percentage of CO_2 released at the second stage. It is also recommended that the optimal CaO/SS ratio is reduced from 1:1, reported for pyrolysis (Fig. 3.4, Chapter 3), to 3:7 for the steam gasification presented in this chapter.

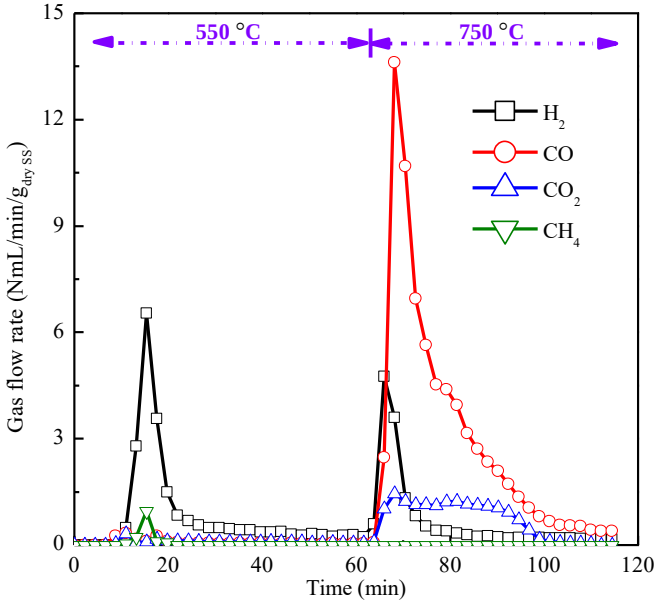

Fig. 4.4. Gas flow rate produced from the TSSE pyrolysis of Ca/SS-3:7. Experimental conditions: 550 °C for the first stage, 750 °C for the second stage.

In order to further study the influence of steam on the syngas production from the TSSE steam gasification of SS, the H_2 and CO production from the TSSE steam gasification of Ca/SS-3:7 is plotted as a function of the S/C ratios, as shown in Fig. 4.5. The increase of the S/C ratios leads to a higher H_2 yield at the first stage due to the enhanced WGS reaction (Eq. 4) for H_2 production (Fig. 4.5a). However, there is also a threshold limit value for the S/C ratio of 1 beyond which the increase of S/C ratio would not further improve the H_2 production at the first stage. This trend has also been reported in other papers [30, 31]. It is well accepted that the excess of steam would have a detrimental effect on the temperature inside the reactor to reduce the activity of steam-reforming reactions and WGS reaction (Eq. 4). In addition, according to Table 4.1, the mass fraction of $CaCO_3$ decreases in the solid residues obtained after the first stage when the S/C ratio is over 1, indicating that less CO_2 is captured by the CaO, thereby weakening the beneficial effect of CaO on the WGS reaction (Eq. 4) for H_2 production.

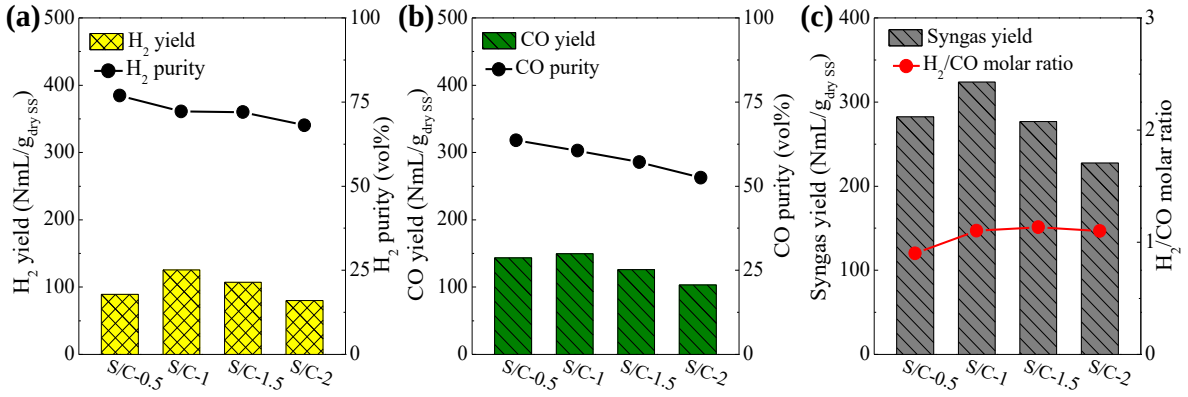

Fig. 4.5. H_2 and CO produced from the TSSE steam gasification of Ca/SS-3:7 as a function of S/C ratios: (a) H_2 yield and purity at the first stage; (b) CO yield and purity at the second stage; (c) total syngas (H_2+CO) yield and H_2/CO molar ratio. Experimental conditions: 550 °C for the first stage, 750 °C for the second stage.

Table 4.1. Quantitative analysis of $CaCO_3$ in the solid residual chars obtained after the first stage.

	I_{CaCO3}	$I_{corundum}$	Mass fraction of $CaCO_3$ X_{CaCO3}
S/C-0.5	136874	173684	19.3%
S/C-1	132465	158128	20.5%
S/C-1.5	133083	168399	19.4%
S/C-2	149334	190985	19.2%

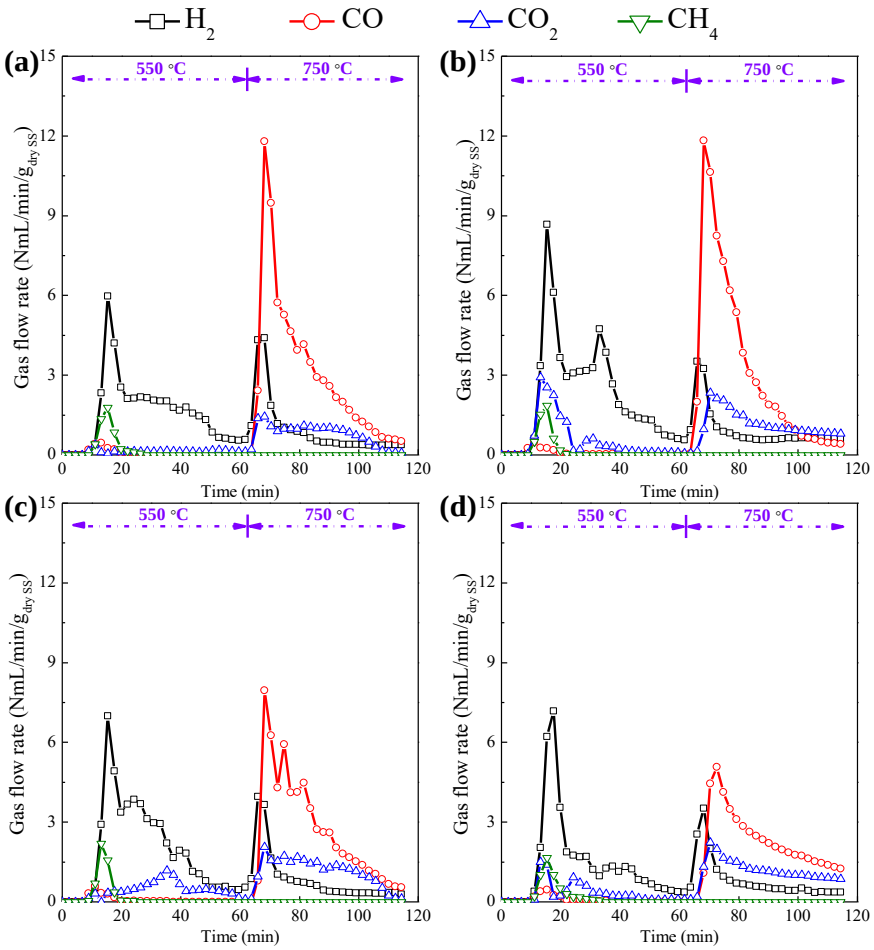

Fig. 4.6. The gas flow rate produced from the TSSE steam gasification of Ca/SS-3:7 as a function of S/C ratios: (a) S/C-0.5; (b) S/C-1; (c) S/C-1.5; (d) S/C-2. Experimental conditions: 550 °C for the first stage, 750 °C for the second stage.

At the second stage, decreasing yield and purity of CO are obtained with the increased S/C ratios (Fig. 4.5b). The results of Table 4.1 indicate that less CO_2 is captured at S/C-1.5 and S/C-1, thereby less CO_2 is released at the second stage for CO production (Fig. 4.6). The syngas production over Ca/SS-3:7 is further compared with that reported in other studies as summarized in Table 4.2. Noteworthy, the H_2 purity (72.2 vol%) obtained at the first stage is higher than or comparable with that reported in the literature. The CO purity of 60.5 vol% obtained at the second stage in this chapter is significantly higher than the range of 2 to 25 vol% reported by the other studies for sorption-enhanced steam gasification of biomass. Hence, the TSSE steam gasification process could achieve high purity H_2 and CO as the dominant gas composition at the first stage and the second stage, respectively. The inherent separation of H_2 and CO generation provides a promising option for direct integration of the TSSE steam gasification of biomass with the syngas applications where H_2 and CO could be mixed in any desirable ratios, ready for use in the downstream synthesis of chemicals or fuels with no need for the additional process for refining the H_2/CO ratio in the syngas.

As shown in Fig. 4.2c, the H_2/CO molar ratios could be systematically tuned from 1.1 to 4.7 by varying the CaO/SS ratios. An H_2-rich syngas is obtained from the TSSE steam gasification of SS-CaO samples when the CaO/SS ratio is below 3:7, thereinto, the H_2/CO ratio decreases with the CaO/SS ratios. When the CaO/SS ratios are above 3:7, the H_2/CO ratios are stable at around 1, which is the desirable ratio for FTS process using iron-based catalysts and the production of aldehydes via hydroformylation of alkenes [10, 11]. In Fig. 4.5c, the H_2/CO ratios of 0.9-1.2 are obtained by changing the S/C ratios. It is noted that a more pronounced effect of the addition of CaO on the tunable H_2/CO ratios is observed, reflected in a wider range of H_2/CO ratios, thereby H_2/CO ratios are more sensitive to the CaO contents compared to the steam contents.

Consequently, the H_2/CO ratios could be effectively controlled in the range of 0.9-4.7 by varying either the CaO contents or the steam contents, which can fully cover the requirements for different downstream synthetic products and FTS optional modes.

Table 4.2. Summary of syngas production via the conventional sorption-enhanced steam gasification of biomass reported in the literature.

Biomass	Temperature (˚C)	CaO type	Gas concentration (vol%)		Ref.
			H_2	CO	
Pine sawdust	650	Calcined limestone	47	5[d]	[32]
Pine sawdust	900	Calcined limestone	53	17	[33]
Pine tree sawdust	650	CaO	58	20	[34]
Larch	650	Calcined limestone	64	5	[35]
Almond shells	770	Calcined dolomite	56	24	[36]
Japanese oak	700	CaO	63	2	[37]
Sawdust	670	CaO	52	24	[38]
Sawdust	580	CaO	71	6	[39]
Municipal solid waste	900	Calcined dolomite	47	15[d]	[40]
Municipal solid waste	750	CaO	48	13	[29]
SS	600	CaO	59	25	[41]
SS	650	CaO	72	5	[42]
SS	**550/750[a]**	**CaO**	**72.2[b]**	**60.5[c]**	**This chapter**

[a] The sample was treated in sequence at 550 °C and 750 °C.
[b] The value was obtained at 550 °C.
[c] The value was obtained at 750 °C.
[d] The gas concentration was expressed as the mol%.

4.3.2. Performance characterisation of the TSSE thermochemical conversion process

4.3.2.1. Product distributions

To clearly understand the specific transformation of SS via the TSSE thermochemical conversion process, the distributions of char, tar, and gas produced from Ca/SS-3:7 are shown in Fig. 4.7.

After the first stage, the percentages of tar and char generated from the sole pyrolysis of Ca/SS-3:7 are at a similar level of around 45%. From the steam gasification of Ca/SS-3:7, an enhancement in the proportion of tar from 46.1 to 76.3% is observed with the increased S/C ratios. Correspondingly, the proportion of gas reduces from 11.7 to 2.0% with the increased S/C ratios. However, as discussed in Fig. 4.5c, the yield of gas exhibits an opposite tendency to some extent. Moreover, the percentage of char declines from 42.2 to 21.3% with the increased S/C ratios, while no significant change in the mass of char is observed (Table 4.3). Thereby, the reduction in the proportions of char and gas could be ascribed to the increased reactants consisting of Ca/SS-3:7 and steam with the increased S/C ratios as the denominator in the calculation of the percentage of char and gas.

Table 4.3. The mass of the residual char obtained after the first stage.

	Mass of residual char (g)
Pyrolysis	0.3133
S/C-0.5	0.3149
S/C-1	0.3130
S/C-1.5	0.3109
S/C-2	0.3086

After the second stage, no significant variation in the tar percentage is observed compared to that after the first stage, revealing that no devolatilization of organic matters of SS for tar production and no tar reforming and cracking reactions occur, and only gas-solid reactions happen at the second stage. Taking the product distributions from Ca/SS-3:7 at S/C-1 as an example, compared to the first stage, the percentage of char diminishes by 17.3% while the percentage of gas enhances by 18.1% after the second stage. This might be attributed to the release of CO_2 via the

decomposition of the $CaCO_3$ formed at the first stage and the char gasification by the release of CO_2 for CO production (Eq. 5) at the second stage.

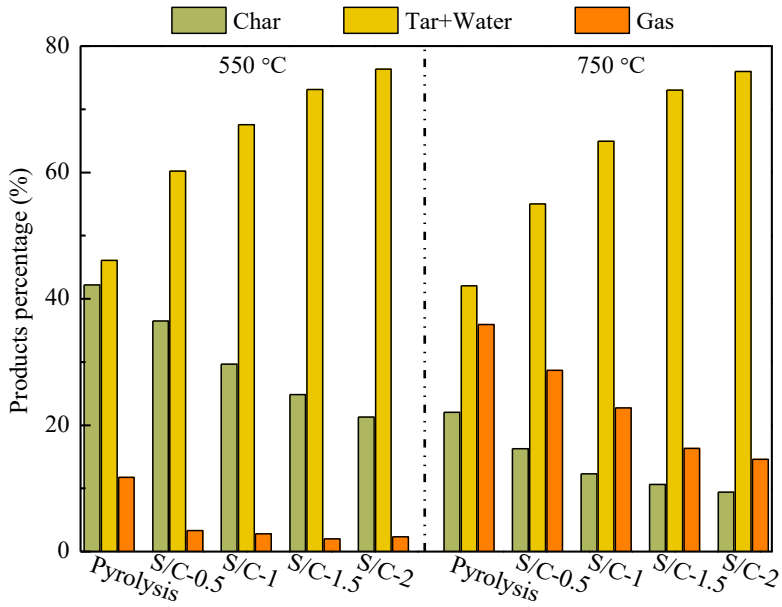

Fig. 4.7. Effects of S/C ratios on the distributions of char, tar, and gas from the TSSE thermochemical conversion of Ca/SS-3:7, **left:** after the first stage (550 °C); **right:** after the second stage (750 °C).

4.3.2.2. Tar composition

Considered as an undesirable by-product, tar is expected to further undergo cracking and reforming reactions for syngas production. Therefore, it is important to identify the composition of tar for the subsequent promotion of tar decomposition for syngas production. The tar composition obtained from the TSSE thermochemical conversion of Ca/SS-3:7 is complex including a wide variety of organic compounds. In this chapter, each GC/MS measurement was carried out under identical conditions for comparison. The constituents identified in the tars can be divided into the following five groups: (1) aliphatic hydrocarbons with the number of carbon ranging from C_6 to C_{35}; (2) mono-aromatic compounds including toluene, styrene, phenol, benzene and their corresponding alkyl derivatives; (3) two-ring aromatics which include naphthalene, benzofuranone and their

corresponding alkyl derivatives; (4) oxygen-containing compounds, such as alcohols (ROH), ketones (ROR'), carboxylic acids (RCOOH), esters (RCOOR'), where R and R' represent long aliphatic chains and cyclanes with the number of carbon ranging between C_5 and C_{39}; (5) nitrogen-containing compounds, which include indol, pyridine, amide, and their alkyl derivative.

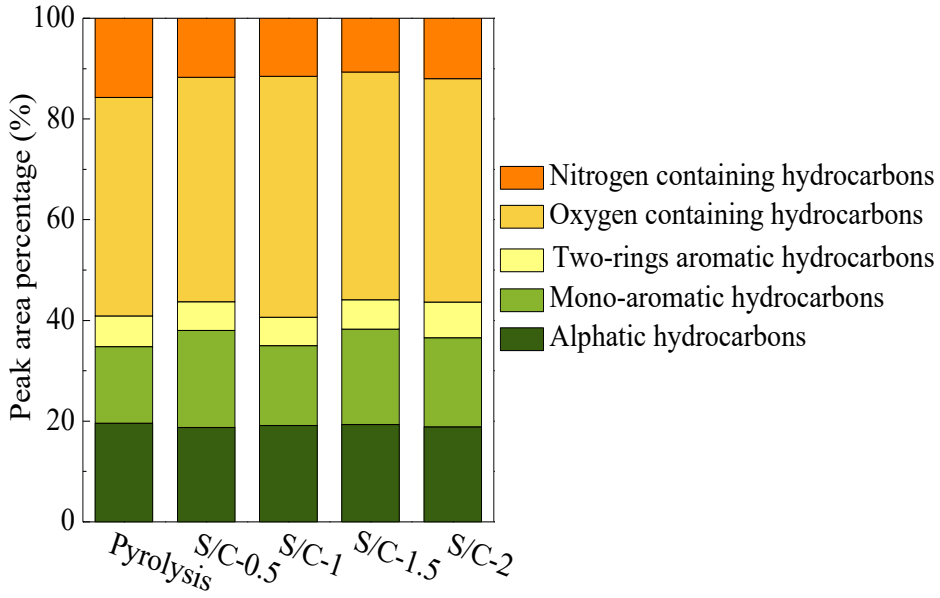

Fig. 4.8. Effects of S/C ratios on the tar compositions obtained from the TSSE thermochemical conversion of Ca/SS-3:7.

Fig. 4.8 shows the variations of tar composition as a function of the S/C ratios, expressed as the peak area fractions of each group. It can be seen that the steam contents exert only a negligible influence on the tar composition. The tar composition is dominated by oxygen-containing hydrocarbons in the range of 43.4-47.9%, aligning well with the previous studies [43, 44]. Conventional petroleum fuels have lower oxygen contents and consequently higher energy values. Therefore, extensive researches in the upgrading of bio-oil by hydrodeoxygenation have been carried out to promote the wide application of bio-oil [45, 46]. The percentages of aliphatic hydrocarbons and mono-aromatic hydrocarbons are at a similar level of 18.8-19.6% and 15.2-

19.2%, respectively, followed by nitrogen-containing hydrocarbons and two-ring aromatic hydrocarbons. In addition, polycyclic aromatic hydrocarbons (PAHs) are considered as carcinogenic and mutagenic chemicals, which is an important constituent of tar reported by other papers [47, 48]. In this chapter, no PAHs is identified in the tars. It was reported that the PAHs could be formed when the temperature is above 700 ˚C [49], while the tar in this chapter is produced at 550 ˚C, leading to the negligible amounts of PAHs and avoid increasing the toxicity of tar.

4.3.2.3. Elemental utilization efficiency

The CO and H_2 in the syngas are mainly derived from the carbon and hydrogen containing compounds in the SS. To understand the transformation of elements during the TSSE thermochemical conversion process, the elemental utilization efficiency was explored by comparing the carbon and hydrogen distributions in the char, tar and gas between the TSSE pyrolysis and steam gasification of Ca/SS-3:7 (Fig. 4.9). The carbon in the char (char-C) and gas (gas-C) are expressed as percentage of the fresh Ca/SS-3:7, while the hydrogen in the char (char-H) and gas (gas-H) are expressed as proportion in the total hydrogen fed into the system, including the hydrogen contents of fresh Ca/SS-3:7 and the introduced steam. The carbon and hydrogen in the tar (tar-C and tar-H) were obtained by the difference of those in the char and gas.

As for the carbon distribution from the TSSE pyrolysis of SS at the first stage, the carbon in the tar, char, and gas is around 61.4%, 36.6%, and 2.0%, respectively. Compared to the carbon distribution from the TSSE pyrolysis of SS, a slight reduction of carbon distribution in the char is ascribed to the char-steam gasification reactions leading to a slight increase in the percentage of gas-C to 6.2% from the TSSE steam gasification of SS at S/C-1 at the first stage. When the temperature increases to 750 °C at the second stage, the increase of tar-C is negligible for both the

TSSE pyrolysis and steam gasification, as discussed above. However, 57.4% of char-C emitted from the first stage into the second stage is converted into gas-C for the TSSE pyrolysis, and 42.1% of char-C remains in the char. Upon the TSSE steam gasification, the conversion efficiency of char-C emitted from the first stage into the second stage to the gas-C increases to 74.8%, and the residual char-C reduces to 22.0%.

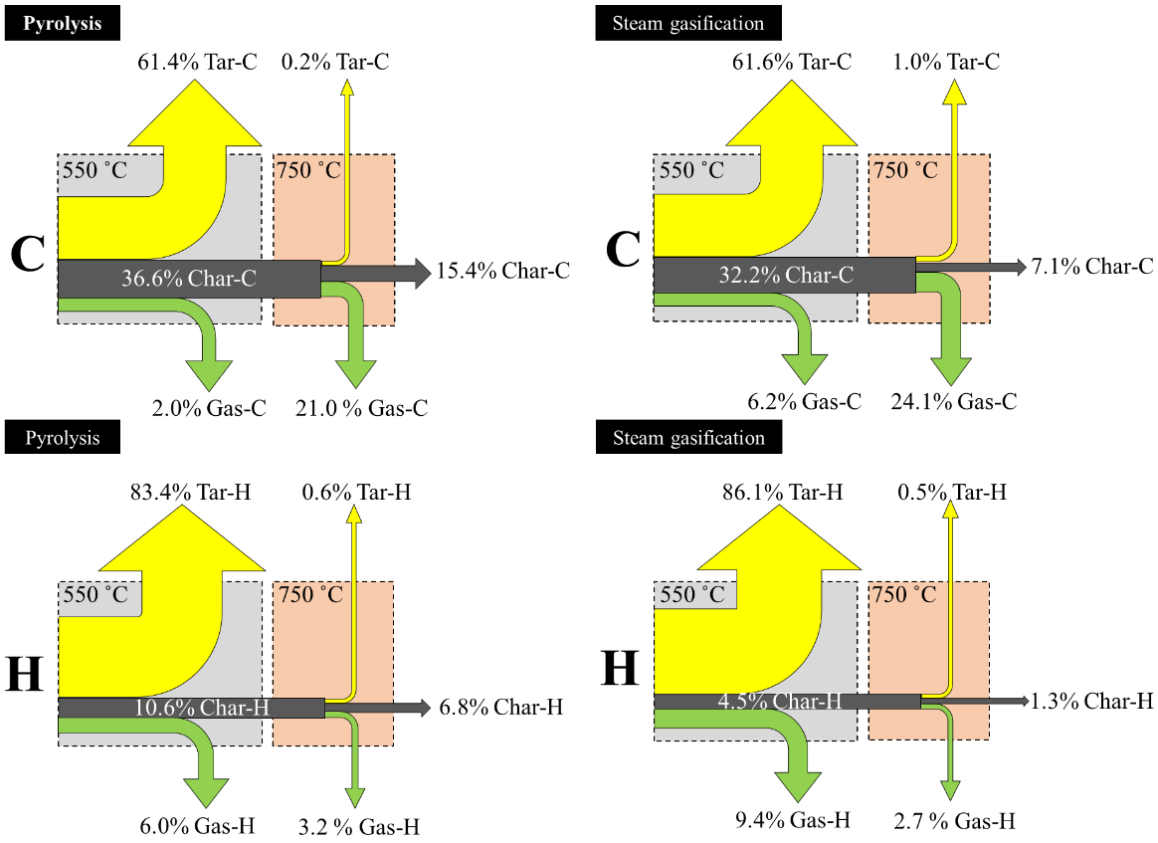

Fig. 4.9. Comparison of the elemental (C and H) distribution in the char, tar, and gas obtained from the TSSE thermochemical conversion of Ca/SS-3:7.

For the hydrogen distribution at the first stage, most of the hydrogen of up to 83.4% and 86.1% distributed in the tar was generated from the TSSE pyrolysis and steam gasification of SS, respectively. The percentage of char-H decreases from 10.6% obtained from the TSSE pyrolysis to 4.5% obtained from the TSSE steam gasification, while the proportion of gas-H increases from

6.0% obtained from the TSSE pyrolysis to 9.4% obtained from the TSSE steam gasification. Regarding the hydrogen distribution at the second stage, the fraction of gas-H to the char-H emitted from the first stage into the second stage increases from 30.2% generated from the TSSE pyrolysis to 60.0% generated from the TSSE steam gasification, and the fraction of the remaining char-H reduces from 64.2% generated from the TSSE pyrolysis to 28.9% generated from the TSSE steam gasification.

In summary, the addition of steam has little influence on the distribution of carbon and hydrogen in the tar, while it could promote the conversion of carbon and hydrogen from solid-phase (char) to gas-phase, with 7.1% of char-C and 1.3% of char-H generated from the TSSE steam gasification. Considering the syngas is the target product of TSSE steam gasification, the promotional conversion efficiencies of carbon and hydrogen in the char to the gas could improve the utilization efficiency of carbon and hydrogen. The conversion efficiency of carbon and hydrogen in the tar to the gas can still be further improved, since up to 62.6% of carbon and 86.6% of hydrogen remain in the tar which would be discharged from the reactor at the first stage and not take part in the reactions at the second stage. This is mainly ascribed to the relatively low temperature (550 °C) at the first stage, which favors the devolatilisation of SS for tar production [50]. The high levels of tar-C and tar-H from the mixture of SS and CaO at 600 °C were also observed by Liu et al. [51]. It is imperative to promote the transformation of tar to gas at the first stage in order to further increase the syngas production. Previous studies have examined several methods for the elimination of tar, among which, thermal and catalytic cracking and reforming of tar for syngas production are generally preferred [52]. For the TSSE thermochemical conversion process, the development of cost-effective catalysts is of great importance to further eliminate tar production and promote syngas production. In addition, it is worth further employing the optimal temperature

at the first stage which would achieve the best compromise between tar elimination and CaO carbonization.

4.4. Conclusions

In order to achieve a tunable H_2/CO ratio in the syngas produced from the TSSE steam gasification process of SS, steam was introduced into the first stage of the TSSE steam gasification process, resulting in significantly enhanced H_2 production at the first stage with 3 times as high as the H_2 production from the TSSE steam gasification compared to that from the TSSE pyrolysis of Ca/SS-3:7. For the TSSE steam gasification of SS, the maximum syngas production is generated from Ca/SS-3:7 reaching 323.8 NmL/$g_{dry\ ss}$ with 72.2 vol% of H_2 at the first stage and 60.5 vol% of CO at the second stage. Moreover, a wide range of H_2/CO ratio in the syngas from 0.9 to 4.7 is obtained from the TSSE steam gasification of SS. The H_2-rich and CO-rich gas stream are produced at the first stage and the second stage, respectively, providing a promising option for direct integration of the TSSE steam gasification of SS with the syngas applications where H_2 and CO could be mixed in desirable ratios for the downstream synthesis of value-added chemicals and fuels. Based on a detailed analysis of product distributions from the TSSE thermochemical conversion of SS, the tar is mainly produced at the first stage, while the second stage is dominated by the conversion of char into gas. The steam contents exert only a negligible influence on the tar composition. Considering a majority of carbon and hydrogen remain in the tar, there is plenty of room for further improvement of the conversion efficiency of the tar into the syngas. Future work on promoting the decomposition of tar is in progress for optimising the TSSE thermochemical conversion process to achieve high-quality syngas production from SS.

References

1. Schulz, H., *Short history and present trends of Fischer-Tropsch synthesis.* Applied Catalysis A: General, 1999. **186**(1-2): p. 3-12.
2. Calderone, V.R., et al., *De Novo design of nanostructured Iron-Cobalt Fischer-Tropsch catalysts.* Angewandte Chemie International Edition, 2013. **52**(16): p. 4397-4401.
3. Dry, M.E., *The Fischer-Tropsch process: 1950-2000.* Catalysis Today, 2002. **71**(3-4): p. 227-241.
4. Chen, Z., et al., *High quality syngas production from catalytic coal gasification using disposable $Ca(OH)_2$ catalyst.* Chemical Engineering Journal, 2017. **316**: p. 842-849.
5. Wu, H. and K. Lin, *Thermodynamic analysis of hydrogen-rich syngas production with a mixture of aqueous urea and biodiesel.* International Journal of Hydrogen Energy, 2018. **43**(14): p. 6804-6814.
6. Hegarty, M.E.S., A.M. O'Connor, and J.R.H. Ross, *Syngas production from natural gas using ZrO_2-supported metals.* Catalysis Today, 1998. **42**(3): p. 225-232.
7. Navarro, R.M., et al., *Hydrogen production from renewable sources: biomass and photocatalytic opportunities.* Energy & Environmental Science, 2008. **2**(1): p. 35-54.
8. Huber, G.W., S. Iborra, and A. Corma, *Synthesis of transportation fuels from biomass: chemistry, catalysts, and engineering.* Chemical reviews, 2006. **106**(9): p. 4044.
9. Shen, Y., et al., *By-products recycling for syngas cleanup in biomass pyrolysis-An overview.* Renewable and Sustainable Energy Reviews, 2016. **59**: p. 1246-1268.
10. Lee, J.S., et al., *Widely controllable syngas production by a dye‐sensitized TiO_2 hybrid system with Re^{I} and Co^{III} catalysts under visible‐light irradiation.* Angewandte Chemie International Edition, 2017. **56**(4): p. 976-980.

11. Beller, M., et al., *Progress in hydroformylation and carbonylation.* Journal of Molecular Catalysis A: Chemical, 1995. **104**: p. 17-85.

12. De Smit, E. and B.M. Weckhuysen, *The renaissance of iron-based Fischer-Tropsch synthesis: on the multifaceted catalyst deactivation behaviour.* Chemical Society Reviews, 2008. **37**(12): p. 2758-2781.

13. Ail, S.S. and S. Dasappa, *Biomass to liquid transportation fuel via Fischer Tropsch synthesis-Technology review and current scenario.* Renewable and Sustainable Energy Reviews, 2016. **58**: p. 267-286.

14. Buelens, L.C., et al., *Super-dry reforming of methane intensifies CO_2 utilization via Le Chatelier's principle.* Science (New York, N.Y.), 2016. **354**(6311): p. 449-452.

15. Nipattummakul, N., et al., *Hydrogen and syngas production from sewage sludge via steam gasification.* International Journal of Hydrogen Energy, 2010. **35**(21): p. 11738-11745.

16. Sikarwar, V., et al., *An overview of advances in biomass gasification.* Energy & Environmental Science, 2016. **9**(10).

17. He, C., et al., *Hydrothermal gasification of sewage sludge and model compounds for renewable hydrogen production: A review.* Renewable and Sustainable Energy Reviews, 2014. **39**: p. 1127-1142.

18. Al-Rahbi, A.S. and P.T. Williams, *Hydrogen-rich syngas production and tar removal from biomass gasification using sacrificial tyre pyrolysis char.* Applied Energy, 2017. **190**: p. 501-509.

19. Florin, N.H. and A.T. Harris, *Enhanced hydrogen production from biomass with in situ carbon dioxide capture using calcium oxide sorbents.* Chemical Engineering Science, 2008. **63**(2): p. 287-316.

20. Ji, G., et al., *Enhanced hydrogen production from Sawdust decomposition using hybrid-functional Ni-CaO-Ca_2SiO_4 materials.* Environmental Science & Technology, 2017. **51**(19): p. 11484.

21. Chen, F.W., C. Dong, L. Vassallo, A. Williams, P. Huang, J., *Characteristics and catalytic properties of Ni/CaAlOx catalyst for hydrogen-enriched syngas production from pyrolysis-steam reforming of biomass sawdust.* Appl. Catal., B, 2016. **183**: p. 168-175.

22. Pimenidou, P., et al., *High purity H_2 by sorption-enhanced chemical looping reforming of waste cooking oil in a packed bed reactor.* Bioresource Technology, 2010. **101**(23): p. 9279-9286.

23. Zhao, X., et al., *Biomass-based chemical looping technologies: the good, the bad and the future.* Energy & Environmental Science, 2017. **10**(9): p. 1885-1910.

24. Onwudili, J.A., P. Radhakrishnan, and P.T. Williams, *Application of hydrothermal oxidation and alkaline hydrothermal gasification for the treatment of sewage sludge and pharmaceutical wastewaters.* Environmental Technology, 2013. **34**(4): p. 529-537.

25. Arregi, A., et al., *Hydrogen production from biomass by continuous fast pyrolysis and in-line steam reforming.* RSC Advances, 2016. **6**(31): p. 25975-25985.

26. Klerk, A.d., *Fischer-Tropsch fuels refinery design.* Energy & Environmental Science, 2011. **4**(4): p. 1177-1205.

27. Sansaniwal, S.K., et al., *Recent advances in the development of biomass gasification technology: A comprehensive review.* Renewable and Sustainable Energy Reviews, 2017. **72**: p. 363-384.

28. Zhou, X., et al., *XRD-based quantitative analysis of clay minerals using reference intensity ratios, mineral intensity factors, Rietveld, and full pattern summation methods: A critical review.* Solid Earth Sciences, 2018. **3**(1): p. 16-29.

29. Hu, M., et al., *Hydrogen-rich gas production by the gasification of wet MSW (municipal solid waste) coupled with carbon dioxide capture.* Energy, 2015. **90**: p. 857-863.

30. Sharma, S. and P.N. Sheth, *Air-steam biomass gasification: Experiments, modeling and simulation.* Energy Conversion and Management, 2016. **110**: p. 307-318.

31. Chang, A.C.C., et al., *Biomass gasification for hydrogen production.* International Journal of Hydrogen Energy, 2011. **36**(21): p. 14252-14260.

32. Wei, L., et al., *Hydrogen production in steam gasification of biomass with CaO as a CO_2 absorbent.* Energy & Fuels, 2008. **22**(3): p. 1997-2004.

33. Luo, S., et al., *Hydrogen-rich gas from catalytic steam gasification of biomass in a fixed bed reactor: Influence of temperature and steam on gasification performance.* International Journal of Hydrogen Energy, 2009. **34**(5): p. 2191-2194.

34. Guoxin, H. and H. Hao, *Hydrogen rich fuel gas production by gasification of wet biomass using a CO_2 sorbent.* Biomass and Bioenergy, 2009. **33**(5): p. 899-906.

35. Weerachanchai, P., M. Horio, and C. Tangsathitkulchai, *Effects of gasifying conditions and bed materials on fluidized bed steam gasification of wood biomass.* Bioresource Technology, 2009. **100**(3): p. 1419-1427.

36. Rapagnà, S., et al., *Steam-gasification of biomass in a fluidised-bed of olivine particles.* Biomass and Bioenergy, 2000. **19**(3): p. 187-197.

37. Hanaoka, T., et al., *Hydrogen production from woody biomass by steam gasification using a CO_2 sorbent.* Biomass and Bioenergy, 2005. **28**(1): p. 63-68.

38. Acharya, B., A. Dutta, and P. Basu, *An investigation into steam gasification of biomass for hydrogen enriched gas production in presence of CaO.* International Journal of Hydrogen Energy, 2010. **35**(4): p. 1582-1589.

39. Acharya, B., A. Dutta, and P. Basu, *Chemical-looping gasification of biomass for hydrogen-enriched gas production with in-process carbon dioxide capture.* Energy & Fuels, 2009. **23**(10): p. 5077-5083.

40. Luo, S., Y. Zhou, and C. Yi, *Syngas production by catalytic steam gasification of municipal solid waste in fixed-bed reactor.* Energy, 2012. **44**(1): p. 391-395.

41. Zhang, Q., et al., *Effect of Fe/Ca-based composite conditioners on syngas production during different sludge gasification stages: Devolatilization, volatiles homogeneous reforming and heterogeneous catalyzing.* International Journal of Hydrogen Energy, 2017. **42**(49): p. 29150-29158.

42. Chen, S., et al., *Steam gasification of sewage sludge with CaO as CO_2 sorbent for hydrogen-rich syngas production.* Biomass and Bioenergy, 2017. **107**: p. 52-62.

43. Duan, D., et al., *Renewable jet-fuel range hydrocarbons production from co-pyrolysis of lignin and soapstock with the activated carbon catalyst.* Waste Management, 2019. **88**(C): p. 1-9.

44. Yang, Z., et al., *Process design and economics for the conversion of lignocellulosic biomass into jet fuel range cycloalkanes.* Energy, 2018. **154**: p. 289-297.

45. Mortensen, P.M., et al., *A review of catalytic upgrading of bio-oil to engine fuels.* Applied Catalysis A: General, 2011. **407**(1): p. 1-19.

46. Xiu, S. and A. Shahbazi, *Bio-oil production and upgrading research: A review.* Renewable and Sustainable Energy Reviews, 2012. **16**(7): p. 4406-4414.

47. Sánchez, M.E., et al., *Effect of pyrolysis temperature on the composition of the oils obtained from sewage sludge.* Biomass and Bioenergy, 2009. **33**(6): p. 933-940.

48. Jordan, C.A. and G. Akay, *Occurrence, composition and dew point of tars produced during gasification of fuel cane bagasse in a downdraft gasifier.* Biomass and Bioenergy, 2012. **42**: p. 51-58.

49. Zhang, B., et al., *Mechanism of wet sewage sludge pyrolysis in a tubular furnace.* International Journal of Hydrogen Energy, 2011. **36**(1): p. 355-363.

50. Alvarez, J., et al., *Sewage sludge valorization by flash pyrolysis in a conical spouted bed reactor.* Chemical Engineering Journal, 2015. **273**: p. 173-183.

51. Liu, H., et al., *Product distribution and sulfur behavior in sewage sludge pyrolysis: Synergistic effect of Fenton peroxidation and CaO conditioning.* Fuel, 2015. **159**: p. 68-75.

52. Guo, F., et al., *Catalytic cracking of biomass pyrolysis tar over char-supported catalysts.* Energy Conversion and Management, 2018. **167**: p. 81.

Chapter 5 Syngas production from co-gasification of sewage sludge and biochar using two-stage sorption-enhanced catalytic thermochemical conversion process

Published as: Yang, X., Gu, S., Kheradmand, A., Jiang, Y. (2021) Syngas production from two-stage sorption-enhanced steam gasification of sewage sludge over bifunctional Ni-Ca catalyst, *Energy Fuels,* Vol. 35(6), pp. 4997-5005. https://doi.org/10.1021/acs.energyfuels.0c04395.

5.1. Introduction

Syngas is a critical precursor for the production of synthetic fuels, which has great potential to combat the energy crisis [1, 2]. Syngas production from the gasification of biomass, a renewable energy source, has attracted extensive attention worldwide [3, 4]. However, there are some undesirable impurities in the biomass-derived syngas restricting the commercial feasibility and industrial implementation of biomass gasification for syngas production.

One bottleneck of the existing gasification technology is the tar removal from syngas [5, 6]. Tar is a kind of viscous liquid of hydrocarbons and free carbon with low condensation temperature, which is often accompanied by syngas production and can easily lead to blockage and corrosion of downstream equipment [7]. Thermal and catalytic cracking of tar into syngas can achieve the purpose of simultaneously purifying the syngas and enhancing the syngas yield, recognized as a sustainable and economical promising approach to eliminate the tar. Regarding the thermal tar elimination, a higher temperature results in a lower yield of tar and a higher yield of gas [8, 9]. It was reported that temperatures over 1000 °C are required to remove the tar completely [10]. The large energy input makes it hard to eliminate tar thermally alone. Catalytic elimination of tar has been demonstrated to facilitate its conversion into the gas at lower temperatures [11-13]. Various types of catalysts such as alkali metals [14, 15], noble metal-based catalysts [16-18] and nickel (Ni)-based catalysts [19-21], have been developed for tar elimination during the gasification of

biomass. The noble metal-based catalysts, such as Rh, Ru, Pt, exhibit excellent catalytic activity, thermal stability and coke resistance [22]. However, high cost and limited availability restrict their large-scale applications. The previous research demonstrated that Ni-based catalysts are also highly active for tar elimination and cost-effective, especially under steam atmosphere [20, 23-25]. Bi-functional Ni-CaO/Al_2O_3 catalyst is an appealing candidate for the sorption-enhanced process to maximise H_2 production, posing dual roles in tar cracking/reforming for gas production and promoting H_2 production with the *in situ* CO_2 capture simultaneously, which has been applied for the dry reforming of methane [26], steam gasification of ethanol [27] or tar model compounds [28]. Ashok et al. [28] demonstrated that Ni-CaO/Al_2O_3 catalyst shows a superior catalytic performance on steam reforming of toluene reflected by high H_2 production, stable CO_2 adsorption capacity and significant coke resistance.

Removal of undesirable incondensable gases, like CO_2, is another challenge for the utilization of the biomass-derived syngas. Recent studies suggest that biochar is carbon-rich, and high-temperature biochar may reach carbon contents of more than 95 wt% [29-31]. To date, the applications of the carbon-rich biochar mainly focus on its carbon sequestration properties. Since the carbon in biochar has been demonstrated to be stable and refractory, the biochar in the soil could be one possible means of reducing the atmospheric CO_2 concentration [32]. It is estimated that the maximum sequestration potential of biochar might be as large as 1.8 Gt of carbon per year, which accounts for 12% of the total global carbon anthropogenic emissions [33]. On the other hand, biochar can also be used for upgrading the flue gas or syngas. Several studies have investigated that the carbon-rich biochar can react with the CO_2 gas in the biomass-derived syngas to produce CO via reverse Boudouard reaction [34-36]. It was reported that the concentration of cumulative CO volume increased by 76.4% using CO_2 compared to N_2 as an agent [37].

A new two-stage sorption-enhanced (TSSE) thermochemical conversion of sewage sludge (SS) integrating with a CaO-based CO_2 carrying cycle has been proposed in Chapter 3 and 4, in which, CaO works as a CO_2 carrier in the sludge matrix, capturing the CO_2 generated from the SS to promote the H_2 production at the first stage (a lower temperature) and releasing it to gasify the SS char for CO production at the second stage (a higher temperature). However, this process is still facing the following two challenges: (1) tar elimination for syngas production; and (2) a certain amount of CO_2 released at the second stage without being efficiently converted into CO. To address the first issue, the effect of increasing temperature and a series of Ni-CaO/Al_2O_3 catalysts with different Ni and CaO ratios on the elimination of tar for syngas production were investigated in this chapter. And a co-gasification process of SS and carbon-rich biochar from pyrolysis of Eucalyptus was proposed, in which the biochar acts as an extra carbon source to *in situ* eliminate the CO_2 for CO production. Moreover, the synergistic effect of steam, Ni-CaO/Al_2O_3 catalyst and biochar on the syngas production from the TSSE catalytic steam gasification of SS was also studied.

5.2. Material and methods

5.2.1. Material preparation

The SS used in this chapter was obtained prior to anaerobic digestion from a municipal wastewater treatment plant in Sydney, Australia. The mixture of SS and CaO (SS-CaO pellets, 0.85-1.00 mm) used in this chapter containing 30% of the mass ratio of CaO, is notated as Ca/SS-3:7. The detailed SS-CaO pellet preparation methods, and the SS properties including ultimate and proximate analysis were described in Section 3.2.1 in Chapter 3.

The Ni-CaO/Al_2O_3 catalysts were prepared using a co-precipitation method. Certain amounts of $Ca(NO_3)_2 \cdot 4H_2O$, $Al(NO_3)_3 \cdot 9H_2O$ and $Ni(NO_3)_2 \cdot 6H_2O$ were dissolved in deionised water, and then

Na_2CO_3 solution (1 M) was added dropwise to the solution under vigorous stirring. The pH value was adjusted to 9 using NaOH solution. The suspension was aged under agitation for 3 h and then filtered under vacuum. The obtained filter cake was rinsed with deionised water several times, then dried at 80 °C for 24 h. The dried solid was calcined at 800 ˚C for 4 h with a heating rate of 2 °C/min in the static air, followed by grinding, pressing, and sieving to obtain the Ni-CaO/Al_2O_3 pellets (0.5-0.85 mm) ready for use. The Ni-CaO/Al_2O_3 catalysts are labelled as Ni*x*Ca*y*/Al, where *x* and *y* denote the weight fraction of Ni and CaO, respectively.

Table 5.1. Proximate analysis of air-dried Eucalyptus, and ultimate analysis of air-dried Eucalyptus and Eucalyptus-derived biochar.

Proximate analysis [a]	**(wt%, dry basis)**	**Ultimate analysis** [b]	**(wt%, dry ash free basis)**	
			Eucalyptus	**Eucalyptus-derived biochar**
Moisture	7.3	C	52.0	72.2
Volatile matter	83.1	H	6.8	1.5
Ash	4.0	N	1.4	1.63
Fixed carbon	5.6			

[a] The proximate analysis was conducted using a thermogravimetric analyzer (TGA, TGA/DSC 1, Mettler Toledo).
[b] The ultimate analysis was conducted using an elemental analyzer (Vario EL III, Elementar).

The biochar used in this chapter was obtained from the pyrolysis of Eucalyptus (size: 1 mm) at 800 °C for 60 min with a heating rate of 10 °C/min under a continuous pure N_2 flow rate (15 mL/min). The proximate analysis of the air-dried Eucalyptus is shown in Table 5.1, and the contents of volatile matter, ash and fixed carbon are comparable with the typical values as reported in other studies [38, 39]. The volatile matter content of the air-dried Eucalyptus is much higher than that of SS reported in Table 3.1 in Chapter 3, while the ash content is much lower. There is a significant rise of up to 72.2 wt% in the proportion of carbon in the Eucalyptus-derived biochar (Table 5.1).

5.2.2. Experimental procedures

The TSSE catalytic thermochemical conversion (including pyrolysis and steam gasification) of the SS were performed in a fixed-bed reactor at atmospheric pressure, as shown in Fig. 5.1. The biochar pellets, Ni-CaO/Al_2O_3 pellets, and SS-CaO pellets were loaded on the quartz wool in sequence in a stainless-steel tube (length: 300 mm; inner diameter: 6 mm). A nitrogen flow of 15 mL/min was used as the carrier gas during the experiment, and a constant flow pump and a preheater were employed to introduce steam into the reactor. Detailed procedures of the TSSE catalytic thermochemical conversion process are as follows: (1) heating the loaded pellets from room temperature to the first stage temperature at a rate of 30 °C/min and keeping for 45 min, as the first stage; (2) subsequently, heating the remaining sample to the second stage temperature at a rate of 30 °C/min and keeping for another 45 min, as the second stage. As for the TSSE catalytic steam gasification, the steam was introduced into the reactor for the first 30 min at the first stage, and the corresponding molar ratio of steam to carbon (S/C) in the SS was 1. The tar was collected by a condenser system and incondensable gases (H_2, N_2, CH_4, CO, and CO_2) were on-line analysed by a comprehensive two-dimensional gas chromatograph (GC, 7890B, Agilent). The detailed tar collection and gaseous products detection were described in Section 4.2.2 in Chapter 4.

5.2.3. Sample characterization and product distribution analysis

The powder X-ray diffraction (XRD) was performed to identify the crystal phase of the fresh Ni-CaO/Al_2O_3 catalysts using an X-ray diffractometer (X'Pert PRO, PANalytical) with the Cu Kα radiation in the 2θ range of 10-80°.

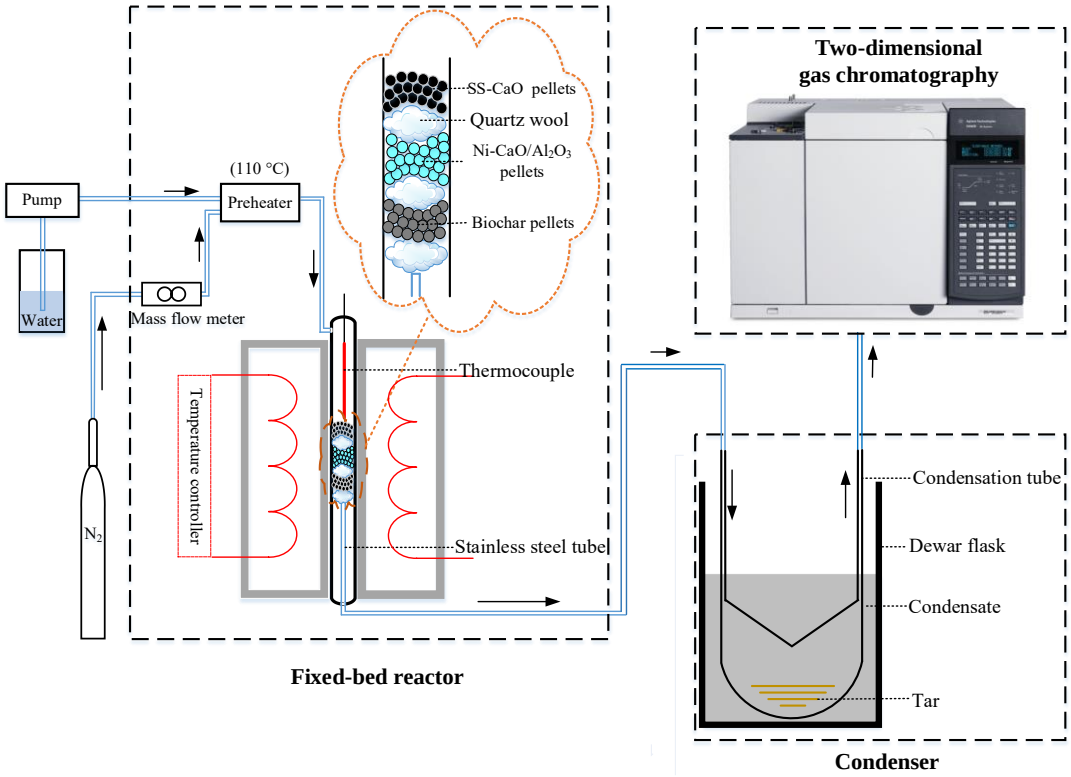

Fig. 5.1. Illustration of the experimental setup used for the TSSE catalytic thermochemical conversion of SS in this chapter.

H_2 temperature-programmed reduction (H_2-TPR) was employed to analyse the reduction behaviour of the fresh Ni-CaO/Al_2O_3 catalysts using an automated chemisorption flow analyser (ChemBET PULSAR TPR/TPD, Quantachrome Instruments). About 50 mg catalyst pellets were loaded in a quartz U-tube and heated to 800 °C at a rate of 10 °C/min under a gas flow of 50 mL/min containing 10 vol% of H_2 with N_2 as the balance gas.

The CO_2 adsorption capacity of Ni_5Ca_{40}/Al catalyst was conducted by a thermogravimetric analyzer (TGA/DSC 2, Mettler Toledo). Approximately 30 mg of the Ni_5Ca_{40}/Al catalyst was placed in a 70 µL alumina pan and heated from room temperature to 600 °C for 30 min at a rate of 10 °C/min under a 20 vol% CO_2 flow of 80 mL/min, and then heated to 800 °C for another 30 min at a rate of 10 °C/min under a N_2 flow rate of 80 mL/min. The carbonation-calcination cycles were

repeated for 5 times. The CO_2 adsorption capacity was expressed as the mass fraction of the added weight after the carbonation process at 600 °C in the CaO weight of the Ni_5Ca_{40}/Al catalyst.

The morphology of fresh and spent Ni_5Ca_{40}/Al catalyst was observed using a JEOL-7100F field emission scanning electron microscope equipped with an energy-dispersive x-ray spectrometer.

The distributions of SS-derived char, biochar and tar are expressed in mass fractions of them in the sum of Ca/SS-3:7, steam and biochar, while the percentage of gas was calculated by the difference between total and the fractions of SS-derived char, biochar and tar. For each case, the mass of SS-derived char, biochar and tar were gained as the weight differences of the Ca/SS-3:7, biochar and condenser before and after the TSSE thermochemical conversion process, respectively. Regarding the yield of SS-derived char, the mass of CaO was excluded, as CaO has no potential to be converted into tar or gas. Since the steam could take part in the steam reforming reactions and it was condensed together with the liquid tar, the mass of steam was included in the yield of tar.

5.3. Results and discussion

5.3.1. Process description

On the basis of the TSSE thermochemical conversion process proposed in Chapter 3 and 4, Ni-CaO/Al_2O_3 catalyst and biochar were introduced into the process to eliminate tar and enhance syngas production simultaneously in this Chapter. The TSSE catalytic thermochemical conversion process diagram is shown in Fig. 5.2. To avoid cross-contamination between SS-CaO, biochar and catalyst, the SS-CaO, Ni-CaO/Al_2O_3 catalyst and biochar pellets are layer loaded. At the first stage (a lower temperature around 600 °C), the SS devolatilization is occurred to generate tar and gaseous products (H_2, CO_2, CO and CH_4). And thereby, the CaO and Ni in the SS-CaO and Ni-

CaO/Al_2O_3 catalyst would catalyse the tar cracking/reforming (Eq. 1, 2) and water-gas shift (WGS, Eq. 3) reactions to produce H_2 and CO_2. Meanwhile, the released CO_2 from the above reactions would be *in situ* captured by CaO, which shift the equilibrium of those reactions toward higher yield and purity of H_2 at the first stage. When it comes to the second stage (a higher temperature around 800 °C), the captured CO_2 is released from $CaCO_3$ decomposition and *in situ* gasifies SS-derived char to produce CO via the reverse Boudouard reaction (Eq. 4). The unconverted CO_2 from SS-CaO layer and released CO_2 from Ni-CaO/Al_2O_3 catalyst layer would react with biochar for CO production.

$$Tar \rightarrow H_2+CO+CO_2+C_mH_n,\ \Delta H_{298K}>0 \quad (1)$$

$$Tar+H_2O \rightarrow H_2+CO+CO_2+C_mH_n+H_2O,\ \Delta H_{298K}>0 \quad (2)$$

$$CO+H_2O \leftrightharpoons CO_2+H_2,\ \Delta H_{298K}= -41.2\ KJ/mol \quad (3)$$

$$C+CO_2 \leftrightharpoons 2CO,\ \Delta H_{298K}= +172.4\ KJ/mol \quad (4)$$

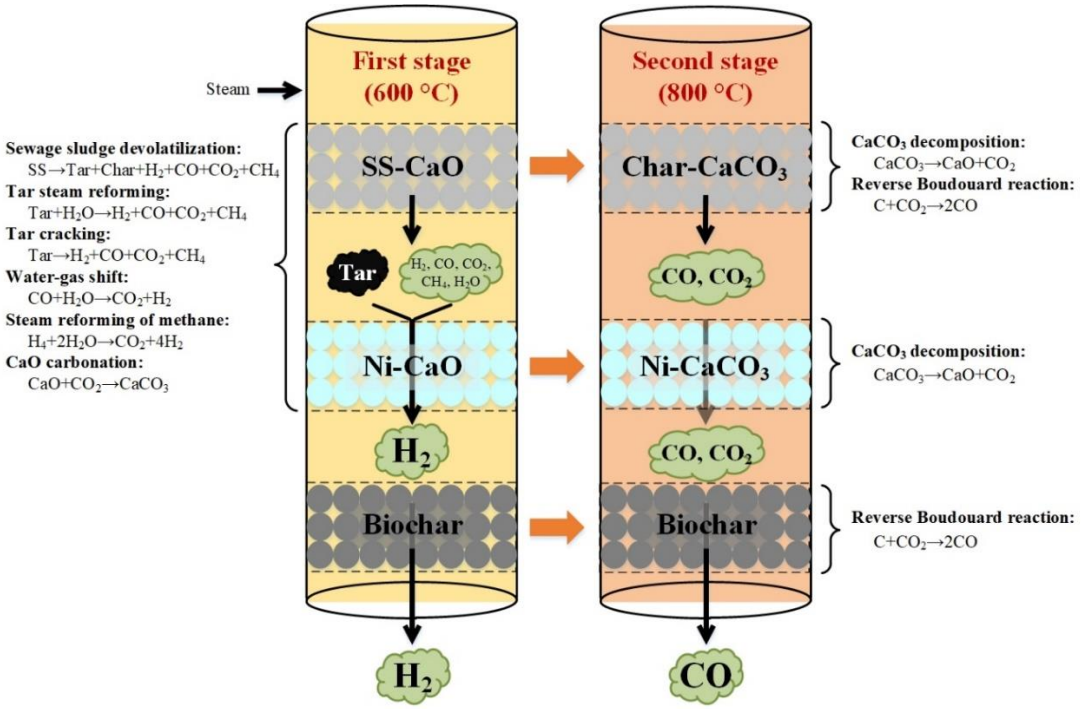

Fig. 5.2. Process diagram of the TSSE catalytic thermochemical conversion of SS in this chapter.

5.3.2. Role of temperature on syngas production

To study the effect of temperature on the syngas production from the TSSE catalytic steam gasification of SS, the yield and purity of H_2, CO, CO_2 and CH_4 as a function of temperature are shown in Fig. 5.3. The key point of the proposed TSSE thermochemical conversion process is the CaO act as a sorbent to capture CO_2 and promote H_2 production at the first stage. Therefore, restricted by the thermodynamic equilibrium of the CaO carbonation reaction at the first stage [40], the temperature range of the first stage was set from 550 °C to 650 °C at intervals of 50 °C. As shown in Fig. 5.3a, the yield of H_2, which is the target product at the first stage, increases from 256.0 NmL/$g_{dry\ SS}$ at 550 °C to 543.9 NmL/$g_{dry\ SS}$ at 650 °C, whereas the purity of H_2 decreases from 90.2 vol% at 550 °C to 79.4 vol% at 650 °C. The enhancement in the H_2 yield is mainly ascribed to the favored endothermic tar cracking/reforming reactions at the high temperature for H_2 production, which is accompanied with the decrease in the yield of tar at the elevated temperatures (Fig. 5.3a (insert)). However, the high yield of H_2 production always accompanies with a high yield of CO_2 generated, and part of which is not captured by CaO and then released, leading to a decrease in the purity of H_2. Taking both the yield and purity of H_2 into account, the temperature of the first stage is determined as 600 °C for H_2 production.

The target product at the second stage, CO, is mainly generated via the reverse Boudouard reaction (Eq. 4). This is a highly endothermic reaction and favourable at high temperatures. The yield and purity of CO and CO_2 in the gas product generated from the second stage of the TSSE catalytic steam gasification process as a function of temperature ranging from 750 °C to 900 °C at 50 °C intervals are shown in Fig. 5.3b. The CO yield increases by 60.6% from 129.8 NmL/$g_{dry\ SS}$ at 750°C to 208.4 NmL/$g_{dry\ SS}$ at 800 °C, while the CO_2 yield decreases from 750 °C to 800 °C. However, no obvious change in the production of CO and CO_2 was observed when the temperature

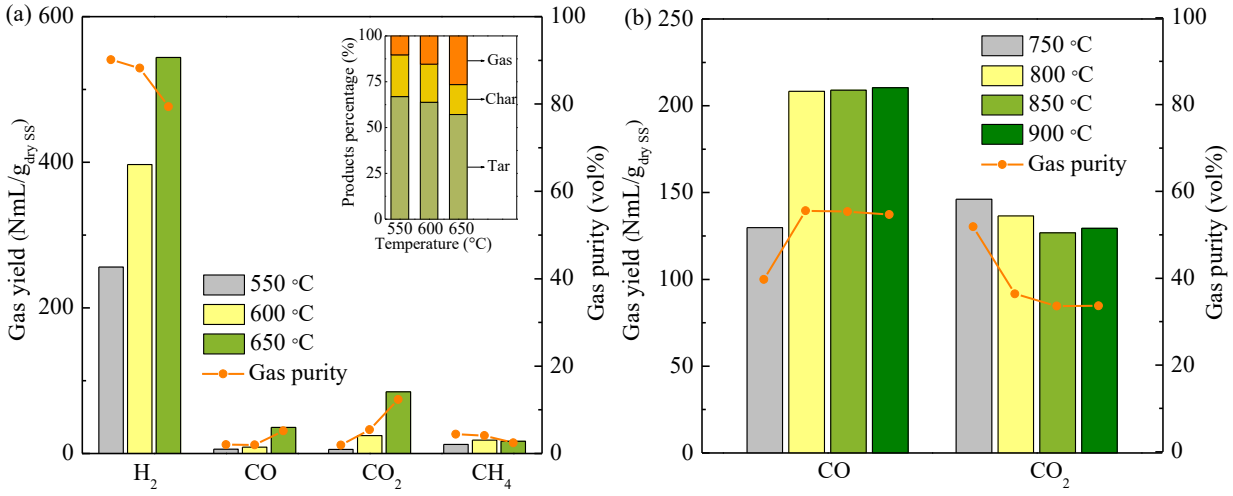

Fig. 5.3. Influence of temperatures on the gas production at (a, insert: product distribution) the first stage and (b) the second stage of the TSSE catalytic steam gasification of Ca/SS-3:7. Experimental conditions: 0.3 g Ca/SS-3:7 pellets, 0.3 g Ni_5Ca_{40}/Al pellets, 0.1g biochar pellets, S/C-1.

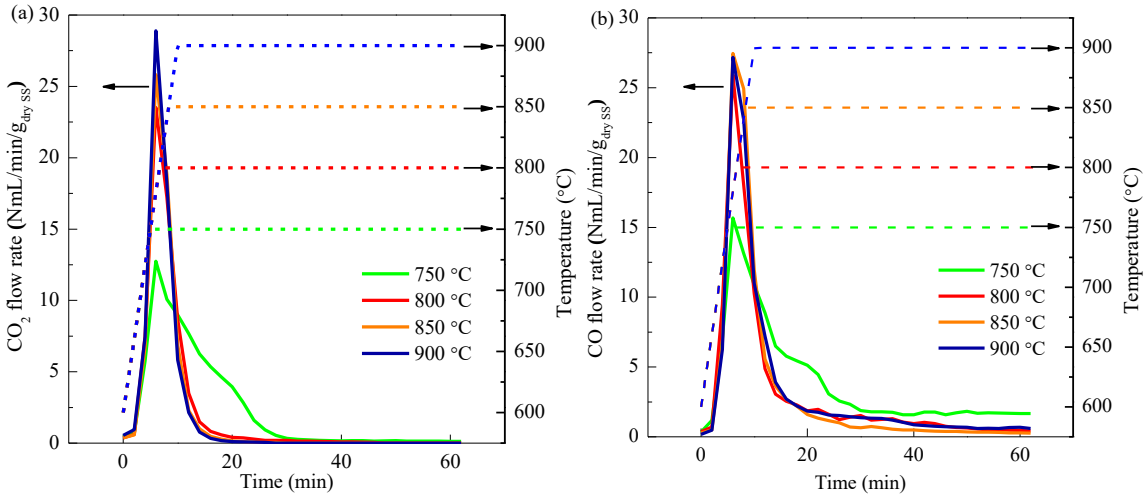

Fig. 5.4. Influence of temperature on the (a) CO_2 and (b) CO flow rate from the second stage of the TSSE catalytic steam gasification of Ca/SS-3:7. Experimental conditions: 0.3 g Ca/SS-3:7 pellets, 0.3 g Ni_5Ca_{40}/Al pellets, 0.1 g biochar pellets, S/C-1, 600 °C for the first stage. Solid lines represent CO_2 and CO generated flow rate along with the reaction time; Short dash lines represent the reaction temperature along with the reaction time.

of the second stage is above 800 °C. As the reactant gas that produces CO at the second stage, CO_2 is mainly released from the decomposition of $CaCO_3$ formed at the first stage. However, whether the temperature of the second stage increases to 850 °C or 900 °C, Fig. 5.4 shows that the flow rate of CO_2 still peaks at 800 °C. Therefore, despite the thermodynamic and kinetic favourability of the reverse Boudouard reaction (Eq. 4) at a higher temperature, large quantities of reactant gas CO_2 is released at 800 °C, leaving less reactant gas CO_2 at 850 °C or 900 °C for CO production and resulting in little change in CO production at 850 °C and 900 °C. Consequently, 800 °C is chosen as the temperature for the second stage for CO production.

5.3.3. Role of Ni-CaO/Al_2O_3 catalyst on syngas production

5.3.3.1. Role of the Ni content of Ni-CaO/Al_2O_3 catalyst

Fig. 5.5 shows the performance of Ni-CaO/Al_2O_3 catalysts at various Ni contents (2.5, 5, 7.5 and 10 wt%) with a fixed CaO content of 40 wt% in the syngas production. It appears that among the studied catalysts, the highest H_2 yield and purity at the first stage were obtained over Ni_5Ca_{40}/Al catalyst, and just slightly lower yields were obtained when $Ni_{7.5}Ca_{40}$/Al and $Ni_{10}Ca_{40}$/Al catalysts were used, whereas the lowest yield was observed for $Ni_{2.5}Ca_{40}$/Al catalyst (Fig. 5.5a). As for the CO production at the second stage (Fig. 5.5b), no obvious change of CO production was observed between the catalysts with various Ni contents. It was reported by Osaki and Mori [41] that the degree of contact of catalyst and carbon is one of the concerning factors influencing the rate of reverse Boudouard reaction (Eq. 4). The layer loaded SS-CaO, Ni-CaO/Al_2O_3 catalyst, and biochar pellets greatly reduces the degree of contact of Ni-CaO/Al_2O_3 catalyst and carbon in the SS-CaO and biochar pellets, resulting in a weak catalytic activity of Ni on the reverse Boudouard reaction (Eq. 4). As shown in Fig. 5.5c, there is a stable H_2/CO ratio of 1.6-2.0 in the syngas by adjusting the Ni content.

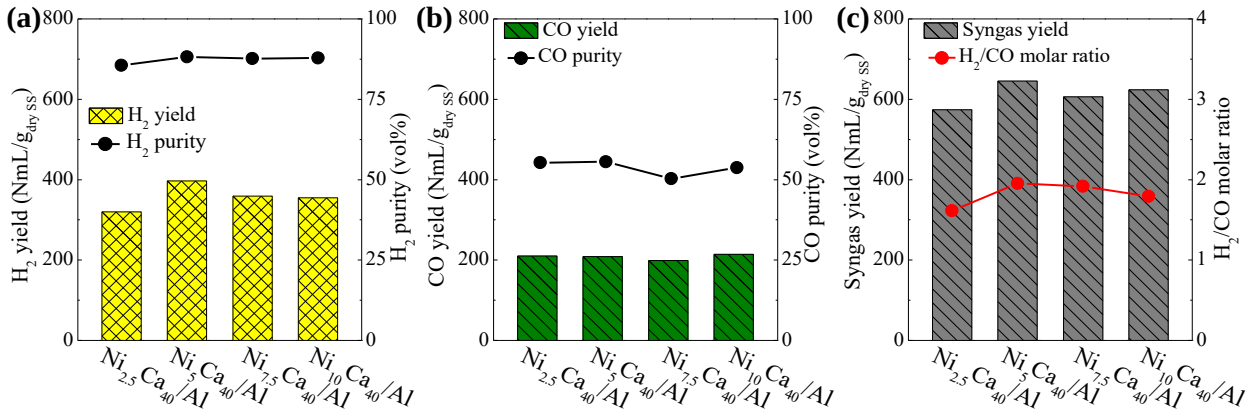

Fig. 5.5. H_2 and CO production as a function of Ni content of Ni-CaO/Al_2O_3 catalyst from the TSSE catalytic steam gasification of Ca/SS-3:7: (a) H_2 yield and purity generated at the first stage; (b) CO yield and purity generated at the second stage; (c) total syngas (H_2+CO) yield and H_2/CO molar ratio. Experimental conditions: 0.3 g Ca/SS-3:7 pellets, 0.3 g Ni-CaO/Al_2O_3 catalyst pellets, 0.1 g biochar pellets, S/C-1, 600 °C for the first stage, 800 °C for the second stage.

The X-ray diffraction analyses were conducted to identify the crystalline phases in the Ni-CaO/Al_2O_3 catalysts with various Ni contents as shown in Fig. 5.6a. The fresh $Ni_{2.5}Ca_{40}$/Al catalyst dominates by CaO-Al_2O_3 mixed oxides, while free CaO and $Ca(OH)_2$ are the main crystalline phases in the fresh Ni-CaO/Al_2O_3 catalysts when the Ni contents are over 2.5 wt%. The existence of free CaO and $Ca(OH)_2$ act as CO_2 sorbents to favour H_2 production. The small diffractions of NiO were detected in all Ni-CaO/Al_2O_3 catalysts. The presence of the NiO phase indicates the availability of catalytic sites to promote the tar cracking/reforming and WGS reactions (Eq. 1-3) [42, 43]. Except for the NiO phase, the $NiAl_2O_4$ crystalline phase appears in the Ni-CaO/Al_2O_3 catalysts when the Ni content is over 2.5 wt%. The $NiAl_2O_4$ is assigned to the spine structure providing high stability and strong dispersion for the metallic particles [44]. Besides, the characteristic peak of Al_2O_3 is also identified in all catalysts.

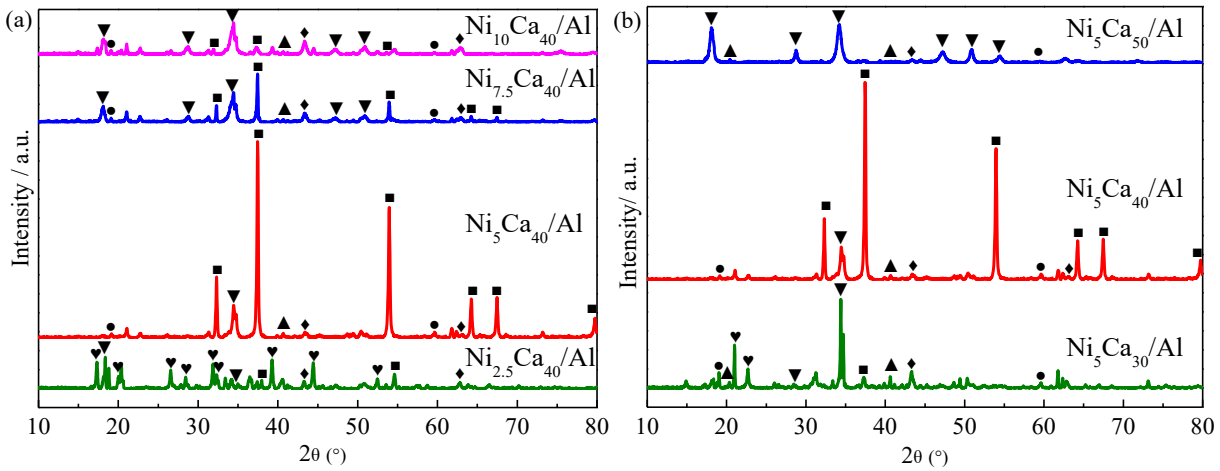

Fig. 5.6. XRD pattern of the fresh Ni-CaO/Al_2O_3 catalysts with various (a) Ni contents and (b) CaO contents. ■ CaO; ▼$Ca(OH)_2$; ♦ NiO; ▲Al_2O_3; ● $NiAl_2O_4$; ♥ CaO-Al_2O_3 mixed oxides.

The H_2-TPR profiles of Ni-CaO/Al_2O_3 catalysts with various Ni contents are shown in Fig. 5.7. The peak appearing at a high temperature around 840 °C is ascribed to the $NiAl_2O_4$ phase which has a spinel structure with the characteristic of thermal stability requiring high temperature for its reduction [45]. In agreement with the XRD results, no reducible peak assigned to the $NiAl_2O_4$ phase at ca. 840 °C is observed for the $Ni_{2.5}Ca_{40}$/Al catalyst. There are two Ni reduction peaks between 550 °C and 800 °C observed for all the Ni-CaO/Al_2O_3 catalysts, which are ascribed to the NiO species interacting with CaO and Al_2O_3 [46]. However, the Ni reducible peaks of Ni_5Ca_{40}/Al catalyst between 550 °C and 800 °C slightly shift towards higher temperatures, which might indicate that NiO is dispersed more thoroughly and even more strongly interaction with CaO and Al_2O_3 [47]. The high dispersion and strong metal-support interaction probably facilitate the catalytic performance for H_2 production at the first stage.

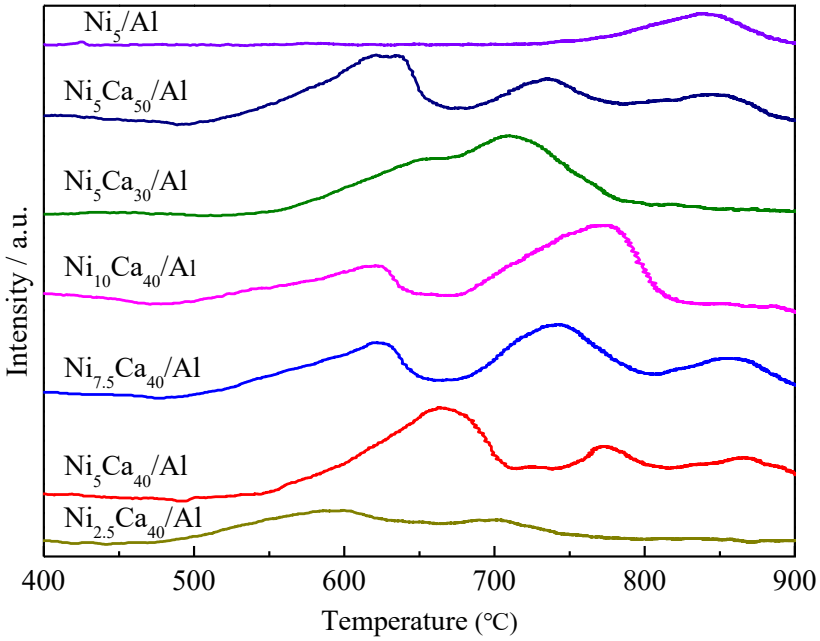

Fig. 5.7. H_2-TPR profiles of the fresh Ni-CaO/Al_2O_3 catalysts.

5.3.3.2. Role of the CaO contents of Ni-CaO/Al_2O_3 catalyst

Further investigations for the syngas production performance of the Ni-CaO/Al_2O_3 catalysts as a function of CaO contents (30, 40 and 50 wt%) with the optimal Ni content of 5 wt% were conducted as shown in Fig. 5.8. Of these three catalysts, Ni_5Ca_{40}/Al catalyst shows the highest H_2 production at the first stage, followed by Ni_5Ca_{50}/Al, while the lowest H_2 production was obtained using Ni_5Ca_{30}/Al catalyst (Fig. 5.8a). At the second stage, CO production is enhanced with the increased CaO contents in the Ni-CaO/Al_2O_3 catalyst (Fig. 5.8b). As the XRD patterns are shown in Fig. 5.6b, CaO, $Ca(OH)_2$, and the CaO-Al_2O_3 mixed oxides are identified in the fresh Ni_5Ca_{30}/Al catalyst. With the increasing CaO contents, the CaO and $Ca(OH)_2$ phases are dominant in the fresh Ni_5Ca_{40}/Al and Ni_5Ca_{50}/Al catalysts. The changes in the Ca species and contents would influence the CO_2 sorption capacity, thereby affecting the H_2 production at the first stage and the CO production at the following second stage. The existence of NiO and $NiAl_2O_4$ is also identified in all three catalysts as shown in the XRD phases in Fig. 5.6b and H_2-TPR profiles in Fig. 5.7. The

Ni reducible peaks of Ni_5Ca_{40}/Al catalyst between 550 °C and 800 °C shifting towards higher temperatures were also observed compared to Ni_5Ca_{30}/Al and Ni_5Ca_{50}/Al catalysts. The H_2/CO ratio ranges from 1.2 to 2.0 by controlling the CaO contents (Fig. 5.8c).

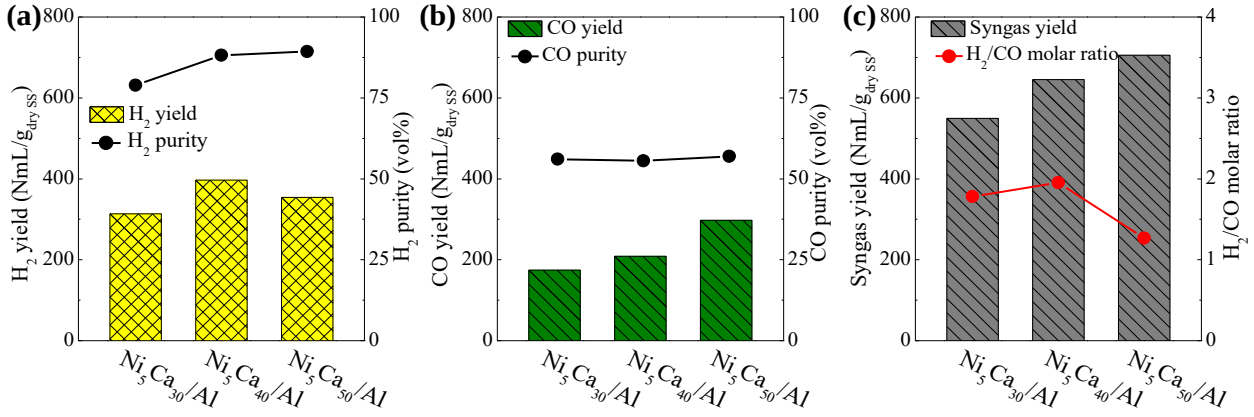

Fig. 5.8. H_2 and CO production performance as a function of CaO contents of Ni-CaO/Al_2O_3 catalysts from the TSSE catalytic steam gasification of Ca/SS-3:7: (a) H_2 yield and purity generated at the first stage; (b) CO yield and purity generated at the second stage; (c) total syngas (H_2+CO) yield and H_2/CO molar ratio. Experimental conditions: 0.3 g Ca/SS-3:7 pellets, 0.3 g Ni-CaO/Al_2O_3 catalyst pellets, 0.1 g biochar pellets, S/C-1, 600 °C for the first stage, 800 °C for the second stage.

5.3.3.3. Role of the composition of Ni-CaO/Al_2O_3 catalyst on the syngas production

The aforementioned results show that the Ni_5Ca_{40}/Al catalyst exhibits the highest selectivity of syngas production from the TSSE catalytic steam gasification of SS. It has been demonstrated that both components of the catalysts, Ni and CaO could affect the syngas production performance of SS (Fig. 5.5 and Fig. 5.8). Therefore, it is critical to investigate the synergistic effect of Ni and CaO in the Ni-CaO/Al_2O_3 catalyst on syngas production. Fig. 5.9 shows the syngas production from the Ni-CaO/Al_2O_3 catalysts consisting of different components. The Ni_5Ca_{40}/Al catalyst, containing Ni, exhibits a higher yield of H_2 produced at the first stage than the Ca_{40}/Al catalyst, and the same trend was observed between the Ni_5/Al and Al catalysts (Fig. 5.9a), which is

attributed to the presence of Ni that could enhance the catalytic cracking/reforming of tar (Eq. 1, 2) for H_2 production [42]. It was reported that Ni could promote the cleavage of C-C, C-H, C-O bonds in the tar, and the formed cracking products are more likely to be dehydrogenated and thus increase the H_2 production [47]. Additionally, Ni shows high catalytic activity in the WGS reaction (Eq. 3) to promote H_2 production [43, 48]. However, no significant improvement in CO production at the second stage was observed between the catalysts with or without Ni. As the above-mentioned, the layer loading of SS-CaO, Ni-CaO/Al_2O_3, and biochar pellets reduces the contact degree of Ni with the reactants of the reverse Boudouard reaction (Eq. 4) and thereby fails to enhance the CO production at the second stage.

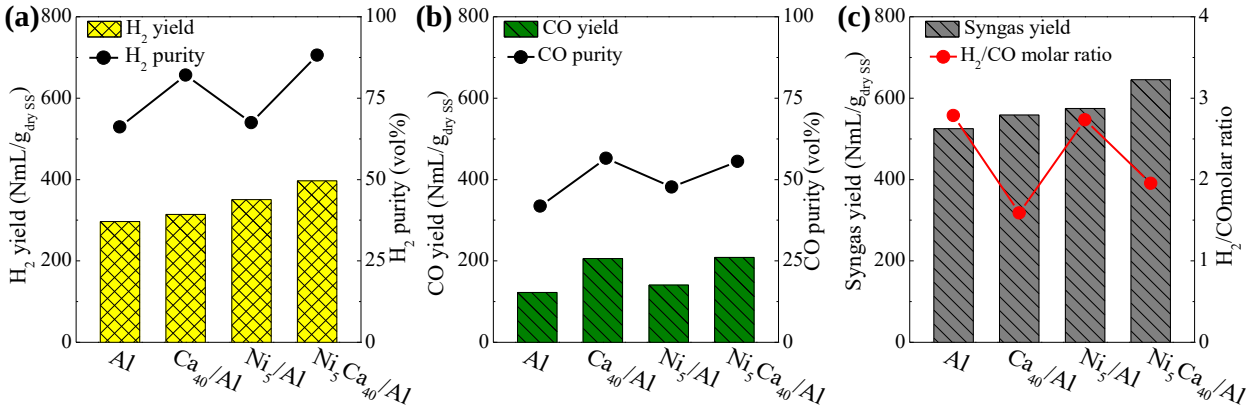

Fig. 5.9. Syngas production performance as a function of the presence of Ni and CaO in the Ni-CaO/Al_2O_3 catalyst from TSSE catalytic steam gasification of Ca/SS-3:7: (a) H_2 yield and purity generated at the first stage; (b) CO yield and purity generated at the second stage; (c) total syngas (H_2+CO) yield and H_2/CO molar ratio. Experimental conditions: 0.3 g Ca/SS-3:7 pellets, 0.3 g Ni-CaO/Al_2O_3 catalyst pellets, 0.1 g biochar pellets, S/C-1, 600 °C for the first stage, 800 °C for the second stage.

For the CaO-containing catalysts, a higher yield of H_2 was observed over the Ni_5Ca_{40}/Al and Ca_{40}/Al catalysts at the first stage compared to the Ni_5/Al and Al, respectively (Fig. 5.9a). The presence of CaO would capture the CO_2 to shift the equilibrium of reactions (Eq. 1-4) that

produced CO_2, thereby favouring the H_2 production at the first stage. Taking the WGS reaction (Eq. 3) as an example, the time evolution of CO and CO_2 release rate, as shown in Fig. 5.10b and Fig. 5.10c, shows that less CO and CO_2 amounts were released from Ca/SS-3:7 with the Ca_{40}/Al and Ni_5Ca_{40}/Al catalysts at the first stage compared to Al and Ni_5/Al catalysts. Not only for the enhancement of H_2 yield, but the presence of CaO would also increase the purity of H_2 obtained at the first stage. For instance, the purity of H_2 increases from 67.4 vol% with the Ni_5/Al catalyst to 88.2 vol% with the Ni_5Ca_{40}/Al catalyst. Regarding the CO production at the second stage, the Ca_{40}/Al and Ni_5Ca_{40}/Al catalysts show an outstanding performance in both the yield and purity of CO compared to Al and Ni_5/Al catalysts, respectively (Fig. 5.9b). Fig. 5.10c indicates that more CO_2 was captured by CaO in the Ca_{40}/Al and Ni_5Ca_{40}/Al catalysts at the first stage, resulting in high CO_2 emissions at the second stage, along with high CO production via the reverse Boudouard reaction (Eq. 4). Consequently, the addition of CaO in the catalysts has greatly improved the H_2 production at the first stage and CO production at the second stage.

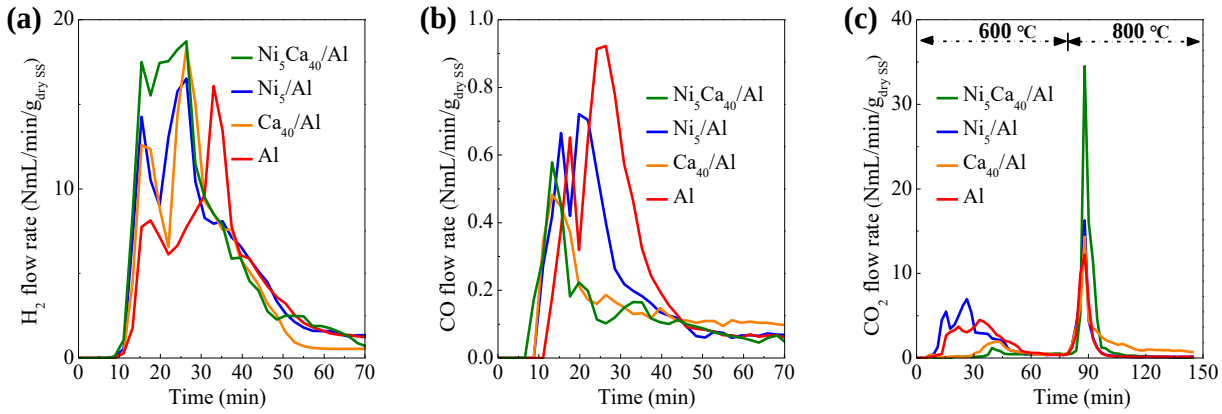

Fig. 5.10. Comparison of the generated flow rate of (a) H_2 at the first stage, (b) CO at the first stage, and (c) CO_2 at the two-stages from Ni_5Ca_{40}/Al, Ni_5/Al, Ca_{40}/Al, and Al.

Moreover, Ni_5Ca_{40}/Al catalyst shows a higher H_2 yield and purity compared to Ni or CaO alone catalysts (Ni_5/Al and Ca_{40}/Al catalysts), concluding a synergistic effect between the Ni and CaO

for H_2 production. And the presence of CaO poses critical influence on CO production at the second stage. The produced syngas is rich in H_2 with the H_2/CO ratios ranging from 1.6 to 2.8, while the presence of CaO in the catalyst would produce a lower H_2/CO ratio of below 2 (Fig. 5.9c).

5.3.3.4. Stability test of Ni_5Ca_{40}/Al catalyst

The above findings indicate high selectivities of H_2 at the first stage and CO at the second stage was achieved over the Ni_5Ca_{40}/Al catalyst. From an industrial perspective, it is of great significance to investigate the stability of this bi-functional catalyst in practical application. Thus, the Ni_5Ca_{40}/Al catalyst was tested for 5 cycles to demonstrate its stability for syngas production. The residual char from the spent Ca-SS/3:7 and biochar after each TSSE catalytic steam gasification process were replenished by fresh Ca-SS/3:7 and biochar. As shown in Fig. 5.11, H_2 and CO production reach maximum values at the 1st cycle, and then exhibit a decrease at the 2nd cycle and keep stable until the 5th cycle, indicating a good stability of H_2 and CO production after the first run. A similar tendency on the CO_2 adsorption capacity of Ni_5Ca_{40}/Al is shown in Fig. 5.12. The CO_2 adsorption capacity peaks at the 1st cycle reaching 39.0%, and then steeply decreases to 17.4% in the 2nd cycle and tends to be stable until the 5th cycle because of the sintering of CaO and the change of physical properties over cyclic carbonation-calcination reactions [46, 49]. The CO_2 adsorption capacity is one of the vital factors for syngas production. The decrease in the cyclic CO_2 capture capacity of the Ni_5Ca_{40}/Al catalyst would weaken the promotional effect of tar cracking/reforming and WGS reaction (Eq. 1-3) for H_2 production at the first stage, thereby resulting in less CO_2 being available for CO production in the following second stage.

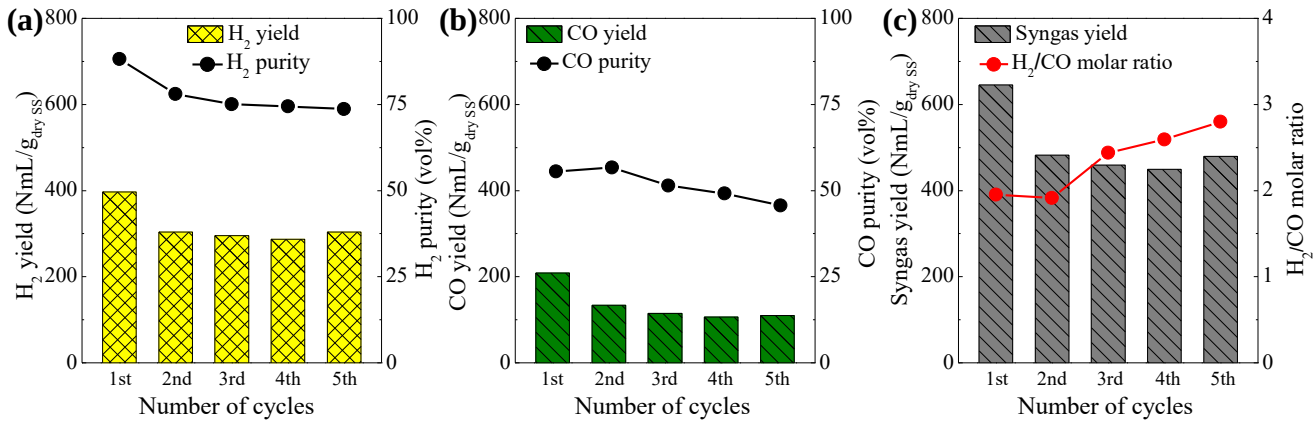

Fig. 5.11. The stability of the Ni_5Ca_{40}/Al catalyst in the syngas production from the TSSE catalytic steam gasification of Ca/SS-3:7**:** (a) H_2 yield and purity generated at the first stage; (b) CO yield and purity generated at the second stage; (c) total syngas (H_2+CO) yield and H_2/CO molar ratio. Experimental conditions: 0.3 g Ca/SS-3:7, 0.3 g Ni_5Ca_{40}/Al catalyst, 0.1 g biochar pellets, S/C-1, 600 °C for the first stage, 800 °C for the second stage.

In addition, the catalytic effect of Ni is another important factor for syngas production. The change in the distribution of elements in the Ni_5Ca_{40}/Al catalyst was investigated by comparing TEM-EDS images of the fresh and spent Ni_5Ca_{40}/Al catalyst after 5 cycles, as shown in Fig. 5.13. The Ca and Ni elements in the fresh Ni_5Ca_{40}/Al catalyst exhibit a homogeneous distribution (Fig. 5.13 top). After 5 cycles, most Ni in the spent catalyst is agglomerated compared to the fresh catalyst (Fig. 5.13, bottom). The sintering of Ni could suppress its catalytic activity in tar cracking/reforming and WGS reactions (Eq. 1-3) for syngas production [50]. Hence, the synthesis of highly active, robust, and sinter-resistant catalysts to facilitate tar conversion for syngas production is still one of the urgent research topics. There is an increase in the H_2/CO ratio from 1.9 to 2.8 with the increase of cycle number, indicating a large reduction in CO production at the second stage (Fig. 5.11c).

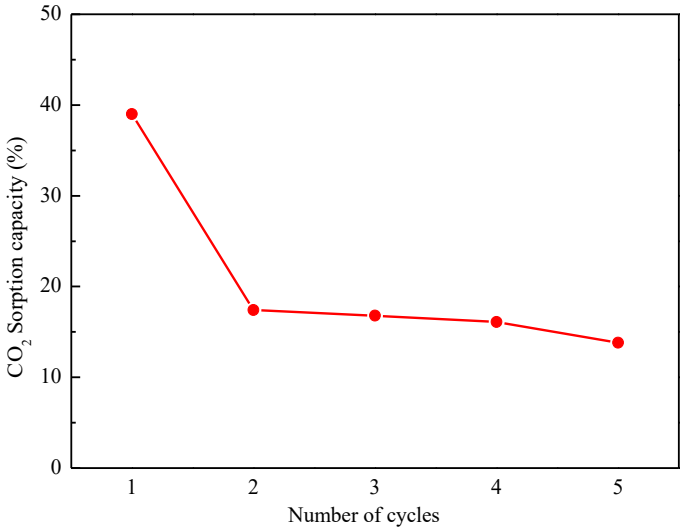

Fig. 5.12. Cyclic CO_2 sorption capacity of the Ni_5Ca_{40}/Al catalyst.

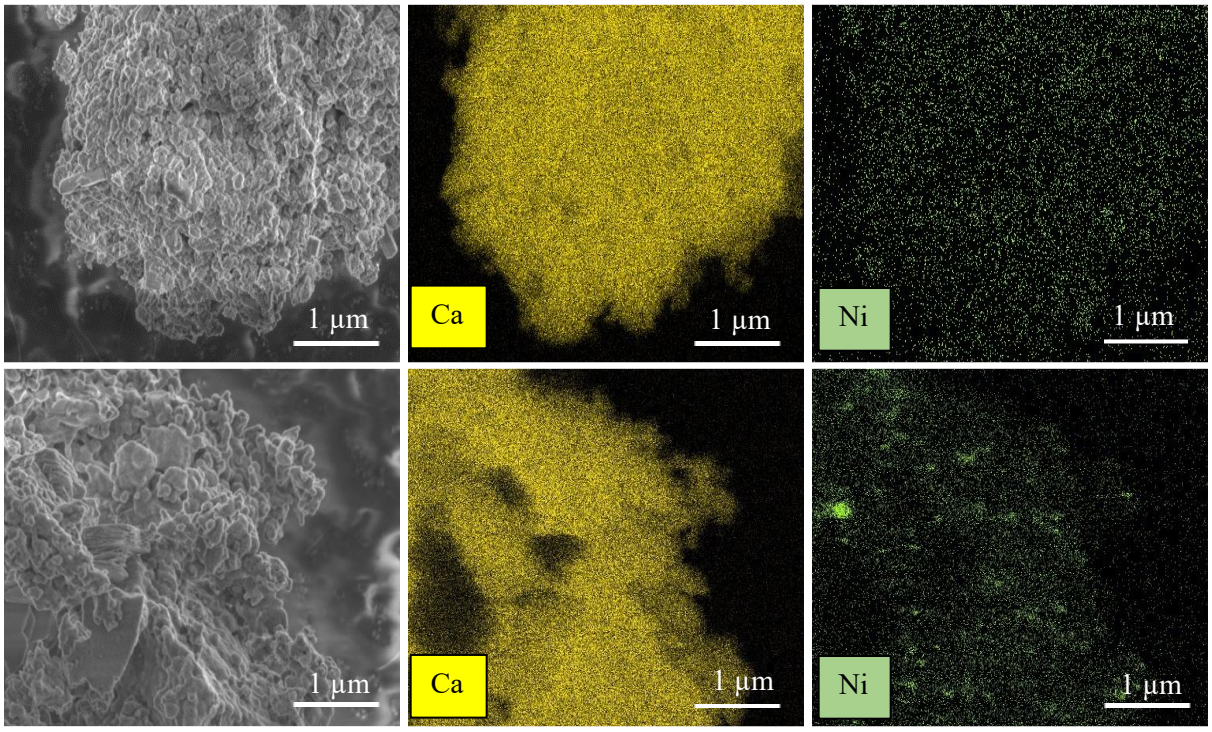

Fig. 5.13. TEM-EDX images of the (top) fresh and (bottom) spent Ni_5Ca_{40}/Al catalyst after 5 cycles.

5.3.4. Synergistic effect of steam, Ni_5Ca_{40}/Al catalyst and biochar on syngas production

5.3.4.1. Role of steam on syngas production

Fig. 5.14 shows the synergistic effect of steam gasification (SG), pyrolysis (P), Ni_5Ca_{40}/Al catalyst (Cat) and biochar on the syngas production from Ca/SS-3:7 using the TSSE catalytic thermochemical conversion process. As shown in Fig. 5.14a, the lowest yield and purity of H_2 at the first stage were obtained from the SS-Cat-Biochar-P, at 120.2 NmL/$g_{dry\ SS}$ and 64.7 vol%, respectively. Upon introduction of steam, 3.3 times higher H_2 yield was achieved from the SS-Cat-Biochar-SG, reaching 396.9 NmL/$g_{dry\ SS}$, and the purity of H_2 reaches 88.2 vol% at the first stage. In Fig. 5.15a, in contrast to a sharp peak of the generated flow rate of H_2 from SS-Cat-Biochar-P, a slowly decreasing trend was observed from SS-Cat-Biochar-SG, resulting in a higher production of H_2. The H_2 generation over a longer period of time was triggered by the addition of steam which could enhance the steam-reforming reactions for H_2 production, such as the WGS reaction (Eq. 3). This is supported by the less CO generated from SS-Cat-Biochar-SG compared to SS-Cat-Biochar-P, as shown in Fig. 5.15b. An increase in the generated flow rate of H_2 is always accompanied by a decrease in the generated flow rate of CO, and vice versa. For the CO production at the second stage in Fig. 5.14b, a CO yield of 157.2 NmL/$g_{dry\ SS}$ was obtained from the SS-Cat-Biochar-P, and 208.4 NmL/$g_{dry\ SS}$ from SS-Cat-Biochar-SG, with a 32.6 % increase. The purity of CO decreases from 64.0 vol% to 54.2 vol% after the addition of steam. As a reactant for CO production via the reverse Boudouard reaction (Eq. 4), a higher amount of CO_2 was released at the second stage from SS-Cat-Biochar-SG as shown in Fig. 5.15c, resulting in a higher yield of CO, while a lower purity of CO. In summary, the addition of steam could significantly increase both the yield and purity of H_2 at the first stage. Correspondingly, a high amount of CO_2 was captured at the first stage and then released at the second stage, leading to high yield of CO at the second stage on the premise of sufficient residual carbon in the char.

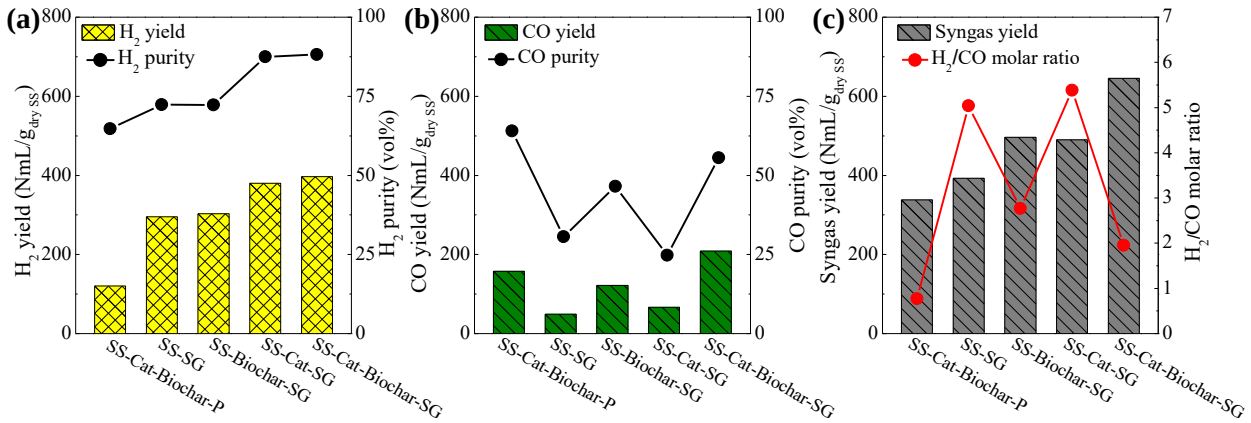

Fig. 5.14. Syngas production as a function of the use of steam, Ni_5Ca_{40}/Al catalyst or biochar from the TSSE catalytic thermochemical conversion of Ca/SS-3:7: (a) H_2 yield and purity generated at the first stage; (b) CO yield and purity generated at the second stage; (c) total syngas (H_2+CO) yield and H_2/CO molar ratio. Experimental conditions: SS: 0.3 g Ca/SS-3:7 pellets, Cat: 0.3g Ni_5Ca_{40}/Al catalyst, Biochar: 0.1g biochar pellets, P: Pyrolysis, SG: steam gasification (S/C-1), 600 °C for the first stage, 800 °C for the second stage.

5.3.4.2. Role of biochar on the syngas production

There is a slight increase in H_2 production at the first stage between the SS-SG and SS-Biochar-SG (Fig. 5.14a), indicating the presence of biochar would sightly promote the H_2 production at the first stage. It was reported that the biochar shows a catalytic activity for tar reforming for H_2 production due to its relatively high surface area and containing alkali/alkaline-earth metals [51, 52]. However, the presence of biochar could remarkably enhance the CO production at the second stage (Fig. 5.14b). For instance, the yield of CO reaches 208.4 NmL/$g_{dry\ SS}$ from SS-Cat-Biochar-SG, almost 3.1 times higher than that from SS-Cat-SG (66.6 NmL/$g_{dry\ SS}$). The carbon-rich biochar could act as a carbon source to convert CO_2 via the reverse Boudouard reaction (Eq. 4) for CO production. Hence, the influence of the addition of biochar on the H_2 production at the first stage

is not significant, while it has a drastic promoting effect on the CO production at the second stage to address the issue that the lack of carbon source remains in the SS for the conversion of CO_2.

5.3.4.3. The synergistic effect of steam, Ni_5Ca_{40}/Al catalyst and biochar on the syngas production

The above results demonstrate that steam and Ni_5Ca_{40}/Al catalyst could promote H_2 production at the first stage. As shown in Fig. 5.14, the yield of H_2 from SS-Cat-Biochar-SG increases by 230.3% compared to SS-Cat-Biochar-P, while SS-Cat-Biochar-SG only exhibits a 34.4% increase in the yield of H_2 compared to SS-SG. This indicates that the steam performs a higher selectivity in H_2 production than the Ni_5Ca_{40}/Al catalyst and biochar. Besides, The CO production from SS-Cat-Biochar-SG and SS-Biochar-SG enhance by 213.0% and 147.6% and compared to SS-Cat-SG and SS-SG, respectively. Higher increase of CO production for SS-Cat-Biochar-SG (213.0%) than SS-Biochar-SG (147.6%), indicates a beneficial effect of biochar on the CO production pronounced by the presence of Ni_5Ca_{40}/Al catalyst. This is likely because the addition of Ni_5Ca_{40}/Al catalyst makes more CO_2 accessible for the CO production at the second stage. In conclusion, the synergistic effect of steam, Ni_5Ca_{40}/Al catalyst and biochar could maximise the yield of the H_2 and CO production at the first and the second stage, respectively. Besides, a gas stream with high purity of H_2 (88.2 vol%) was obtained at the first stage, and a gas stream with high purity of CO (55.6 vol%) was generated at the following second stage, enabling an inherent separation of H_2 and CO products from the SS.

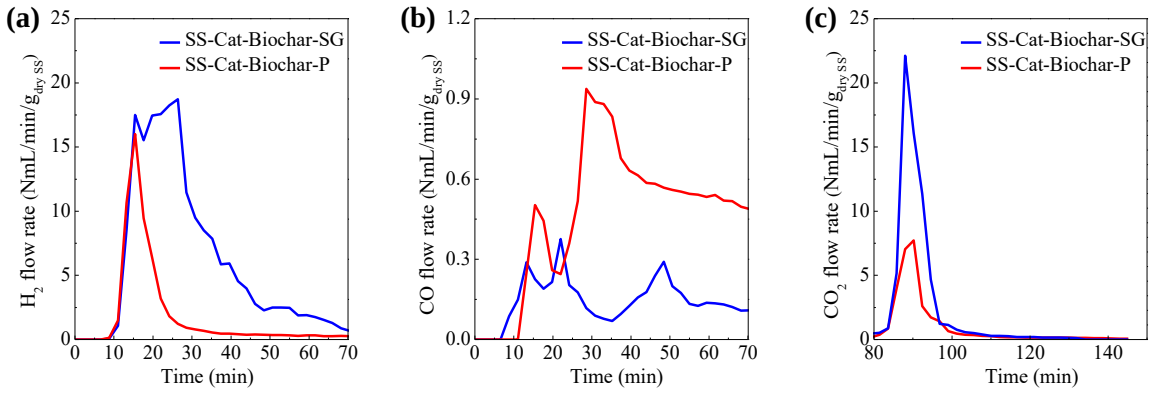

Fig. 5.15. Comparison of the generated flow rate of H_2 at the first stage (a), CO at the first stage (b), and CO_2 at the second stage (c) from the SS-Cat-Biochar-P and SS-Cat-Biochar-SG.

When the syngas production over Ni_5Ca_{40}/Al catalyst and biochar is further compared with that reported in other studies (Table 5.2), it can be observed that the both H_2 and CO purity in this chapter are higher than those reported by other studies. The one of the important reason for the high H_2 purity in this chapter is that the temperature for H_2 production (600 °C) favors CaO carbonation reaction and ensures a fast sufficient CO_2 sorption kinetic, and thereby significantly benefits for the H_2 production by moving WGS reaction (Eq. 3) in the forward direction. However, the catalytical reaction temperature in other studies (Table 5.2) for H_2 production over the catalysts containing CaO is generally up to 800-950 °C which favors the reverse CaO carbonation reaction with a negligible sorption-enhanced effect of CaO. Regarding the higher CO purity in this chapter, the existence of CaO in the catalyst could transfer CO_2 captured at the first stage (600 °C) to release and react with the biochar for CO production at the following second stage (800 °C). Thus, the combined use of Ni-CaO/Al_2O_3 catalyst and biochar exhibits a superior on an inherent separation of high purity H_2 and CO production from SS.

Table 5.2. Summary of syngas production, tar removal efficiency and catalyst stability performance over Ni-CaO/char catalysts via catalytic thermochemical conversion of biomass.

Catalyst	Biomass	Reactor	Operating Temperature	Syngas purity (vol%)		Tar removal efficiency (%) [d]	Catalyst stability	Ref.
				H_2	CO			
Ni/$CaAlO_x$ (the molar ratio of Ca to Al of 1:1)	Sawdust	Dual fixed bed reactors	T_R [a]: 500 °C T_C [b]: 800 °C	50	30	/	The amount of coke deposited on the catalyst was less than 10 wt% of the weight of the reacted catalyst after one cycle. The addition of Ca into the Ni/Al_2O_3 catalyst could improve the catalyst basicity, and thereby reduce coke formation during pyrolysis-reforming of biomass.	[53]
Ni-Ca-Mg-Al (1:1:1:1 mol ratio)	Wood sawdust	Dual fixed bed reactors	T_R: 550 °C T_C: 800 °C	52.3	23.0	/	/	[54]
10 wt% Ni-dolomite (calcined at 900 °C)	Rice husk	Two stages fixed bed reactor system	T_R: 950 °C T_C: 950 °C	59.1	22.8	Only 0.24 g/Nm^3 of tar was obtained.	The amount of carbon deposited on the Ni-dolomite catalyst was only 1.33 wt% after one cycle.	[55]
20 wt% Ni-24 wt% CaO-Ca_2SiO_4	Sawdust	Thermogravimetric mass spectrometry (TG-MS)	850 °C	68	18.5	/	Ni-CaO-Ca_2SiO_4 exhibits superb cyclic stability. After 15 cycles, the H_2 yield decreased by 7%, while the CO yield slightly increased.	[56]
15 wt% NiO/wood char	Sawdust	Dual fixed bed reactors	T_C: 800 °C	33.5	31.1	97	Exhibited an excellent tar removal rate in the first 2 h, and then the rate slightly decreased by 13% but remained stable and high after 2 h until 8 h. (continued on next page)	[57]

Catalyst	Biomass	Reactor	Operating Temperature	Syngas purity (vol%)		Tar removal efficiency (%) [d]	Catalyst stability	Ref.
				H_2	CO			
11.3 wt% Ni-12.1 wt% Co/ lignite char (acid washed)	Corncob	Two stages fixed bed quartz reactor	T_R: 900 °C T_C: 450 °C	63.0	2.0	/	H_2 yield decreased by 23.4% after 7 cycles.	[58]
8 wt% Ni/pine sawdust char	Pine sawdust	Dual fixed bed reactors	T_R: 800 °C T_C: 800 °C	43.8	23.1	90.8	/	[59]
Ni_5Ca_{40}/Al + Biochar	Sewage sludge	Fixed bed reactor	600/800 [c]	88.2	55.6	22.0	The catalyst exhibited an excellent performance of syngas production in the first run. After the first run, stable performance of syngas performance was maintained for at least up to four cycles.	This chapter

[a] T_R: Temperature of pyrolysis/gasification of biomass.
[b] T_C: Temperature of catalytical reforming/cracking of tar.
[c] Sample was treated in sequence at 600 °C and 800 °C.
[d] Tar removal efficiency defined as the percentage of tar removed over catalyst.

As shown in Fig. 5.14c, the H_2/CO molar ratio of syngas is tunable from 0.8 to 5.4. The SS-Cat-Biochar-P in the absence of steam produces CO-rich syngas with the lowest H_2/CO ratio of 0.77. While in the presence of steam and Ni_5Ca_{40}/Al catalyst, the H_2-rich syngas was produced with the highest H_2/CO ratio of 5.4 from SS-Cat-SG. The median H_2/CO ratios of 2.8 and 2.0 were obtained from SS-Biochar-SG and SS-Cat-Biochar-SG which are in the presence of steam and biochar. Therefore, the H_2/CO molar ratio could be tuned by controlling the utilization of steam, Ni_5Ca_{40}/Al catalyst, and biochar. More specifically, the steam and Ni_5Ca_{40}/Al catalyst could improve the selectivity to H_2 production, and the biochar could improve the selectivity to CO production. More importantly, an H_2/CO molar ratio of 2.0 was achieved over the SS-Cat-Biochar-SG, which is an ideal H_2/CO molar ratio for the synthesis of liquid fuels and value-added chemicals, like methanol, via the Fischer-Tropsch process [60, 61].

5.3.5. Product distributions

To clearly understand the thermal and catalytic tar elimination for gas production, the distributions of char, tar and gas are shown in Fig. 5.16. Regarding the TSSE catalytic pyrolysis of Ca/SS-3:7 (Fig. 5.16, left), the tar percentage decreases to 35.4% from 42.0% obtained from the TSSE pyrolysis of Ca/SS-3:7, while the gas production slightly increases to 36.2% from 35.9%. Fig. 5.16 (right) exhibits that the distributions of tar and gas from the TSSE catalytic steam gasification of Ca/SS-3:7 account for 50.6% and 32.4%, respectively. Compared to the TSSE steam gasification of Ca/SS-3:7 shown in Fig. 5.16 (right), the percentage of tar from the TSSE catalytic steam gasification decreases by 22.0%, while the proportion of gas increases by 42.7%. Therefore, the elevated temperature and the presence of steam, Ni-CaO/Al_2O_3 catalyst and biochar could promote the tar cracking/reforming for gas production.

Whereas, the tar removal efficiency in this chapter is lower compared to that in other studies reaching up to 90.8-98.8% (Table 5.2). In this chapter, the tar vaporization and then cracking/reforming over catalyst happens at 600 °C (the first stage), while a beneficial catalytic tar removal was obtained at higher temperature up to 800-950 °C in other studies (Table 5.2). Additionally, it can be noticed that the dual reactors with separation of a tar vaporization reactor and a catalyst bed reactor would lengthen the residence time of tar inside the reactor to further promote the tar cracking/reforming reactions for tar elimination. Those also point the way to the further efforts on efficient tar elimination for syngas production.

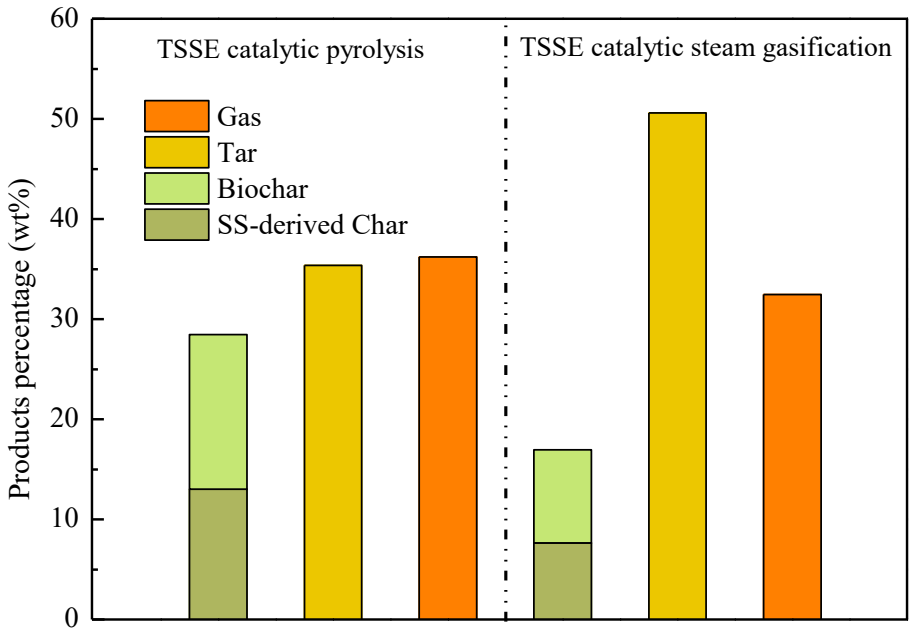

Fig. 5.16. The distributions of char, tar, and gas produced from the TSSE catalytic thermochemical conversion of Ca/SS-3:7.

5.4. Conclusion

To promote tar removal for syngas production from TSSE thermochemical conversion of SS, the thermal and catalytic elimination of tar for syngas production was investigated. It is demonstrated

that the elevated temperature could promote H_2 production at the first stage and CO production at the second stage. And 600 °C and 800 °C are determined as the optimal temperatures for the first and second stage, respectively, at which a perfect integration of tar cracking/reforming, WGS and SRM reactions and CaO carbonation reaction for H_2 production at the first stage, and the reverse Boudouard reaction and $CaCO_3$ decomposition reaction for CO production at the second stage could be achieved. The highest syngas production was obtained from the Ni_5Ca_{40}/Al catalyst, which shows a high dispersion of Ni and strong metal-support interaction. A synergistic effect of CaO and Ni in the Ni_5Ca_{40}/Al catalyst is defined to enhance the H_2 production at the first stage, while CaO is a critical factor for CO production at the second stage. The stability test shows that after the first run, a good performance of H_2 and CO production was maintained for at least up to four cycles.

The elevated temperature and the presence of steam and Ni_5Ca_{40}/Al catalyst play a significant role in H_2 production at the first stage (396.9 NmL/$g_{dry\ SS}$), which is 9.3 times higher than that from the TSSE pyrolysis of Ca/SS-3:7 (in the absence of steam and Ni_5Ca_{40}/Al catalyst, and 550 °C as the first stage temperature) reported previously. The purity of H_2 increases to 88.2 vol% from 49.2 vol% obtained from the TSSE pyrolysis of Ca/SS-3:7. Thereinto, the control experiments indicate that the steam performs a higher selectivity to H_2 than the Ni-CaO/Al_2O_3 catalyst. However, the presences of steam and Ni_5Ca_{40}/Al catalyst have a suppression effect on the CO production at the second stage. Biochar remarkably promotes the CO production at the second stage, which could be further pronounced by the presence of Ni_5Ca_{40}/Al catalyst. The yield of CO (208.4 NmL/$g_{dry\ SS}$) at the second stage triples that in the absence of biochar (66.6 NmL/$g_{dry\ SS}$). The percentage of tar decreases by 22.0% and the gas increases by 42.7% with the elevated temperature and the presence of steam, Ni-CaO/Al_2O_3 catalyst and biochar. Therefore, a synergistic effect of steam,

Ni_5Ca_{40}/Al catalyst and biochar is complementary to drastically eliminate the tar and facilitate syngas production. The highest yield of syngas reaches 645.5 $NmL/g_{dry\ SS}$ with 88.2 vol% of H_2 at the first stage and 55.6 vol% of CO at the second stage, and a desirable H_2/CO ratio of 2 is achieved for the downstream liquid fuels and value-added chemicals synthesis via Fischer-Tropsch process.

References

1. De Smit, E. and B.M. Weckhuysen, *The renaissance of iron-based Fischer-Tropsch synthesis: on the multifaceted catalyst deactivation behaviour.* Chemical Society Reviews, 2008. **37**(12): p. 2758-2781.
2. De Klerk, A., *Fischer-Tropsch refining: technology selection to match molecules.* Green Chemistry, 2008. **10**(12): p. 1249-1279.
3. Udomsirichakorn, J. and P.A. Salam, *Review of hydrogen-enriched gas production from steam gasification of biomass: The prospect of CaO-based chemical looping gasification.* Renewable and Sustainable Energy Reviews, 2014. **30**: p. 565-579.
4. Santos, R.G.d. and A.C. Alencar, *Biomass-derived syngas production via gasification process and its catalytic conversion into fuels by Fischer Tropsch synthesis: A review.* International Journal of Hydrogen Energy, 2019.
5. Sikarwar, V., et al., *An overview of advances in biomass gasification.* Energy & Environmental Science, 2016. **9**(10).
6. Sansaniwal, S.K., et al., *Recent advances in the development of biomass gasification technology: A comprehensive review.* Renewable and Sustainable Energy Reviews, 2017. **72**: p. 363-384.
7. Watson, J., et al., *Gasification of biowaste: A critical review and outlooks.* Renewable and Sustainable Energy Reviews, 2018. **83**: p. 1-17.

8. Anis, S. and Z.A. Zainal, *Tar reduction in biomass producer gas via mechanical, catalytic and thermal methods: A review.* Renewable and Sustainable Energy Reviews, 2011. **15**(5): p. 2355-2377.

9. Peng, W., et al., *Hydrogen and syngas production by catalytic biomass gasification.* Energy Conversion and Management, 2017. **135**: p. 270.

10. Schmidt, S., et al., *Catalytic tar removal from bio syngas-Catalyst development and kinetic studies.* Catalysis Today, 2011. **175**(1): p. 442-449.

11. Cheng, L., et al., *Tar elimination from biomass gasification syngas with bauxite residue derived catalysts and gasification char.* Applied Energy, 2020. **258**.

12. Shen, Y. and K. Yoshikawa, *Recent progresses in catalytic tar elimination during biomass gasification or pyrolysis-A review.* Renewable and Sustainable Energy Reviews, 2013. **21**: p. 371-392.

13. Ren, J., et al., *Recent advances in syngas production from biomass catalytic gasification: A critical review on reactors, catalysts, catalytic mechanisms and mathematical models.* Renewable and Sustainable Energy Reviews, 2019. **116**: p. 109426.

14. Umeki, K., et al., *Reduction of tar and soot formation from entrained-flow gasification of woody biomass by alkali impregnation.* Energy & Fuels, 2017. **31**(5): p. 5104-5110.

15. Pushp, M., et al., *Influence of bed material, additives, and operational conditions on alkali metal and tar concentrations in fluidized bed gasification of biomass.* Energy & Fuels, 2018. **32**(6): p. 6797-6806.

16. Polychronopoulou, K., J.L.G. Fierro, and A.M. Efstathiou, *The phenol steam reforming reaction over MgO-based supported Rh catalysts.* Journal of Catalysis, 2004. **228**(2): p. 417-432.

17. Savuto, E., et al., *Steam reforming of tar model compounds over Ni/Mayenite catalysts: effect of Ce addition.* Fuel, 2018. **224**: p. 676-686.

18. Hoang, T.M.C., et al., *Investigation of Ce-Zr oxide-supported Ni catalysts in the steam reforming of meta-Cresol as a model component for bio-derived tar.* ChemCatChem, 2015. **7**(3): p. 468-478.

19. Kimura, T., et al., *Development of Ni catalysts for tar removal by steam gasification of biomass.* Applied Catalysis B: Environmental, 2006. **68**(3): p. 160-170.

20. Artetxe, M., et al., *Steam reforming of different biomass tar model compounds over Ni/Al_2O_3 catalysts.* Energy Convers. Manag., 2017: p. 119-126. .

21. Ren, J., et al., *Layered uniformly delocalized electronic structure of carbon supported Ni catalyst for catalytic reforming of toluene and biomass tar.* Energy Conversion and Management, 2019. **183**: p. 182-192.

22. Guan, G., et al., *Catalytic steam reforming of biomass tar: Prospects and challenges.* Renewable and Sustainable Energy Reviews, 2016. **58**: p. 450-461.

23. Grams, J., et al., *Mesoporous silicas as supports for Ni catalyst used in cellulose conversion to hydrogen rich gas.* International Journal of Hydrogen Energy, 2016. **41**(20): p. 8656-8667.

24. Sato, K. and K. Fujimoto, *Development of new nickel based catalyst for tar reforming with superior resistance to sulfur poisoning and coking in biomass gasification.* Catalysis Communications, 2007. **8**(11): p. 1697-1701.

25. Richardson, Y., et al., *Catalytic investigation of in situ generated Ni metal nanoparticles for tar conversion during biomass pyrolysis.* Journal of Physical Chemistry C, 2013. **117**(45): p. 23812-23831.

26. Xu, L., H. Song, and L. Chou, *One-pot synthesis of ordered mesoporous NiO-CaO-Al_2O_3 composite oxides for catalyzing CO_2 reforming of CH_4.* ACS Catalysis, 2012. **2**(7): p. 1331-1342.

27. Wu, G., et al., *Sorption enhanced steam reforming of ethanol on Ni-CaO-Al_2O_3 multifunctional catalysts derived from hydrotalcite-like compounds.* Energy & Environmental Science, 2012. **5**(10): p. 8942-8949.

28. Ashok, J., et al., *Bi-functional hydrotalcite-derived NiO-CaO-Al_2O_3 catalysts for steam reforming of biomass and/or tar model compound at low steam-to-carbon conditions.* Applied Catalysis B: Environmental, 2015. **172-173**: p. 116-128.

29. Ronsse, F., et al., *Production and characterization of slow pyrolysis biochar: influence of feedstock type and pyrolysis conditions.* GCB Bioenergy, 2013. **5**(2): p. 104-115.

30. Weber, K. and P. Quicker, *Properties of biochar.* Fuel, 2018. **217**: p. 240-261.

31. Sun, H., et al., *Multiple controls on the chemical and physical structure of biochars.* Industrial & Engineering Chemistry Research, 2012. **51**(9): p. 3587-3597-3587-3597.

32. Zimmerman, A.R., *Abiotic and microbial oxidation of laboratory-produced black carbon (biochar).* Environmental Science & Technology, 2010. **44**(4): p. 1295.

33. Dominic, W., et al., *Sustainable biochar to mitigate global climate change.* Nature Communications, 2010. **1**(5): p. 56.

34. Lahijani, P., et al., *Conversion of the greenhouse gas CO_2 to the fuel gas CO via the Boudouard reaction: A review.* Renewable and Sustainable Energy Reviews, 2015. **41**: p. 615-632.

35. Wu, C., et al., *CO_2 gasification of bio-char derived from conventional and microwave pyrolysis.* Applied Energy, 2015. **157**(C): p. 533-539.

36. Lahijani, P., et al., *Co-gasification of tire and biomass for enhancement of tire-char reactivity in CO_2 gasification process.* Bioresource Technology, 2013. **138**: p. 124-130.

37. Shen, Y., et al., *CO2 gasification of woody biomass: Experimental study from a lab-scale reactor to a small-scale autothermal gasifier.* Energy, 2019. **170**: p. 497-506.

38. Syed-Hassan, S.S.A., et al., *Thermochemical processing of sewage sludge to energy and fuel: Fundamentals, challenges and considerations.* Renewable and Sustainable Energy Reviews, 2017. **80**: p. 888-913.

39. Feng, D., et al., *Experimental comparison of biochar species on in-situ biomass tar H_2O reforming over biochar.* International Journal of Hydrogen Energy, 2017. **42**(38): p. 24035-24046.

40. Kierzkowska, A.M., R. Pacciani, and C.R. Müller, *CaO‐based CO_2 sorbents: From fundamentals to the development of new, highly effective materials.* Chemsuschem, 2013. **6**: p. 1130-1148.

41. Osaki, T. and T. Mori, *Kinetics of the reverse-Boudouard reaction over supported nickel catalysts.* Reaction Kinetics and Catalysis Letters, 2006. **89**(2): p. 333-339.

42. Li, J., et al., *Development of nano-NiO/Al_2O_3 catalyst to be used for tar removal in biomass gasification.* Environmental Science & Technology, 2008. **42**(16): p. 6224.

43. Bian, Z., et al., *A highly active and stable Ni-Mg phyllosilicate nanotubular catalyst for ultrahigh temperature water-gas shift reaction.* Chemical Communications, 2015. **51**(91): p. 16324-16326.

44. Salhi, N., et al., *Steam reforming of methane to syngas over $NiAl_2O_4$ spinel catalysts.* International Journal of Hydrogen Energy, 2011. **36**(17): p. 11433-11439.

45. Li, M., et al., *Hydrogen production from ethanol steam reforming over nickel based catalyst derived from Ni/Mg/Al hydrotalcite-like compounds.* International Journal of Hydrogen Energy, 2010. **35**(13): p. 6699-6708.

46. Wu, G., et al., *Sorption enhanced steam reforming of ethanol on Ni–CaO–Al_2O_3 multifunctional catalysts derived from hydrotalcite-like compounds.* Energy & Environmental Science, 2012. **5**(10): p. 8942-8949.

47. Ruppert, A.M., et al., *Optimization of Ni/ZrO_2 catalytic performance in thermochemical cellulose conversion for enhanced hydrogen production.* Applied Catalysis B: Environmental, 2014. **145**: p. 85-90.

48. Kho, E.T., J. Scott, and R. Amal, *Ni/TiO_2 for low temperature steam reforming of methane.* Chemical Engineering Science, 2016. **140**: p. 161-170.

49. Li, Z.-S., et al., *Synthesis, experimental studies, and analysis of a new calcium-based carbon dioxide absorbent.* Energy & Fuels, 2005. **19**(4): p. 1447-1452.

50. Ji, G., et al., *Enhanced hydrogen production from sawdust decomposition using hybrid-functional Ni-CaO-Ca_2SiO_4 materials.* Environmental Science & Technology, 2017. **51**(19): p. 11484.

51. Shen, Y. and Y. Fu, *Advances in in situ and ex situ tar reforming with biochar catalysts for clean energy production.* Sustainable Energy & Fuels, 2018. **2**(2): p. 326-344.

52. Zhang, Y.-L., et al., *Experimental study on pyrolysis tar removal over rice straw char and inner pore structure evolution of char.* Fuel Processing Technology, 2015. **134**: p. 333.

53. Chen, F., et al., *Characteristics and catalytic properties of Ni/CaAlOx catalyst for hydrogen-enriched syngas production from pyrolysis-steam reforming of biomass sawdust.* Applied Catalysis B: Environmental, 2016. **183**: p. 168-175.

54. Jin, F., et al., *Effect of calcium addition on Mg-AlOx supported Ni catalysts for hydrogen production from pyrolysis-gasification of biomass.* Catalysis Today, 2018. **309**: p. 2-10.

55. Waheed, Q.M.K. and P.T. Williams, *Hydrogen Production from High Temperature Pyrolysis/Steam Reforming of Waste Biomass: Rice Husk, Sugar Cane Bagasse, and Wheat Straw.* Energy & Fuels, 2013. **27**(11): p. 6695-6704.

56. Ji, G., et al., *Enhanced Hydrogen Production from Sawdust Decomposition Using Hybrid-Functional Ni-CaO-Ca2SiO4 Materials.* Environmental Science & Technology, 2017. **51**(19): p. 11484-11492.

57. Wang, D., W. Yuan, and W. Ji, *Char and char-supported nickel catalysts for secondary syngas cleanup and conditioning.* Applied Energy, 2011. **88**(5): p. 1656-1663.

58. Yang, F.-L., et al., *Acid washed lignite char supported bimetallic Ni-Co catalyst for low temperature catalytic reforming of corncob derived volatiles.* Energy Conversion and Management, 2019. **196**: p. 1257-1266.

59. Hu, M., et al., *Catalytic cracking of biomass tar over char supported nickel catalyst.* Energy, 2018. **145**: p. 228-237.

60. Dry, M.E., *The Fischer–Tropsch process: 1950–2000.* Catal Today, 2002. **71**(3-4): p. 227-241.

61. Cho, M., et al., *Silver nanowire/carbon sheet composites for electrochemical syngas generation with tunable H_2/CO ratios.* ACS Omega, 2017. **2**(7): p. 3441-3446.

Chapter 6 Conclusions and future work

6.1. Conclusions

Thermochemical conversion is a promising approach to treat sewage sludge (SS) and recover its embedded energy. Consider that conventional thermochemical conversion process mainly focuses on the H_2 production while ignores the CO production. This thesis proposed a novel two-stage sorption-enhanced (TSSE) thermochemical conversion process of SS for H_2 and CO production, and much effort has been paid on the maximisation of the yield and improvement of the quality of H_2 and CO. The main research innovations and contributions of this thesis are summarised as follows.

A novel two-stage sorption-enhanced (TSSE) pyrolysis process was proposed in Chapter 3. Based on the introduction of a CaO-based CO_2 carrying cycle, large amounts of CO_2 which is released without utilization during conventional sorption-enhanced thermochemical conversion of SS is capable of being utilized for CO production in the proposed TSSE pyrolysis process. More specifically, the CO_2 generated from SS is captured by CaO and stored in the form of $CaCO_3$ at a lower temperature (first stage, 500-600 °C) to facilitate the H_2 production, and is then released at a higher temperature (second stage, 700-800 °C) to gasify the sludge char for CO production. This new TSSE pyrolysis process can improve the utilization efficiency of carbon for CO production, with a remarkably higher yield of CO than that using other conventional sorption-enhanced thermochemical conversion processes. More importantly, the proposed process can achieve the inherent separation of H_2 production at the first stage and CO production at the second stage providing great convenience for the application of H_2 and CO for the downstream synthesis of

chemicals or fuels, which cannot be achieved by the conventional sorption-enhanced thermochemical conversion process.

Chapter 4 presents a TSSE steam gasification process via the introduction of steam at the first stage to obtain a tunable H_2/CO ratio in the syngas to meet different demands of H_2/CO ratios for the downstream application process. By controlling the CaO and steam contents, a wide range of H_2/CO ratio can be adjusted from 0.9 to 4.7 in the SS-derived syngas using the TSSE steam gasification process. Under the optimal conditions, an H_2-rich gas stream (72.2 vol% purity) and CO-rich gas stream (60.5 vol% purity) could be obtained at the first stage and the second stage, respectively. The high purity and inherent separation of H_2 and CO production can avoid imposing severe cost penalties for the cleaning, refining and separation of H_2 and CO before application. This process presents a promising option for direct integration of the TSSE steam gasification of SS with the syngas applications where H_2 and CO could be mixed in any desirable ratios for the downstream synthesis of value-added chemicals and fuels. The studies on the performance characterisation of the TSSE thermochemical conversion process show that a high yield of tar is produced at the first stage, while the conversion of char into gas is dominated at the second stage.

A co-gasification of SS and biochar using TSSE catalytic steam gasification process over Ni-CaO/Al_2O_3 catalyst was proposed in Chapter 5 to address the issue of tar removal in the syngas and simultaneously enhance the syngas production. A 22.0% of reduction in the tar yield and a 42.7% of enhancement in the gas yield is obtained with the addition of biochar and Ni-CaO/Al_2O_3 catalyst. And there is a complementary effect of steam, Ni-CaO/Al_2O_3 catalyst and biochar on the syngas production, thereinto, the addition of steam and Ni-CaO/ Al_2O_3 catalyst triggers a drastic enhancement in the yield and purity of H_2 at the first stage, while the presence of biochar acts as the carbon source to promote the CO production at the second stage. A desirable H_2/CO ratio of 2

is achieved, which is typically desired for the downstream synthesis of value-added chemicals and fuels via FTS process.

The novel proposed TSSE thermochemical conversion process with the inherent separation of H_2 and CO production has great potential to directly integrate with the FTS process to produce high value-added fuels and chemicals, offering a sustainable and environmentally benign approach to convert waste, i.e. SS to energy.

6.2. Future work

In spite of the promising results shown above, related studies are still in progress and further developments are required.

1. Further improve the yield and purity of CO production at the second stage

In this work, it is observed that the increase in H_2 production at the first stage always accompanies by an increase in the amount of CO_2 captured by CaO. Much more CO_2 released from $CaCO_3$ dissociation reaction at the second stage exists in the effluent gas stream without participating in the reverse Boudouard reaction for CO production, leading to a reduction in the purity of CO at the second stage. In further work, it deserves to develop the cost-effective catalysts to accelerate the reaction rate of reverse Boudouard reaction, thereby achieving better integration of the reverse Boudouard and $CaCO_3$ dissociation reaction at the second stage. The released CO_2 from the $CaCO_3$ dissociation reaction can directly be converted into CO via the reverse Boudouard reaction to further promote the yield and purity of CO at the second stage.

2. Extend the utilization of the proposed process to other biomass sources

The technical feasibility to transform SS into syngas with potentially controllable H_2/CO ratios has been demonstrated in this work by using the proposed TSSE thermochemical conversion process, which will be applicable to various forms of biomass other than SS. In principle, a better performance of syngas production could be achieved by the conversion of the lignocellulosic biomass with higher contents of organic matters, e.g., agricultural wastes.

3. Develop efficient and stable additives for industrial application

The naturally abundant and readily available limestone feedstock is one of the vital additive required for the operation of the proposed TSSE thermochemical conversion process. The benefit of recycling the CaO-rich sludge ash and potential synergy with cement manufacture will offer the proposed process techno-economic superiority for industrial application. Additionally, high catalytically active, stable, cost-effective Ni-CaO multifunctional catalysts are also deserved to be exploited for the industrial application of the proposed TSSE thermochemical conversion process.

4. Industrial application of the proposed TSSE thermochemical conversion process

Upon introducing the interconnected fluidized-bed reactor concept, the proposed TSSE thermochemical conversion process can be operated in a continuous mode for practical application. As illustrated in Fig 6.1, the proposed TSSE thermochemical conversion process can be performed on two interconnected fluidized-bed reactors, where the CaO-based CO_2 sorbent is circulated between the first reactor for CaO carbonation to capture CO_2 and the second reactor for $CaCO_3$ calcination to release CO_2. The lime-dried SS is continuously fed into the first reactor operated at 500-600 °C, and mixed with the CaO/ash streams circulated back from the second reactor to produce high-purity H_2 via the steam reforming and CaO carbonation reactions. Meanwhile, the $CaCO_3$/sludge char streams are circulated into the second reactor operated at 700-800 °C to

produce high-purity CO via the $CaCO_3$ calcination and reverse Boudouard reactions. The spent CaO/ash streams discharged from the second reactor are composed of inorganic oxides, such as CaO, SiO_2, MgO, and Al_2O_3, which are potential feedstock readily for the use of cement production. This is a promising way of the practical application of the proposed TSSE thermochemical conversion process in industries.

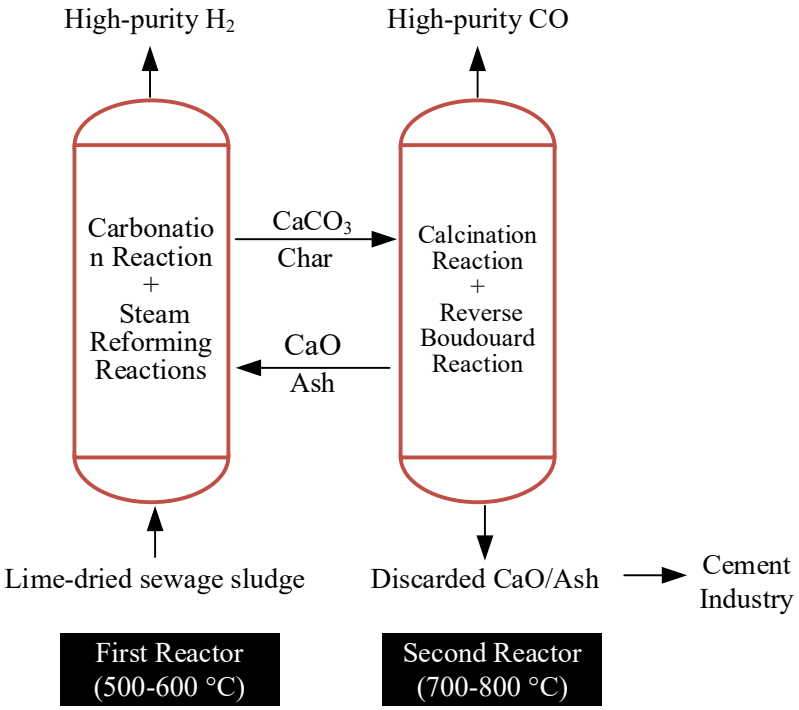

Fig. 6.1. Conceptual design for industrial application of the proposed TSSE thermochemical process of SS based on the calcium-looping scheme.

5. Integration of the proposed TSSE thermochemical conversion process with the application process of syngas

To fully achieve the conversion of waste to energy, it has been demonstrated that high purity of H_2 and CO can be separately collected via the proposed TSSE thermochemical conversion of SS, while the other indispensable step is the conversion of the generated syngas into the common types

of energy, like thermal, electricity, liquid fuels. Hence, extra processes, such as the FTS process for various chemicals and liquid fuels, syngas fermentation for bioethanol, internal combustion engines for heat or electricity are needed. Therefore, it is of great significance for the sustainable management of waste-to-energy to integrate the proposed TSSE thermochemical conversion process with the industrial application process of syngas.